

AD A056044

LEVEL III

A036872

2

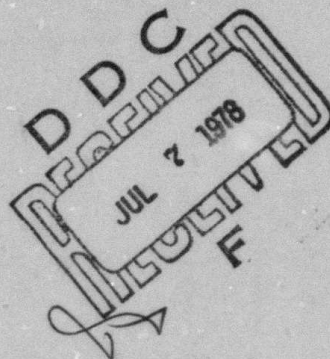
RADC-TR-78-124  
Final Technical Report  
June 1978



LASER ATMOSPHERIC ABSORPTION STUDIES

R. K. Long  
E. K. Damon  
R. J. Nordstrom  
J. C. Peterson  
M. E. Thomas  
J. Sherman

Sponsored by  
Defense Advanced Research Projects Agency (DoD)  
ARPA Order No. 1279



Approved for public release; distribution unlimited.

The views and conclusions contained in this document are those of the authors and should not be interpreted as necessarily representing the official policies, either expressed or implied, of the Defense Advanced Research Projects Agency or the U.S. Government.

DDC FILE COPY

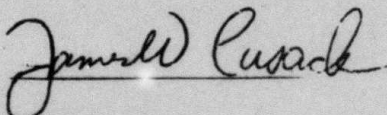
ROME AIR DEVELOPMENT CENTER  
Air Force Systems Command  
Griffiss Air Force Base, New York 13441

78 07 06 003

This report has been reviewed by the RADC Information Office (OI) and is releasable to the National Technical Information Service (NTIS). At NTIS it will be releasable to the general public, including foreign nations.

RADC-TR-78-124 has been reviewed and is approved for publication.

APPROVED:



JAMES W. CUSACK  
Project Engineer

If your address has changed or if you wish to be removed from the RADC mailing list, or if the addressee is no longer employed by your organization, please notify RADC (OCSE) Griffiss AFB NY 13441. This will assist us in maintaining a current mailing list.

Do not return this copy. Retain or destroy.



LASER ATMOSPHERIC ABSORPTION STUDIES

R. K. Long  
E. K. Damon  
R. J. Nordstrom  
J. C. Peterson  
M. E. Thomas  
J. Sherman

Contractor: Ohio State University  
Contract Number: F30602-76-C-0058  
Effective Date of Contract: 1 July 1975  
Contract Expiration Date: 30 Sep 1977  
Short Title of Work: Laser Atmospheric Absorption Studies  
Program Code Number: 6E20  
Period of Work Covered: Jan 77 - Sep 77

Principal Investigator: Dr. Ronald K. Long  
Phone: 614-422-6077

Project Engineer: James W. Cusack  
Phone: 315-330-3145

Approved for public release; distribution unlimited.

This research was supported by the Defense Advanced Research Projects Agency of the Department of Defense and was monitored by James W. Cusack (OCSE), Griffiss AFB NY 13441 under Contract F30602-76-C-0058.

78 07 06 003

UNCLASSIFIED

SECURITY CLASSIFICATION OF THIS PAGE (When Data Entered)

REPORT DOCUMENTATION PAGE		READ INSTRUCTIONS BEFORE COMPLETING FORM
1. REPORT NUMBER RADC TR-78-124	2. GOVT ACCESSION NO.	3. RECIPIENT'S CATALOG NUMBER
4. TITLE (and Subtitle) LASER ATMOSPHERIC ABSORPTION STUDIES		5. TYPE OF REPORT & PERIOD COVERED Final Technical Report, Jul 75--Sep 77
6. AUTHOR(s) R. K./Long, J. C./Peterson E. K./Damon, M. E./Thomas R. J./Nordstrom, J. S. Smetman		7. PERFORMING ORGANIZATION REPORT NUMBER ESL-4232-6 (710338)
9. PERFORMING ORGANIZATION NAME AND ADDRESS The Ohio State University ElectroScience Laboratory Department of Electrical Engineering Columbus OH 43212		8. CONTRACT OR GRANT NUMBER(s) F30602-76-C-0058, ARPA Order-1279
11. CONTROLLING OFFICE NAME AND ADDRESS Defense Advanced Research Projects Agency 1400 Wilson Blvd Arlington VA 22209		10. PROGRAM ELEMENT, PROJECT, TASK AREA & WORK UNIT NUMBERS 62301E 1279053
14. MONITORING AGENCY NAME & ADDRESS (if different from Controlling Office) Rome Air Development Center (OCSE) Griffiss AFB NY 13441		12. REPORT DATE June 1978
		13. NUMBER OF PAGES 129 p.
		15. SECURITY CLASS. (of this report) UNCLASSIFIED
		15a. DECLASSIFICATION/DOWNGRADING SCHEDULE N/A
16. DISTRIBUTION STATEMENT (of this Report) Approved for public release; distribution unlimited.		
17. DISTRIBUTION STATEMENT (of the abstract entered in Block 20, if different from Report) Same		
18. SUPPLEMENTARY NOTES RADC Project Engineer: James W. Cusack (OCSE)		
19. KEY WORDS (Continue on reverse side if necessary and identify by block number) Laser absorption      Molecular absorption      Chemical laser CO <sub>2</sub> laser      White cell      Line shape CO laser      Absorption cell      Absorption coefficient water vapor      DF laser laser propagation      HF laser		
20. ABSTRACT (Continue on reverse side if necessary and identify by block number) This report describes work conducted under Contract F30602-76-C-0058. Measurements of water vapor absorption coefficients for 27 CO <sub>2</sub> laser lines are given. Some measurements were obtained using a spectrophone and others using a long path absorption cell. Measurements were made with pure water vapor, and with samples broadened with N <sub>2</sub> and with O <sub>2</sub> -N <sub>2</sub> mixtures. This is discussed in Section I and Tables II and IV summarize the results obtained. (Cont'd)		

DD FORM 1 JAN 73 1473 EDITION OF 1 NOV 65 IS OBSOLETE

UNCLASSIFIED

SECURITY CLASSIFICATION OF THIS PAGE (When Data Entered)

402 251

act



**UNCLASSIFIED**

SECURITY CLASSIFICATION OF THIS PAGE(When Data Entered)

(20 Cont'd)

Studies of water vapor absorption by CO laser radiation were also conducted. This is discussed in Section II and the results are summarized in Table V.

A new long path White cell was developed under this program. A brief description of this equipment is given in Section III.

A small cw HF/DF chemical laser also was developed. The results obtained are described in Section IV.

**UNCLASSIFIED**

SECURITY CLASSIFICATION OF THIS PAGE(When Data Entered)

# CONTENTS

	Page
I. WATER VAPOR ABSORPTION MEASUREMENTS AT CO <sub>2</sub> LASER FREQUENCIES	1
A. <u>White Cell Measurements</u>	1
B. <u>Spectrophone Measurements</u>	25
II. WATER VAPOR ABSORPTION MEASUREMENTS USING A CO LASER	92
A. <u>Introduction</u>	92
B. <u>Pressure Broadened (N<sub>2</sub>) Water Vapor Measurements</u>	92
III. CONSTRUCTION OF A NEW LONG PATH ABSORPTION CASE	100
IV. DEVELOPMENT OF A SMALL SINGLE-MODE CW HF-DF LASER	101
A. <u>Introduction</u>	101
1. <u>Background</u>	101
2. <u>Research Objectives</u>	102
B. <u>System Configuration</u>	103
C. <u>Operation and Output Characteristics</u>	105
1. <u>Multiline Operation</u>	105
2. <u>Single Line Operation</u>	107
3. <u>Conclusions</u>	109
D. <u>Output Coupling Studies</u>	111
E. <u>Short-Term Stability Measurements</u>	113
F. <u>Summary and Conclusions</u>	117
APPENDIX A. OVERCOUPLING OF HF OUTPUT MIRROR	120
REFERENCES	121

ACCESSION for	
NTIS	White Section <input checked="" type="checkbox"/>
DPC	Buff Section <input type="checkbox"/>
UNANNOUNCED	<input type="checkbox"/>
JUSTIFICATION	
BY	
DISTRIBUTION/AVAILABILITY NOTES	
DI	CIAL
A	



## SECTION I

### WATER VAPOR ABSORPTION MEASUREMENTS AT CO<sub>2</sub> LASER FREQUENCIES

Measurements of the water vapor absorption at CO<sub>2</sub> laser frequencies in the 9.4 and 10.4  $\mu\text{m}$  bands have been conducted using two different instruments. A long path, multi-traversal absorption cell has been used to measure the transmittance of pressure-broadened and pure water vapor samples. A differential, non-resonant spectrophone has also been used to study the absorption caused by pressure-broadened water vapor samples. Both instruments have been described in previous reports and publications<sup>1,2</sup>.

Results of these studies are summarized in the following sections. The laser used for both the long-path absorption cell measurements and the spectrophone measurements is a modified Sylvania 948 multi-line CO<sub>2</sub> laser. The modification has been discussed in an earlier report<sup>3</sup>.

#### A. White Cell Measurements

The monochromatic absorption coefficients of pressure-broadened water vapor samples were measured at 21 wavelengths of the CO<sub>2</sub> laser in both the 9.4 and 10.4  $\mu\text{m}$  bands. The techniques for making measurements with the absorption cell have been refined over the years to yield experimental results which are quite reproducible.

Doubly distilled water is evaporated into the cell. When 15 torr is reached, the cell is filled to 760 torr with nitrogen buffer gas. Mixing fans are turned on and a period of more than 8 hours is required to mix the sample. The water vapor partial pressure is monitored during the mixing with a dew point hygrometer to determine when adequate mixing is achieved.

When the sample is ready, the circulation fans are turned off and the CO<sub>2</sub> laser is aligned through the cell.

A digital computer-based data recording system is used in our experiments. The outputs from two separate detectors are sampled and digitized four hundred times at 100 msec intervals. The signal detector collects the laser radiation which traversed the absorption cell. A reference detector collects the radiation which is reflected from a beam splitter just prior to the entrance window of the absorption cell. The two signals are corrected for nonlinearities in the detector system and then ratioed. This ratioing eliminates any fluctuations in the laser output intensity during the measurement time.

The four hundred sample points are then averaged and the standard deviation is computed. In these experiments, the standard deviation is typically more than three orders of magnitude smaller than the average of the ratioed signals.

Transmission data are recorded by this method at several laser frequencies. The absorption cell is then partially evacuated and refilled to 760 torr with nitrogen. The partial pump-out pressure determines the new water vapor pressure in the next sample. The mixing fans are turned on for a few hours to mix the new sample.

After the mixing fans are turned off and turbulence decays, the water vapor partial pressure is verified with a dew point hygrometer. Data are again recorded and averaged. Typically, four or five different laser lines can be studied at four or five water vapor pressures during a single experimental run.

Once the water vapor transmission data have been collected, a background is collected by pumping the cell out completely and refilling the cell to 760 torr with nitrogen. Transmission data are recorded in the same way at each laser line. The water vapor transmission data are ratioed to the background to produce transmittance values.

Figures 1-21 show experimental results at twenty-one laser lines. The data at each laser frequency were fit to a quadratic of the form

$$k = A_1 p_{H_2O} + A_2 p_{H_2O}^2 \quad (\text{km}^{-1}) \quad (1)$$

where  $p_{H_2O}$  is in Torr.

This fit is in agreement with the concept that absorption at these frequencies is caused by the wings of strong Lorentzian lines. At the R(20) laser line in the 10.4  $\mu\text{m}$  band the  $A_2$  coefficient is negligibly small compared to the  $A_1$  coefficient and the absorption is essentially linear with water vapor partial pressure. This linearity is caused by the near coincidence of the R(20) laser line with a rotational absorption line in water vapor. Table I lists the curve-fit coefficients at each of the twenty-one laser lines.

McCoy et al<sup>1</sup> wrote the monochromatic absorption coefficient in the form

$$k = C p_{H_2O} \left[ P_{\text{Total}} + B p_{H_2O} \right] \quad (2)$$

where  $P_{\text{Total}}$  is the total cell pressure (760 Torr). The coefficients C and B can be evaluated from the coefficients listed in Table I by

$$C = \frac{A_1}{P_{\text{Total}}} \quad (3a)$$

$$B = \frac{A_2 P_{\text{Total}}}{A_1} \quad (3b)$$



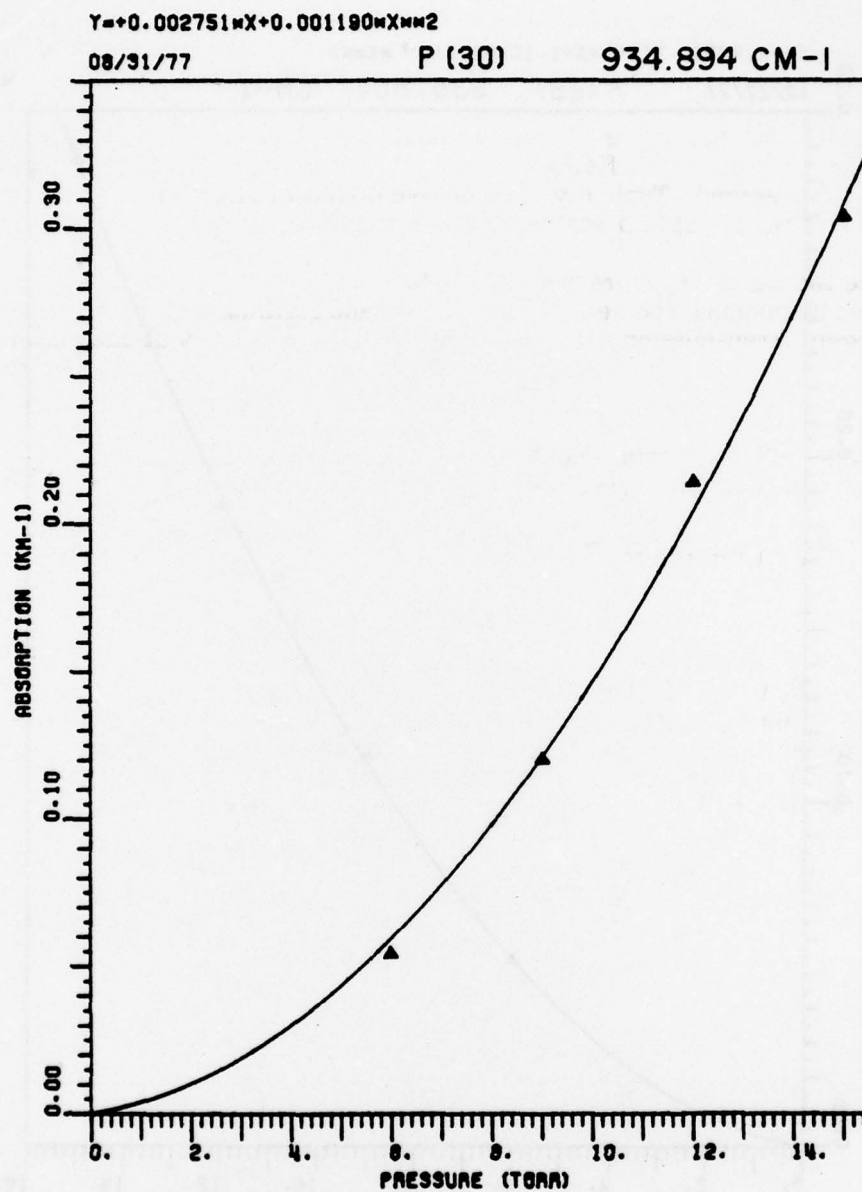


Figure 1. Measured water vapor-nitrogen absorption coefficient  
 at P(30) CO<sub>2</sub> laser line, 934.894 cm<sup>-1</sup> for 760 Torr  
 total pressure and T=22.5±.5°C.

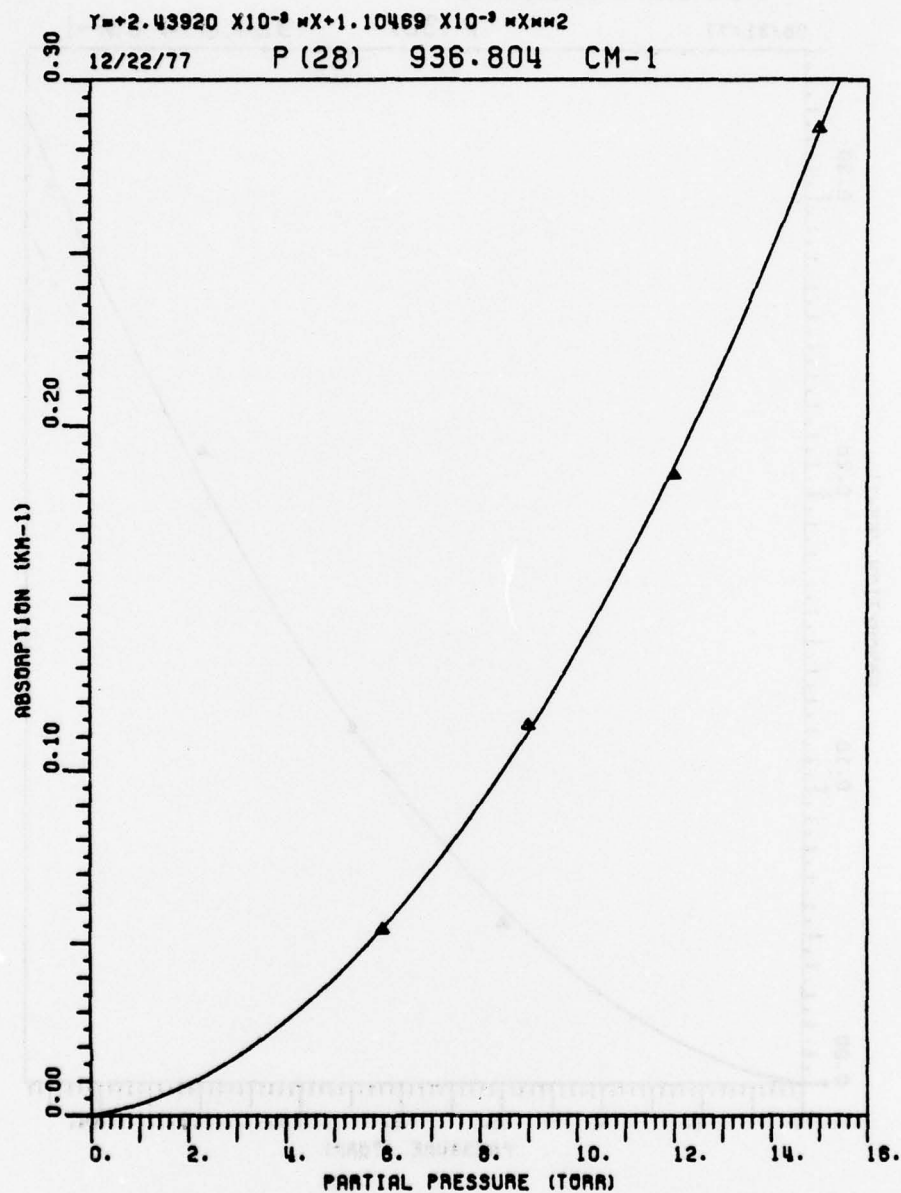


Figure 2. Measured water vapor-nitrogen absorption coefficient  
 at P(28) CO<sub>2</sub> laser line, 936.804 cm<sup>-1</sup> for 760 Torr  
 total pressure and T=22.5±.5°C.



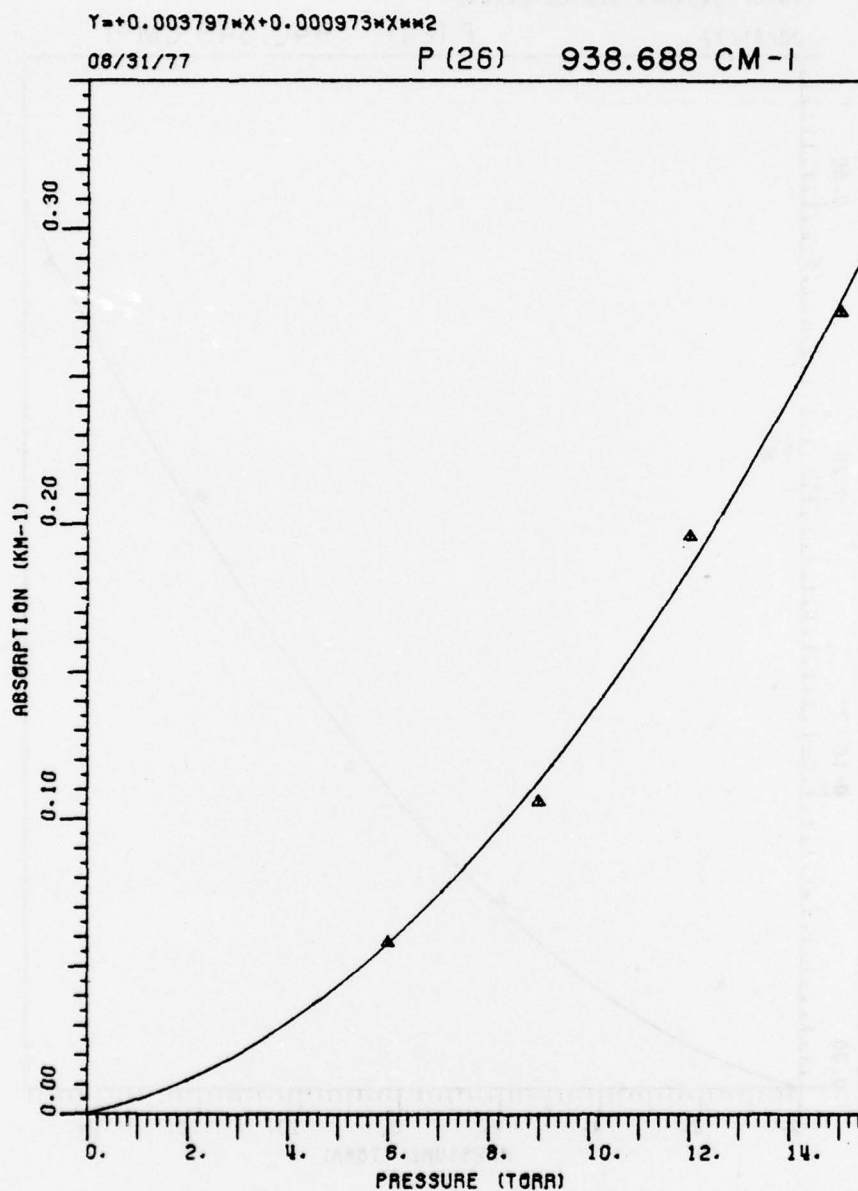


Figure 3. Measured water vapor-nitrogen absorption coefficient  
 at P(26) CO<sub>2</sub> laser line, 938.688 cm<sup>-1</sup> for 760 Torr  
 total pressure and T=22.5±.5°C.

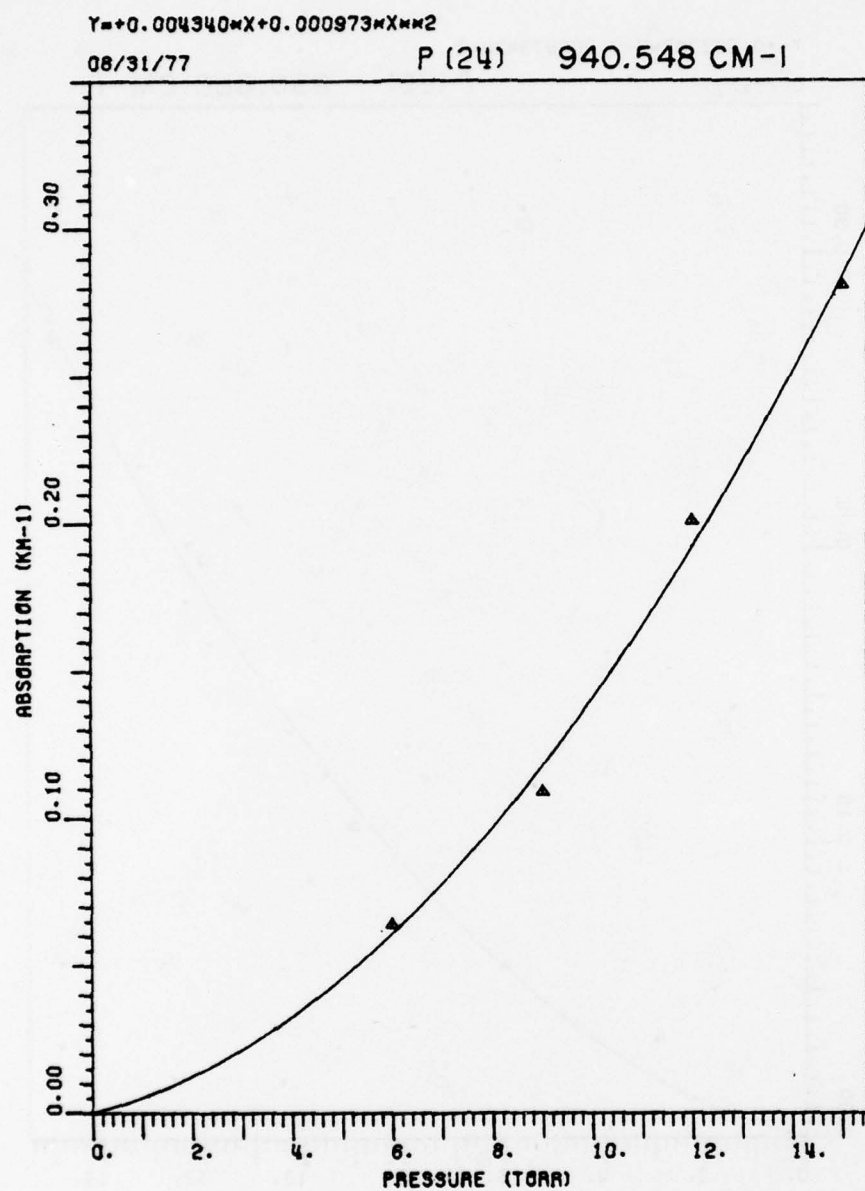


Figure 4. Measured water vapor-nitrogen absorption coefficient  
 at P(24) CO<sub>2</sub> laser line, 940.548 cm<sup>-1</sup> for 760 Torr  
 total pressure and T=22.5<sup>±</sup>.5°C.

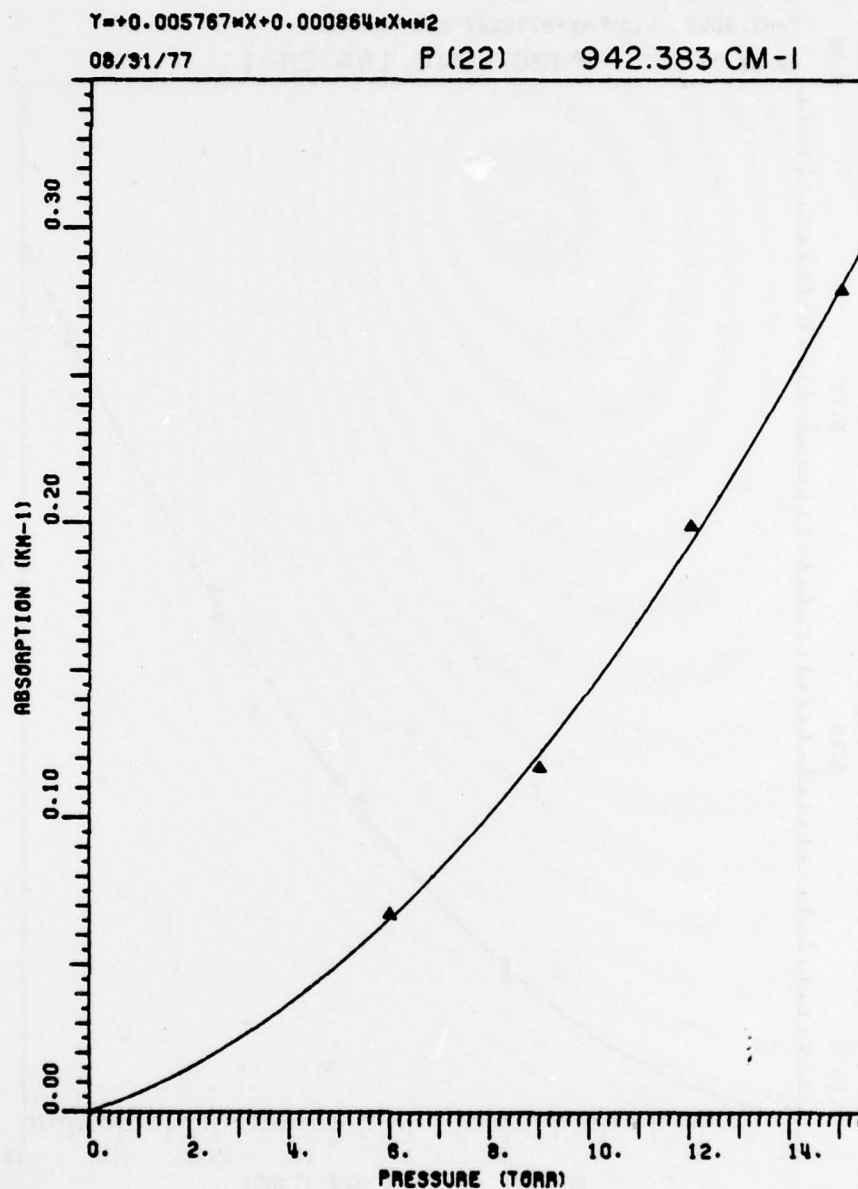


Figure 5. Measured water vapor-nitrogen absorption coefficient  
 at P(22) CO<sub>2</sub> laser line, 942.383 cm<sup>-1</sup> for 760 Torr  
 total pressure and T=22.5±.5°C.



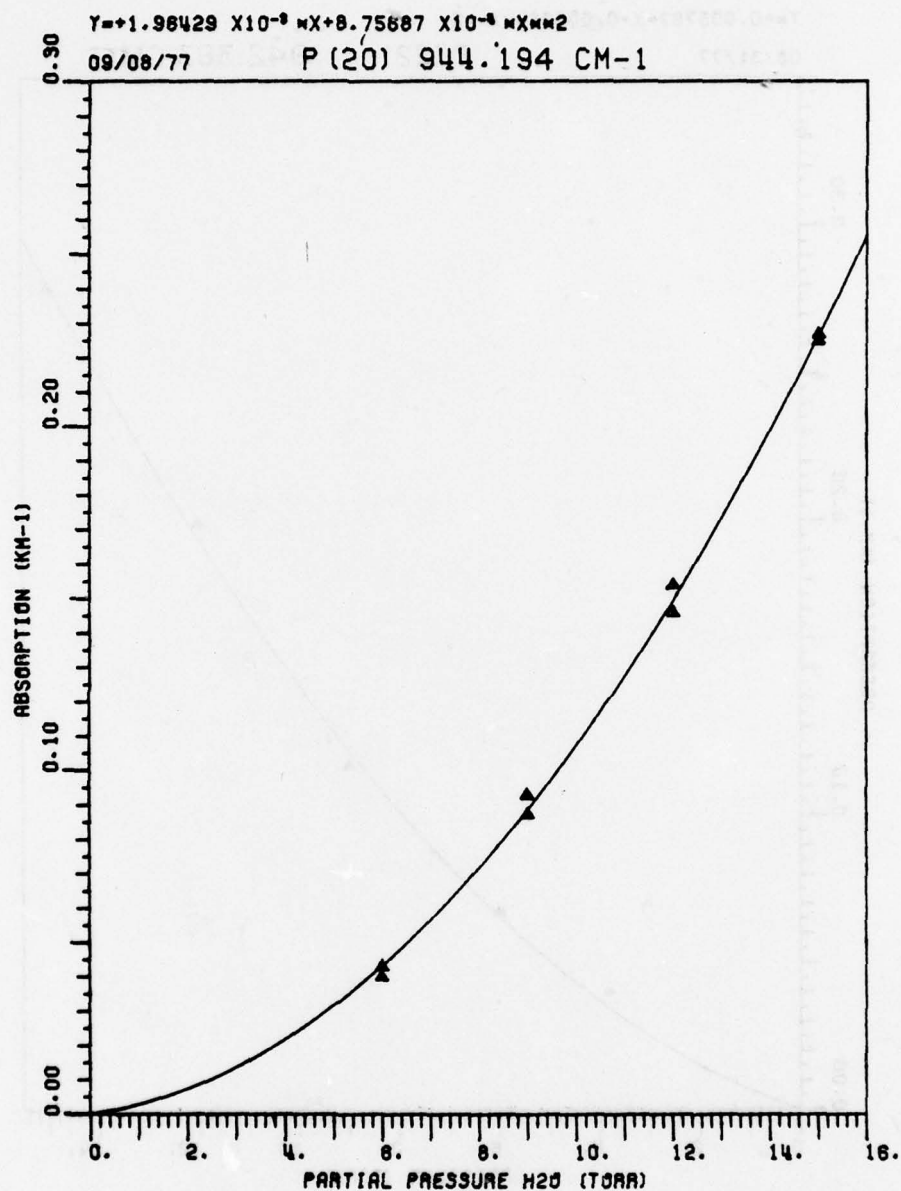


Figure 6. Measured water vapor-nitrogen absorption coefficient  
 at P(20) CO<sub>2</sub> laser line, 944.194 cm<sup>-1</sup> for 760 Torr  
 total pressure and T=22.5±.5°C.

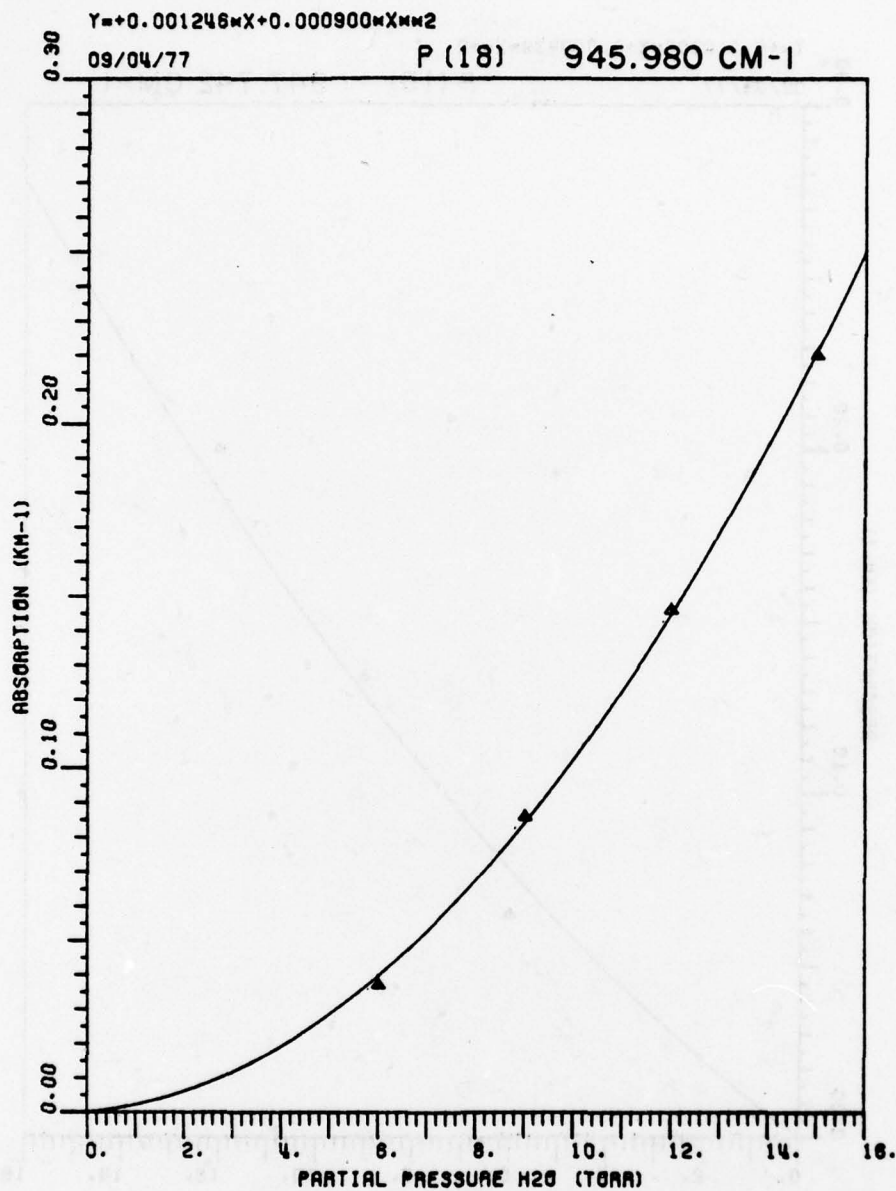


Figure 7. Measured water vapor-nitrogen absorption coefficient  
 at P(18) CO<sub>2</sub> laser line, 945.980 cm<sup>-1</sup> for 760 Torr  
 total pressure and T=22.5±.5°C.

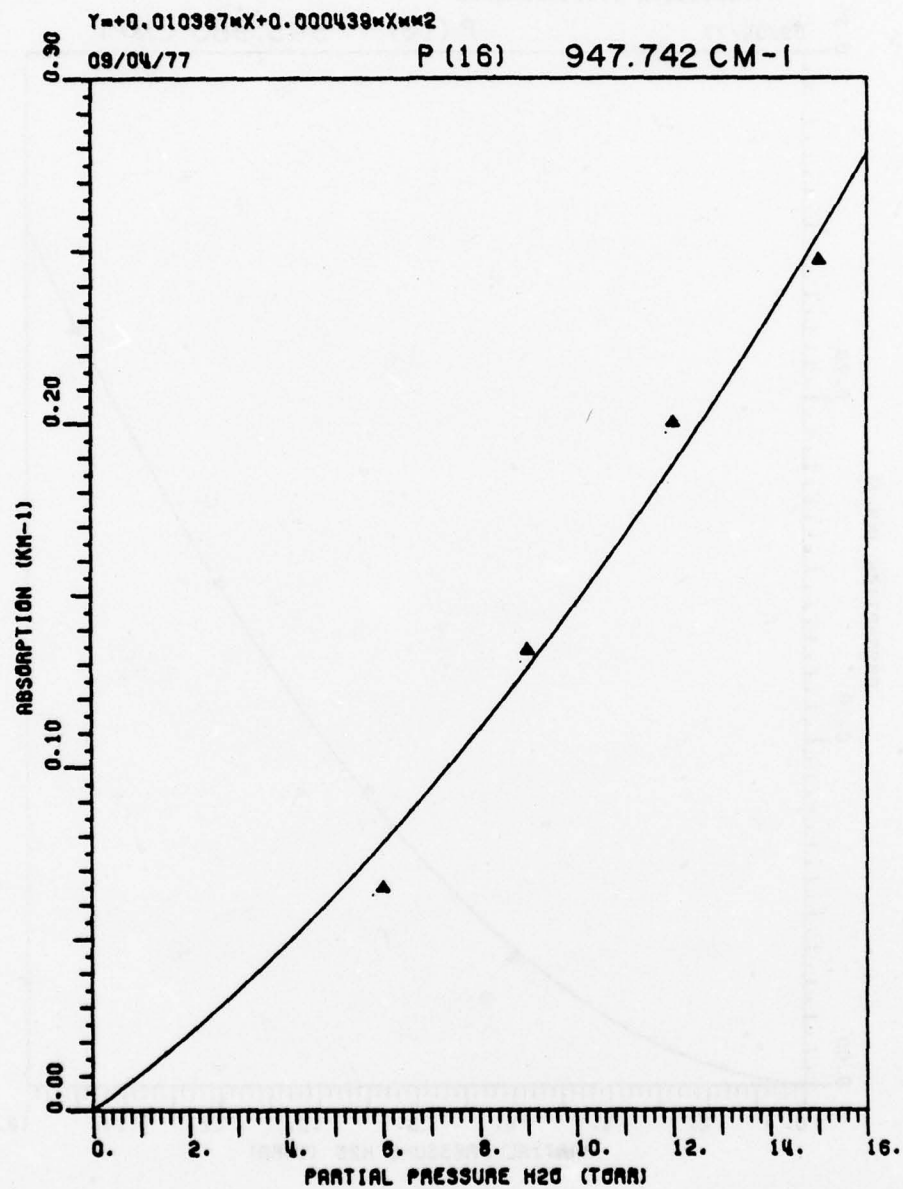


Figure 8. Measured water vapor-nitrogen absorption coefficient  
 at P(16) CO<sub>2</sub> laser line, 947.742 cm<sup>-1</sup> for 760 Torr  
 total pressure and T=22.5±.5°C.



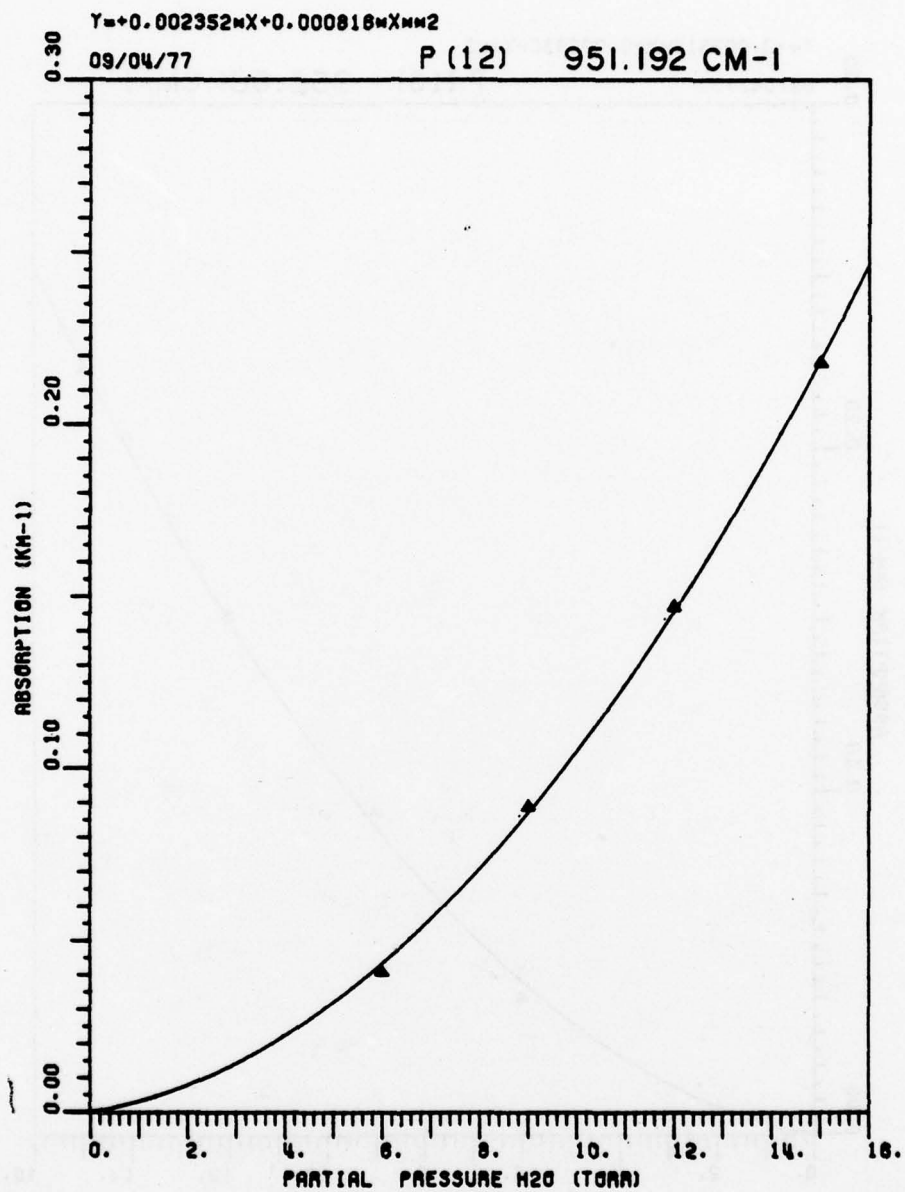


Figure 9. Measured water vapor-nitrogen absorption coefficient at P(12) CO<sub>2</sub> laser line, 951.192 cm<sup>-1</sup> for 760 Torr total pressure and T=22.5±.5°C.

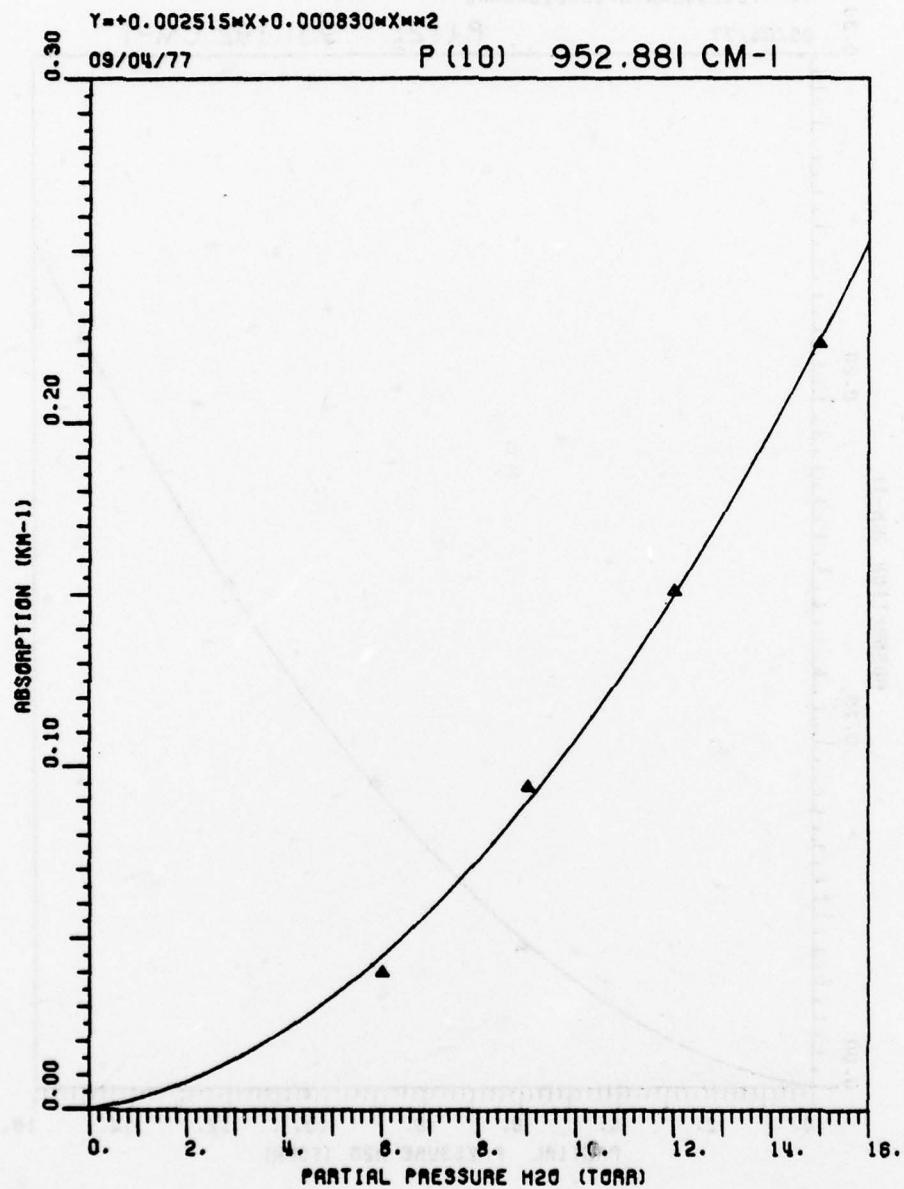


Figure 10. Measured water vapor-nitrogen absorption coefficient at P(10) CO<sub>2</sub> laser line, 952.881 cm<sup>-1</sup> for 760 Torr total pressure and T=22.5<sup>+1.5</sup>°C.

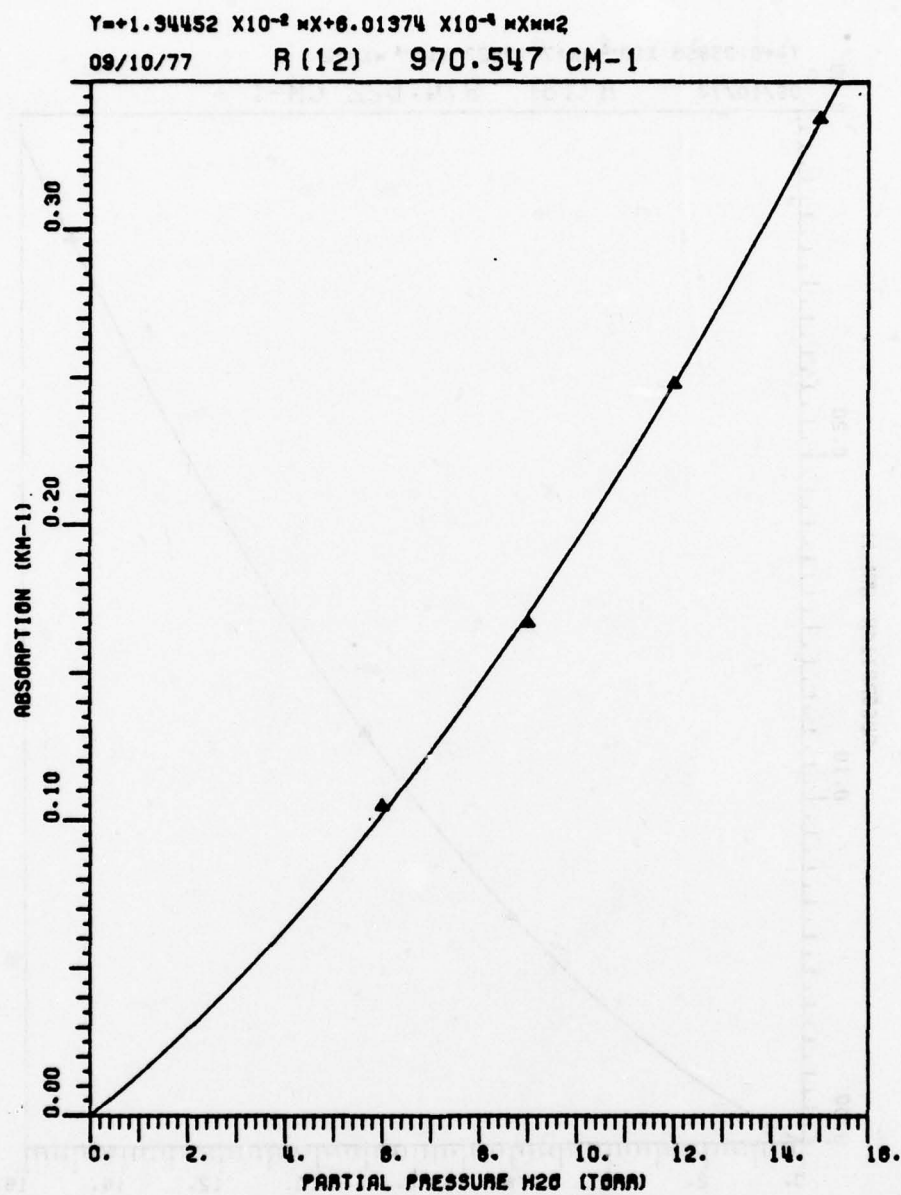


Figure 11. Measured water vapor-nitrogen absorption coefficient  
 at R(12) CO<sub>2</sub> laser line, 970.547 cm<sup>-1</sup> for 760 Torr  
 total pressure and T=22.5±.5°C.



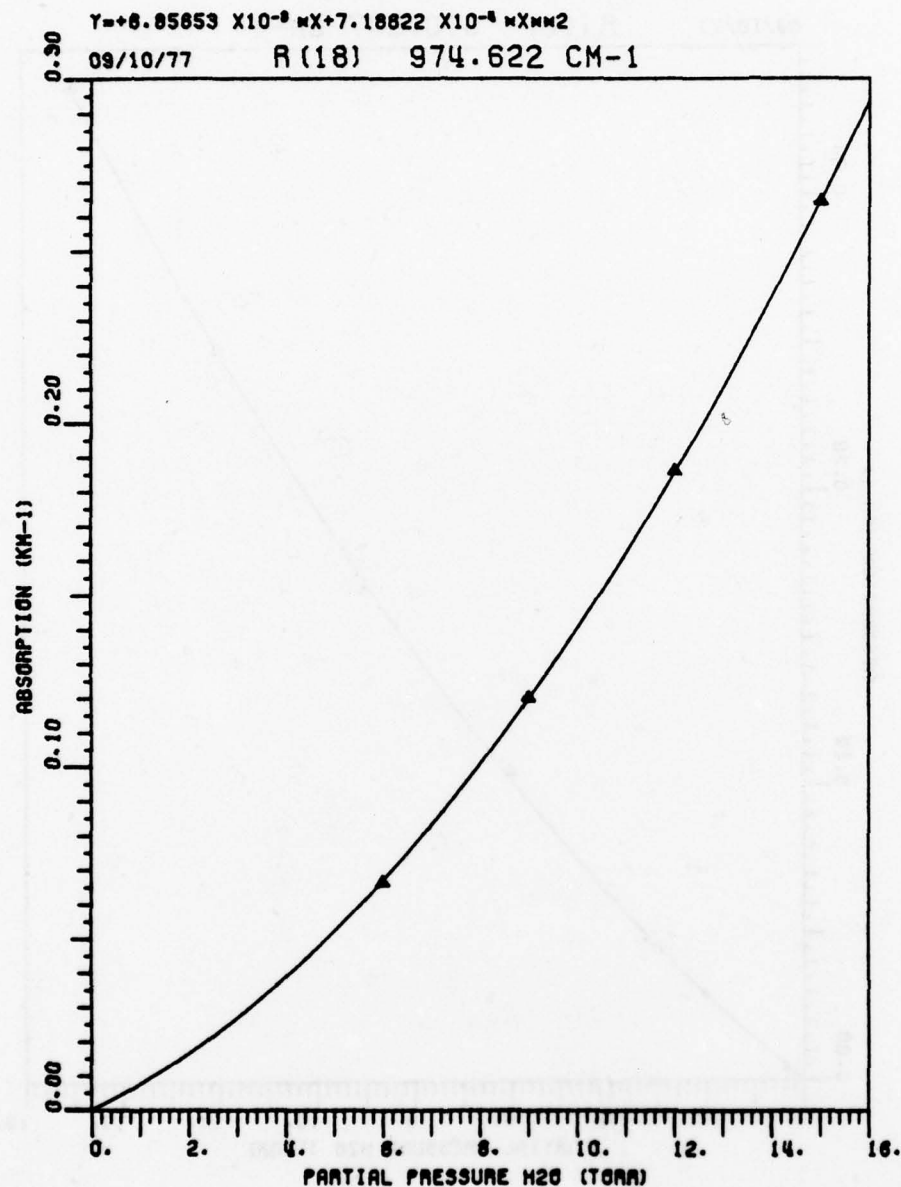


Figure 12. Measured water vapor-nitrogen absorption coefficient  
 at R(18) CO<sub>2</sub> laser line, 974.622 cm<sup>-1</sup> for 760 Torr  
 total pressure and T=22.5±.5°C.

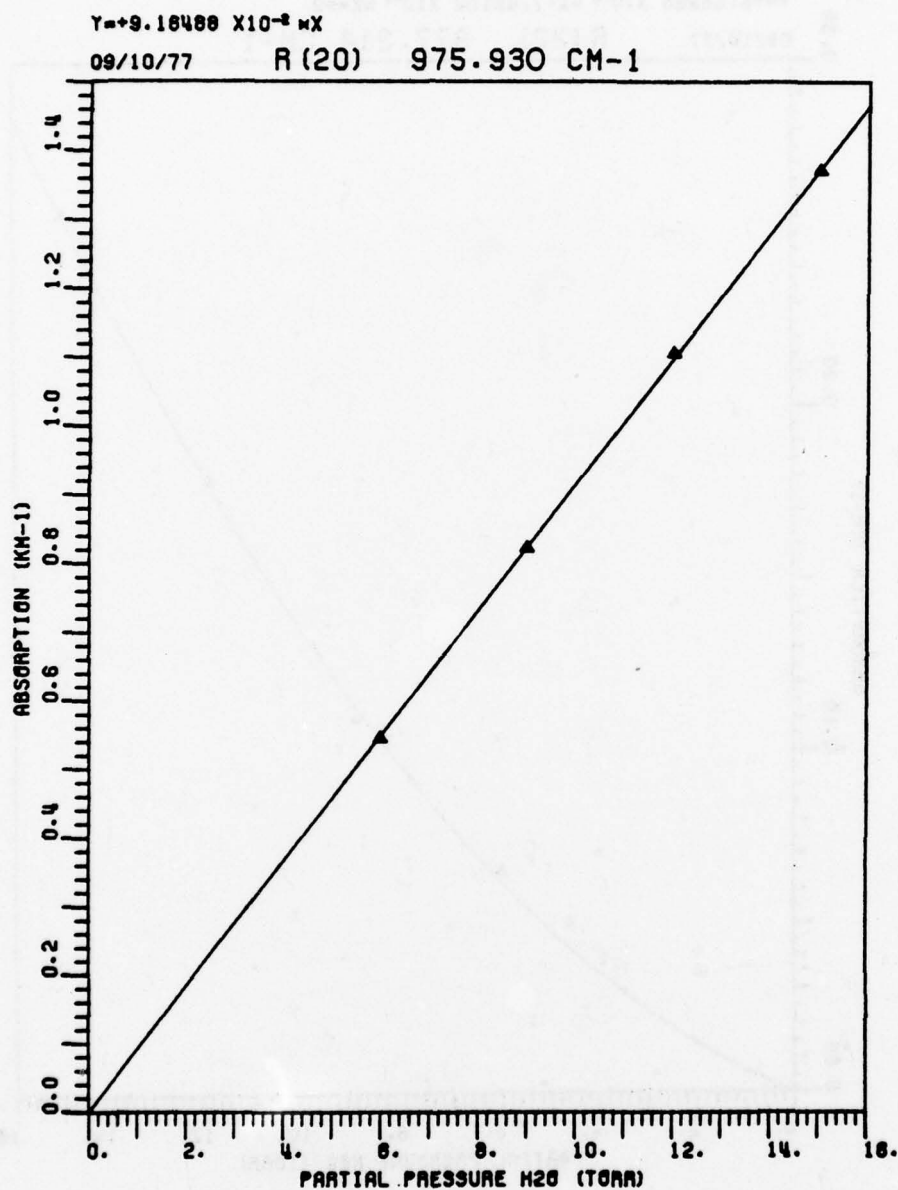


Figure 13. Measured water vapor-nitrogen absorption coefficient at R(20) CO<sub>2</sub> laser line, 975.930 cm<sup>-1</sup> for 760 Torr total pressure and T=22.5±.5°C.

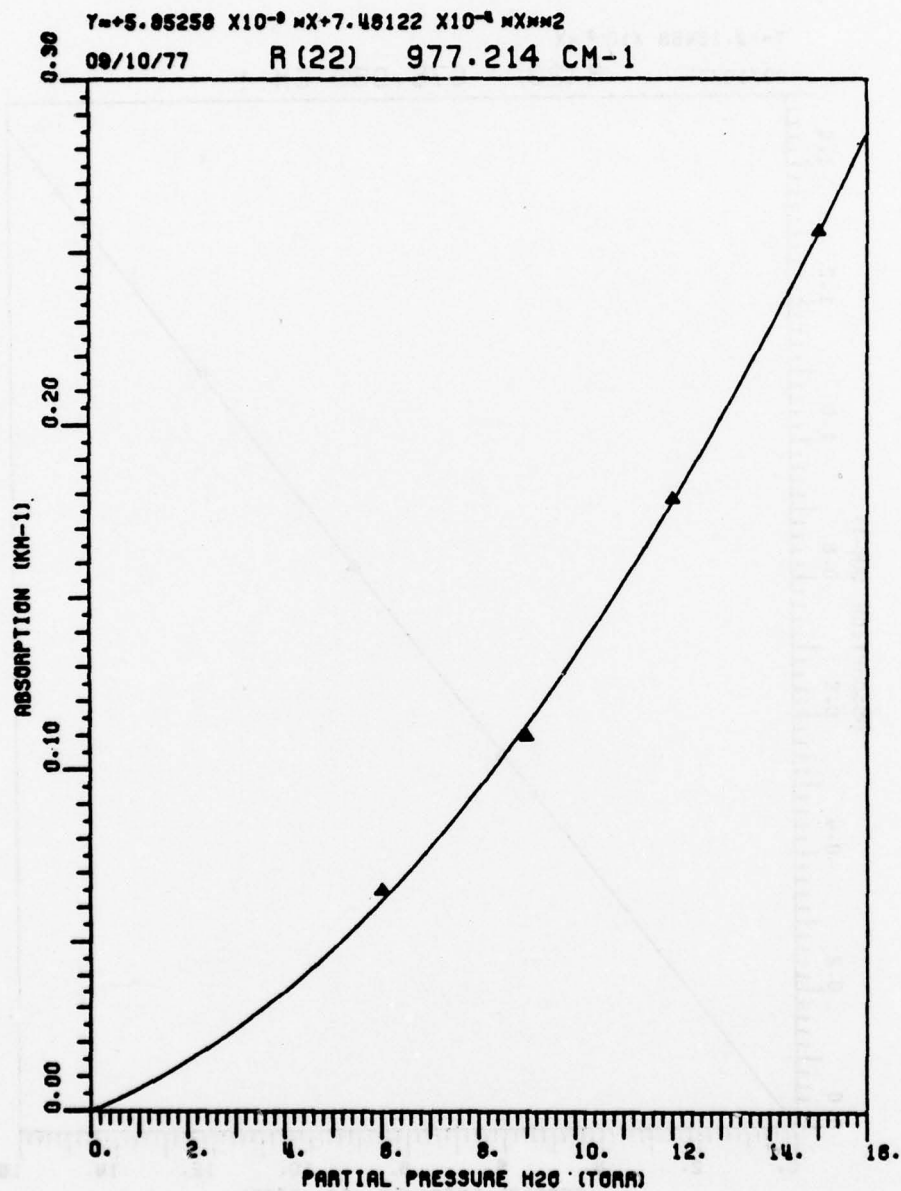


Figure 14. Measured water vapor-nitrogen absorption coefficient  
 at R(22) CO<sub>2</sub> laser line, 977.214 cm<sup>-1</sup> for 760 Torr  
 total pressure and T=22.5±.5°C.



H2O IN N2 - 3/9/77

$Y = 1.24155 \times 10^{-3} \cdot X + 7.80302 \times 10^{-5} \cdot X^2$

03/30/77 R (28) 380.913 CM-1

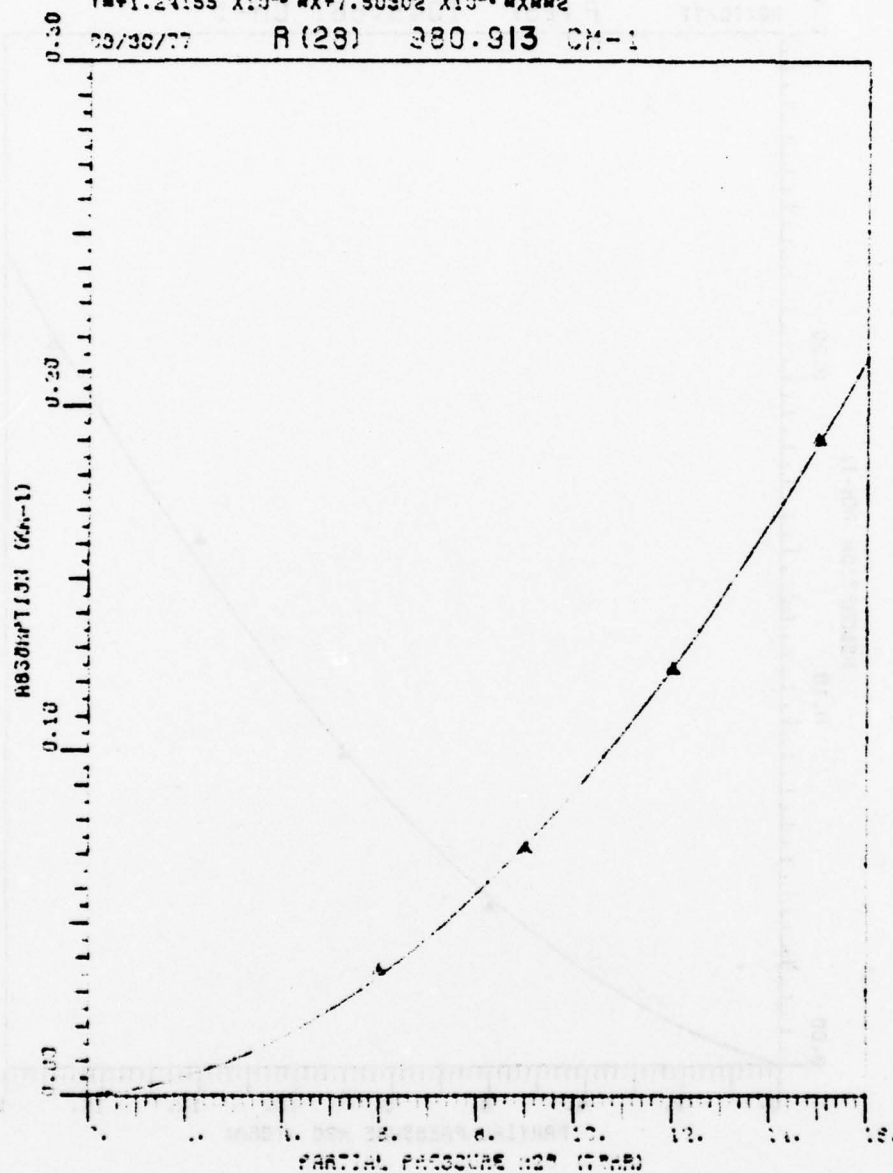


Figure 15. Measured water vapor-nitrogen absorption coefficient at R(28) CO<sub>2</sub> laser line, 988.913 cm<sup>-1</sup> for 760 Torr total pressure and T=22.5±.5°C.

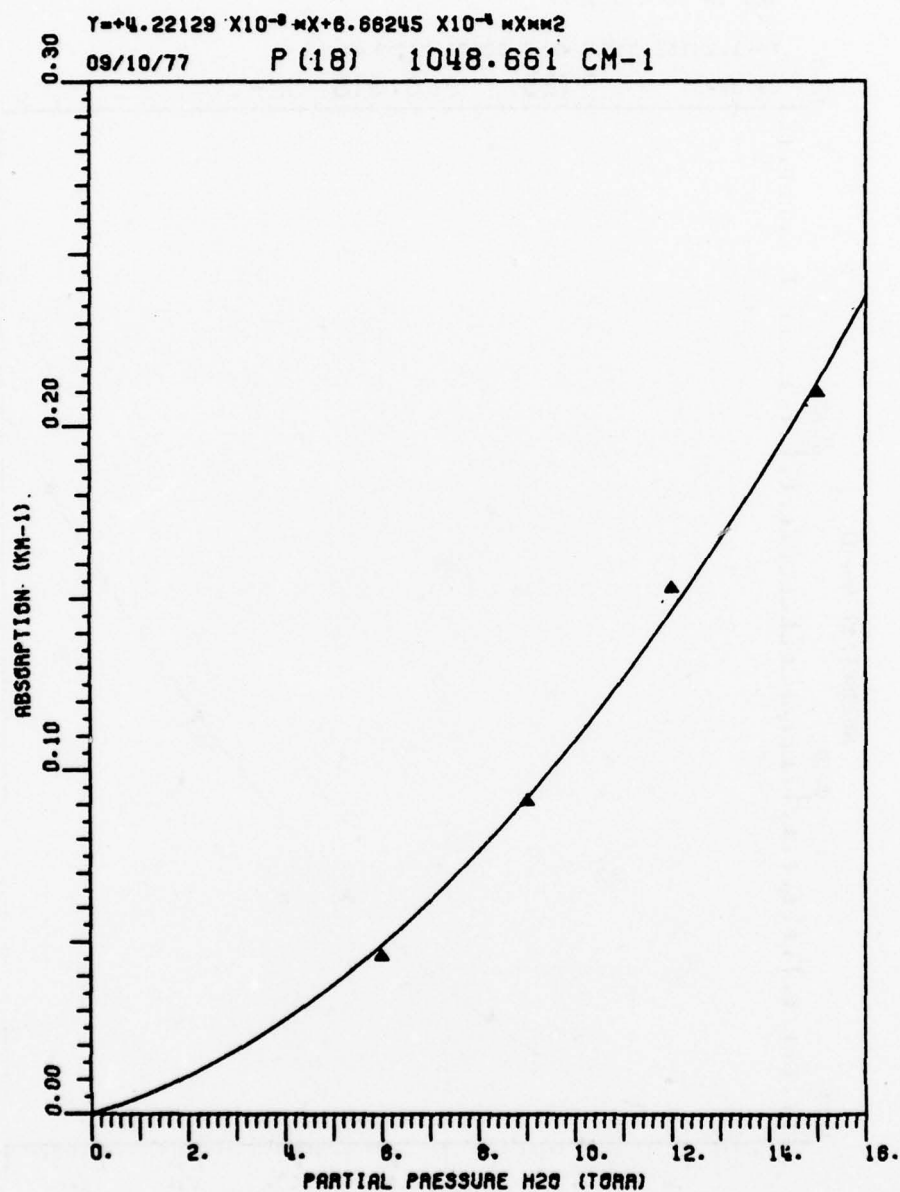


Figure 16. Measured water vapor-nitrogen absorption coefficient  
 at P(18) CO<sub>2</sub> laser line, 1048.661 cm<sup>-1</sup> for 760 Torr  
 total pressure and T=22.5±.5°C.

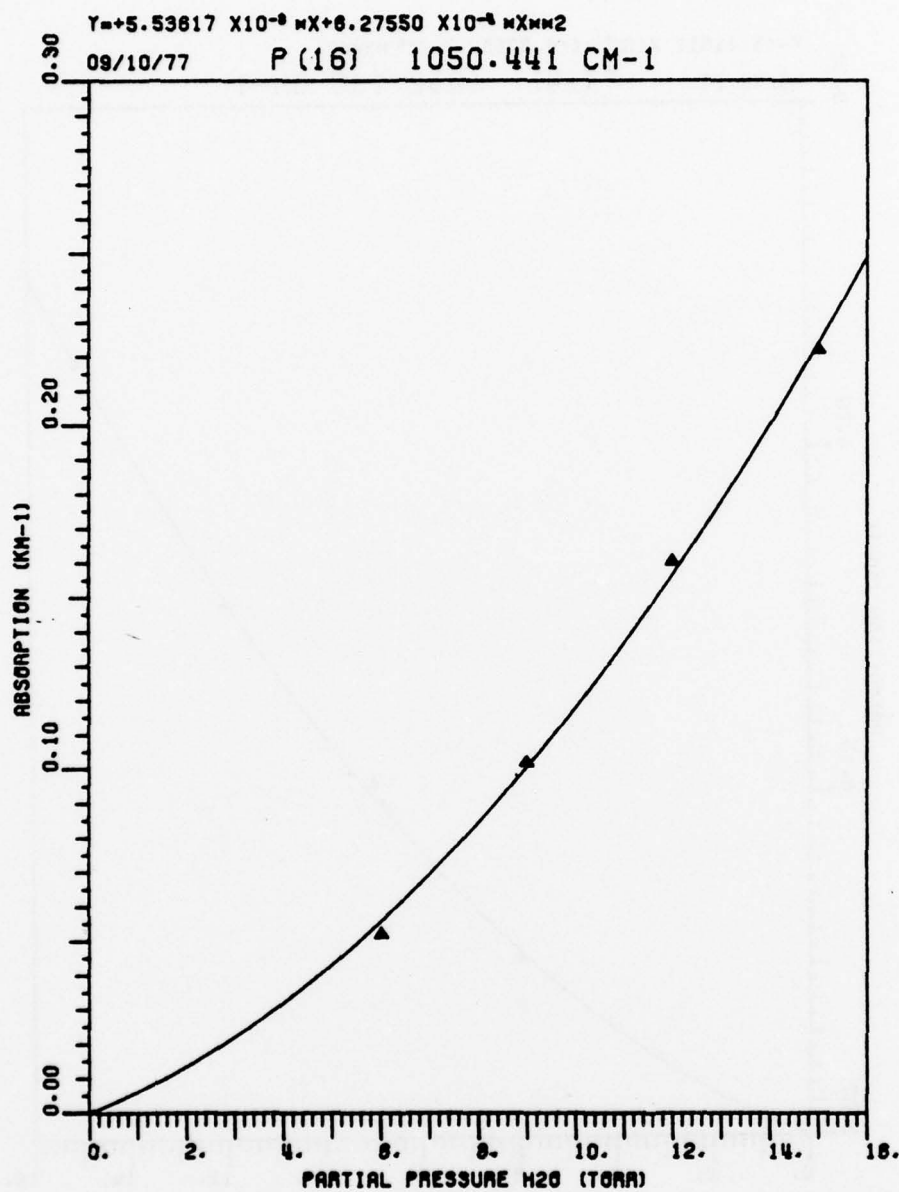


Figure 17. Measured water vapor-nitrogen absorption coefficient  
 at P(16) CO<sub>2</sub> laser line, 1050.441 cm<sup>-1</sup> for 760 Torr  
 total pressure and T=22.5±.5°C.

H2O IN N2 - 9/7/77

$$Y = +5.11611 \times 10^{-3} X + 6.60858 \times 10^{-4} X^2$$

09/30/77 P (14) 1052.196 CM-1

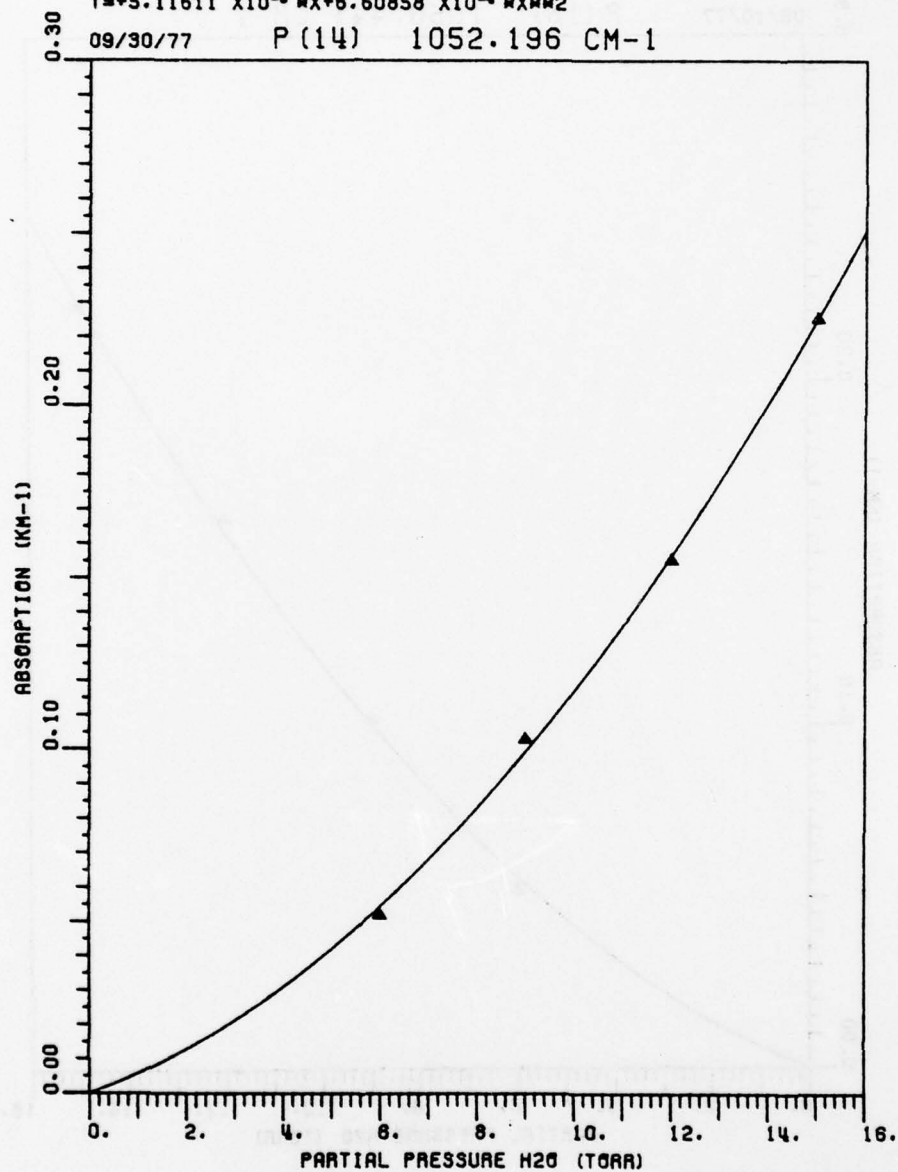


Figure 18. Measured water vapor-nitrogen absorption coefficient at P(14) CO<sub>2</sub> laser line, 1052.196 cm<sup>-1</sup> for 760 Torr total pressure and T=22.5±.5°C.



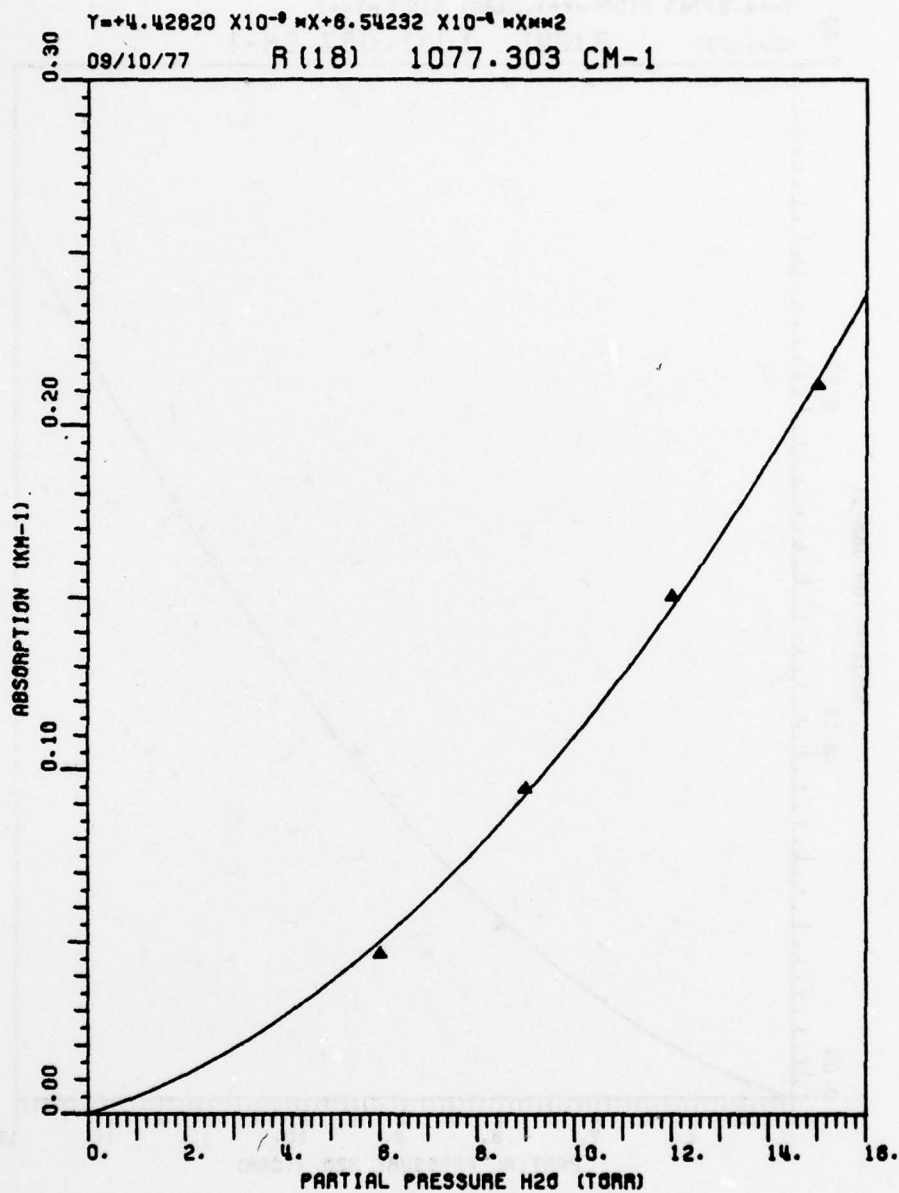


Figure 19. Measured water vapor-nitrogen absorption coefficient  
 at R(18) CO<sub>2</sub> laser line, 1077.303 cm<sup>-1</sup> for 760 Torr  
 total pressure and T=22.5±.5°C.

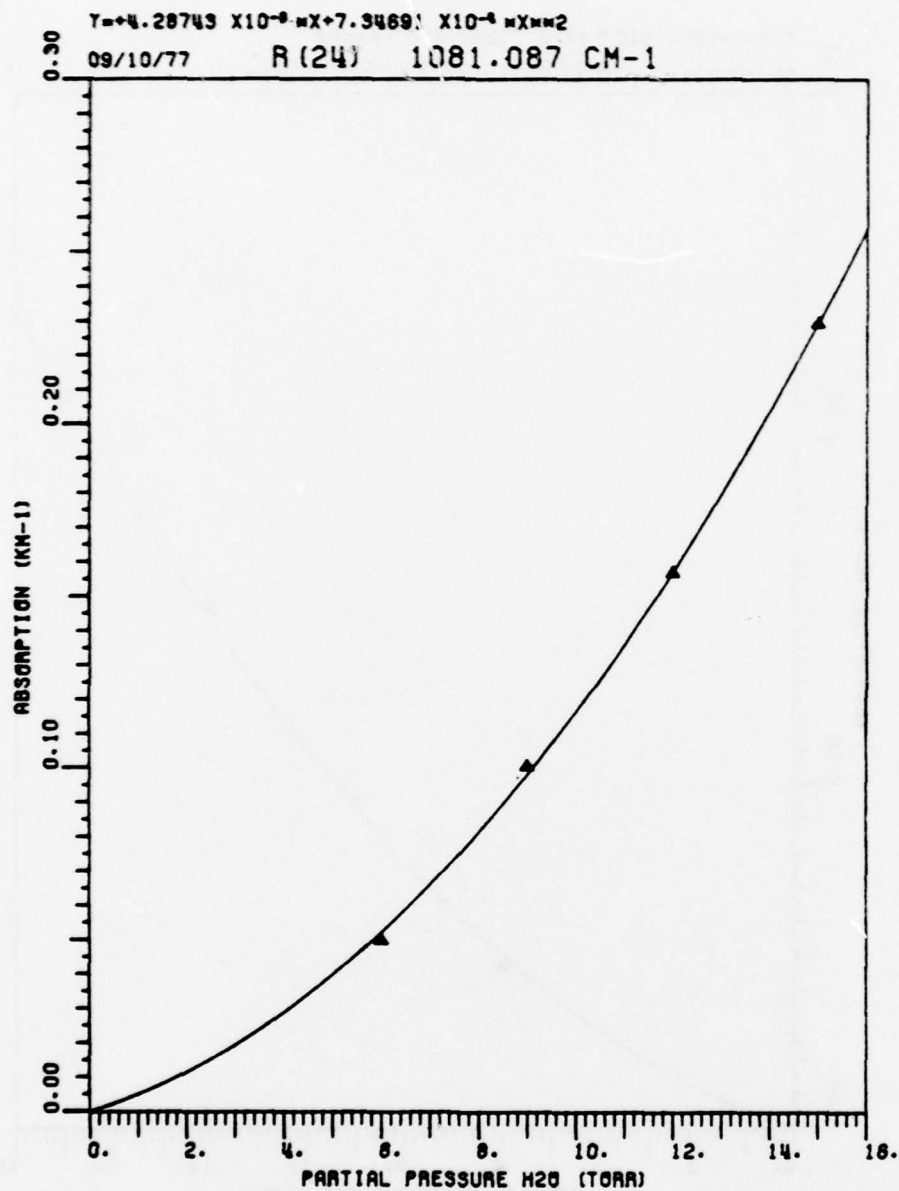


Figure 20. Measured water vapor-nitrogen absorption coefficient  
 at R(24) CO<sub>2</sub> laser line, 1081.087 cm<sup>-1</sup> for 760 Torr  
 total pressure and T=22.5±.5°C.

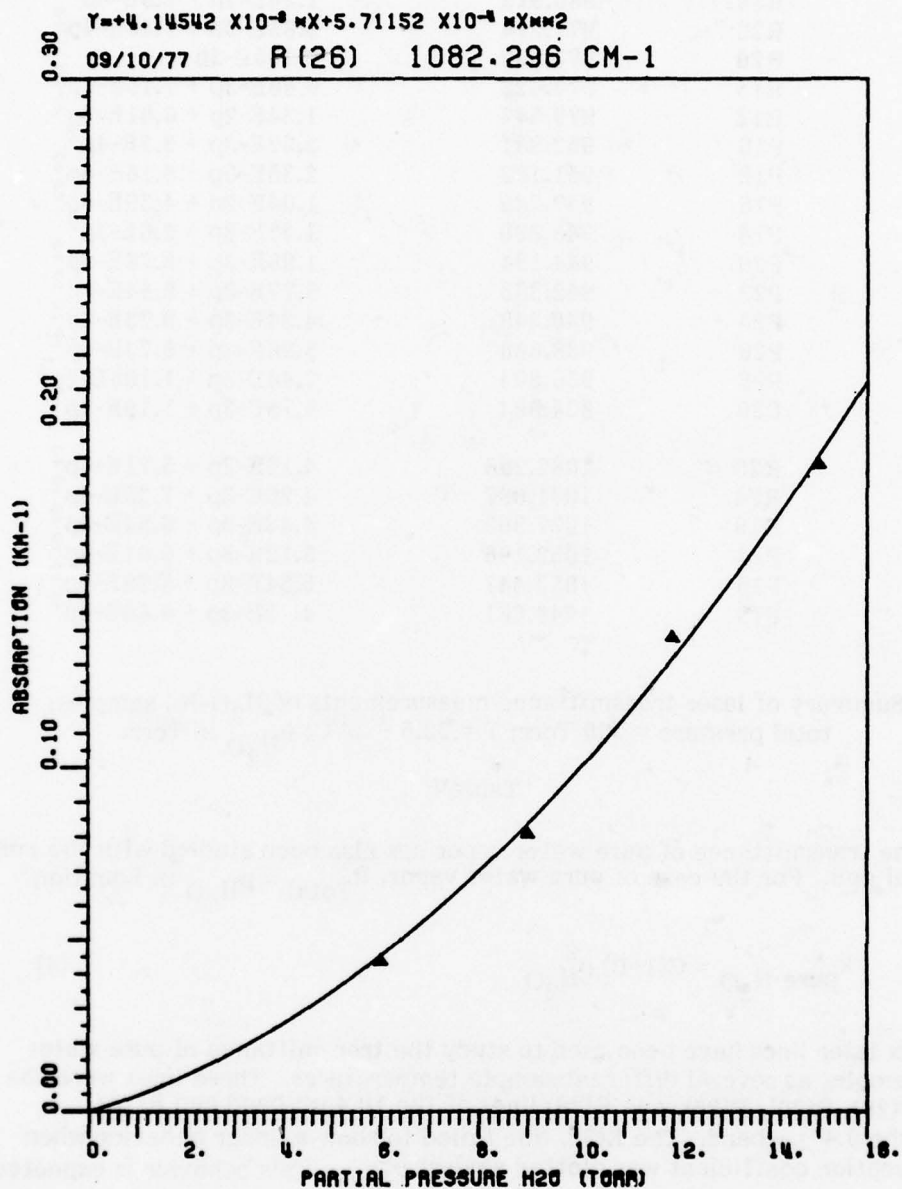


Figure 21. Measured water vapor-nitrogen absorption coefficient  
 at R(26) CO<sub>2</sub> laser line, 1082.296 cm<sup>-1</sup> for 760 Torr  
 total pressure and T=22.5±.5°C.

Band	Iden.	Wavenumber	Extinction Coefficient (km <sup>-1</sup> )
100-001	R28	980.913	1.24E-3p + 7.6E-4p <sup>2</sup>
	R22	977.214	5.85E-3p + 7.46E-4p <sup>2</sup>
	R20	975.930	9.165E-2p
	R18	974.622	6.86E-3p + 7.19E-4p <sup>2</sup>
	R12	970.547	1.34E-2p + 6.01E-4p <sup>2</sup>
	P10	952.881	2.52E-3p + 8.3E-4p <sup>2</sup>
	P12	951.192	2.35E-3p + 8.16E-4p <sup>2</sup>
	P16	947.742	1.04E-2p + 4.39E-4p <sup>2</sup>
	P18	945.980	1.25E-3p + 9.0E-4p <sup>2</sup>
	P20	944.194	1.96E-3p + 8.76E-4p <sup>2</sup>
	P22	942.383	5.77E-3p + 8.64E-4p <sup>2</sup>
	P24	940.548	4.34E-3p + 9.73E-4p <sup>2</sup>
	P26	938.688	3.80E-3p + 9.73E-4p <sup>2</sup>
	P28	936.804	2.44E-3p + 1.105E-3p <sup>2</sup>
	P30	934.894	2.75E-3p + 1.19E-3p <sup>2</sup>
100-020	R26	1082.296	4.15E-3p + 5.71E-4p <sup>2</sup>
	R24	1081.087	4.29E-3p + 7.35E-4p <sup>2</sup>
	R18	1077.303	4.43E-3p + 6.54E-4p <sup>2</sup>
	P14	1052.196	5.12E-3p + 6.61E-4p <sup>2</sup>
	P16	1050.441	5.54E-3p + 6.28E-4p <sup>2</sup>
	P18	1048.661	4.22E-3p + 6.66E-4p <sup>2</sup>

Summary of laser transmittance measurements of H<sub>2</sub>O-N<sub>2</sub> samples;  
total pressure = 760 Torr; T = 22.5 ± .5°C; p<sub>H<sub>2</sub>O</sub> in Torr.

Table I

The transmittance of pure water vapor has also been studied with the multi-traversal cell. For the case of pure water vapor, P<sub>Total</sub> = p<sub>H<sub>2</sub>O</sub> in Equation (2), so

$$k_{\text{pure H}_2\text{O}} = C(1+B) p_{\text{H}_2\text{O}}^2 \quad (4)$$

Six laser lines have been used to study the transmittance of pure water vapor samples at several different sample temperatures. These lines were the P(20), P(28), R(20), R(22), and R(28) lines of the 10.4 μm band and R(18) line in the 9.4 μm band. The R(20) line failed to show a linear behavior when the absorption coefficient was plotted against p<sub>H<sub>2</sub>O</sub><sup>2</sup>. This behavior is expected, however, since the absorption at the R(20) laser line cannot be modeled with a far wings equation.



Figures 22-27 show plots of the absorption coefficient at these laser lines for pure water vapor samples at temperatures noted. At P(20), in the wings of water vapor absorption lines, the absorption decreases as the temperature is increased, but at R(20) the absorption increases. Both trends indicate a narrowing of the halfwidths of the water vapor absorption lines as the temperature increases.

Table II lists the curve fits for the pure water vapor data.

Figure 28 shows a comparison at P(20) of the results obtained at this laboratory with recently published results of Arefev and Dianov-Klovov<sup>4</sup>. The data presented in the reference were digitized on our computer and a least square fit of the form in Equation (4) was made. Table III shows the results of these curve fits at the four temperatures reported by Arefev and Dianov-Klovov. Also shown in Figure 28 and listed in Table III are results obtained at this laboratory.

The room temperature data recorded for this study are somewhat higher than the results reported in Reference 4. It is possible that this error could be caused by a small amount of condensation of water vapor on the mirrors of our absorption cell. Recently, we have tried heating the mirrors slightly, in order to drive off any condensate. However, the results of this procedure were inconclusive, i.e. had no significant effect on the measured absorption coefficient.

#### B. Spectrophone Measurements

This section of the report describes spectrophone measurements of pressure-broadened water vapor absorption at CO<sub>2</sub> laser frequencies. Both nitrogen and artificial air (80% N<sub>2</sub> - 20% O<sub>2</sub>) were used as the buffer gases in these experiments, which were conducted at a total pressure of 760 Torr and room temperature. Twenty-three laser lines in both the 9.4  $\mu$ m and 10.4  $\mu$ m bands were studied using nitrogen as the broadening gas and four lines in the 10.4  $\mu$ m band were studied using artificial air. Calibration of the spectrophone is based upon recent White cell measurements of water vapor at the R(20) laser line at 975.930 cm<sup>-1</sup>.

The instrument used in this study is a stainless steel non-resonant differential spectrophone with ZnSe Brewster windows. This instrument was designed with the goal of eliminating that portion of background noise caused by the absorption of laser radiation in the IR windows. The theory employed here was originally tested and developed on an aluminum spectrophone which served as the prototype for the current stainless steel instrument<sup>2</sup>. Several refinements have been made in the construction of the new instrument which make it more versatile and reliable.

The most significant improvement is the addition of temperature control capability. The stainless steel walls of the spectrophone were drilled with a spiral series of holes that conduct a water-alcohol mixture that is used as the heat exchange fluid. Insulation has been installed around the instrument to improve the temperature range of this system and to insure a uniform temperature distribution. ZnSe windows in this spectrophone permit the study of samples with high relative humidities; the previous aluminum instrument was limited by the

hydroscopic property of NaCl windows. The vacuum system for the spectrophone consists of stainless steel, high vacuum bellows seal valves and Cajon ultra-torr fittings. These valves are pneumatically operated and allow this experiment to be controlled remotely, with the experimental apparatus enclosed in a plexi-glass box. This isolates the spectrophone from laboratory air currents and eliminates the disturbances caused by an operator opening and closing hand operated valves. Figure 29 shows a picture of the stainless steel spectrophone prior to the installation of insulation.

The laser used in these experiments is a sealed off cw CO<sub>2</sub> laser, grating tunable for single line operation, and electronically stabilized to maintain operation at line center. Construction of this laser is based on a Sylvania Model 948 CO<sub>2</sub> laser plasma tube that was mounted together with cavity optics and high voltage power supply on a 7.62 cm thick limestone slab. We have added an original grating ruled with 150  $\lambda$ /mm that permits tuning over both the 10.4  $\mu$ m (00<sup>0</sup>1-10<sup>0</sup>0) and 9.4  $\mu$ m (00<sup>0</sup>1-02<sup>0</sup>0) bands. Output powers ranging from 1/4 to 4 watts were observed on the lines employed in this study. Electronic stabilization is based on the technique which we have applied in several other lasers<sup>5</sup>. A complete description of this laser appeared in an earlier report<sup>3</sup>. Figure 30 shows a picture of the laser enclosed in a plexiglass box.

Calibration of the CO<sub>2</sub> laser lines was made with an Optical Eng. CO<sub>2</sub> spectrum analyzer. This instrument is a grating spectroscope that displays the laser radiation on a thermally sensitive screen that is calibrated for both rotational line number and wavelength.

Laser power was measured with a Scientech model 36-0001 disc calorimeter, having an aperture of 2.54 cm and a nominal output of 100 mv/watt. This detector has a relatively long time constant, 14 sec, which effectively averages out any short term variations in laser power. The detector is enclosed in a plexiglass box to minimize the fluctuations and drifts caused by laboratory air currents present during the course of a measurement.

Data were collected with a computer controlled data acquisition system consisting of an SDS Model 920 computer with 8 K memory, a typewriter, a high speed 24 channel analog to digital converter, and DC amplifiers<sup>6</sup>. This is the same system used for the absorption cell measurements. Each measurement was performed by sampling two channels of the A/D converter 400 times each, and calculating the average and standard deviation for each channel. The ratio of the two channel readings was also calculated. The two channels, called Signal (pressure signal) and Reference (laser power), were sampled 10 nsec apart and there was a delay of 100 msec between pairs of readings. Figure 31 shows a block diagram of this data acquisition system.

The pressure sensor used with the differential spectrophone is a C.G.S. Datametrics Model 523-15 differential electronic manometer, trade name Barocel. This pressure sensor has a full scale range of  $\pm 1$  Torr while the associated electronics unit offers a selection of higher sensitivities down to  $10^{-4}$  Torr full scale; the 0-0.03 Torr range was employed in this study.

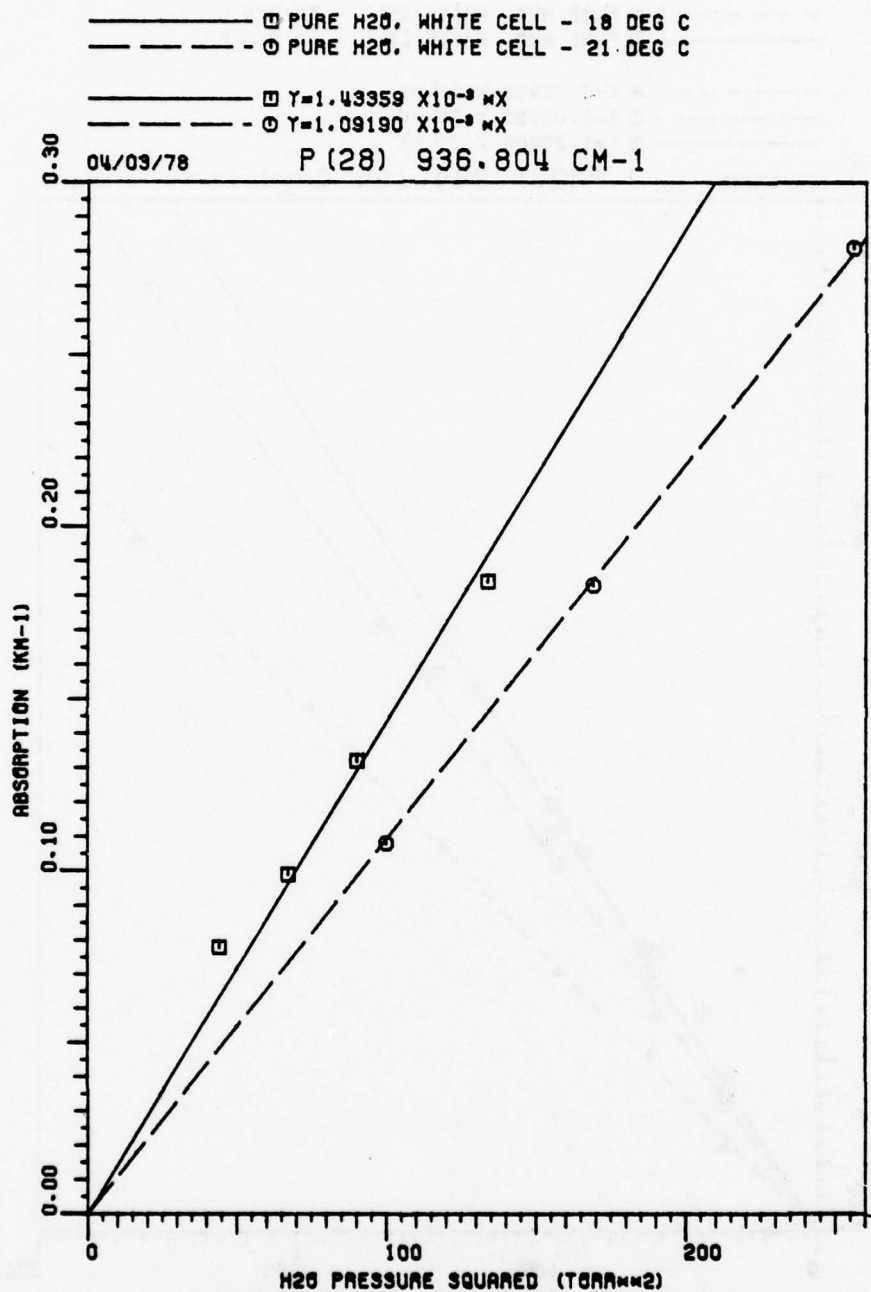


Figure 22. Measured pure water vapor absorption coefficient for the P(28) CO<sub>2</sub> laser line at 936.804 cm<sup>-1</sup> for sample temperatures of 18°C indicated by the symbol □ and 21°C indicated by the symbol ○.

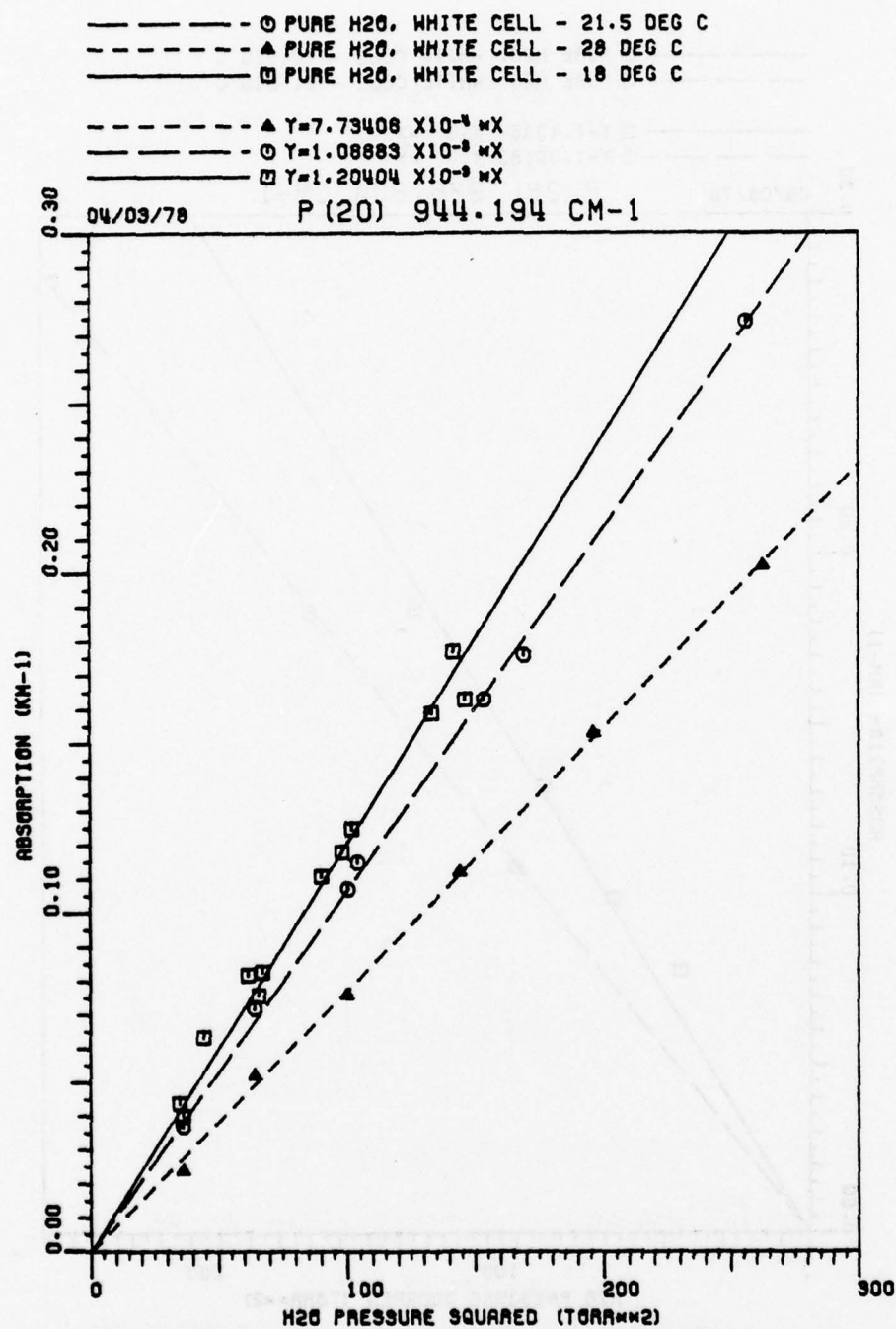


Figure 23. Measured pure water vapor absorption coefficient for the P(20) CO<sub>2</sub> laser line at 944.194 cm<sup>-1</sup> for sample temperatures of 18°C indicated by the symbol □, 21.5°C indicated by the symbol ○ and 28°C indicated by the symbol ▲.



-----  $\Delta$  PURE H<sub>2</sub>O, WHITE CELL - 28 DEG C  
 -----  $\square$  PURE H<sub>2</sub>O, WHITE CELL - 18 DEG C  
 -----  $\circ$  PURE H<sub>2</sub>O, WHITE CELL - 21.5 DEG C

-----  $\Delta$   $Y=1.95854 \times 10^{-2} \text{ mX} + 1.58810 \times 10^{-2} \text{ mXmm}^2$   
 -----  $\square$   $Y=1.92824 \times 10^{-2} \text{ mX} + 1.27317 \times 10^{-2} \text{ mXmm}^2$   
 -----  $\circ$   $Y=3.05309 \times 10^{-2} \text{ mX} + 1.10254 \times 10^{-2} \text{ mXmm}^2$

04/03/78

R (20) 975.930 CM-1

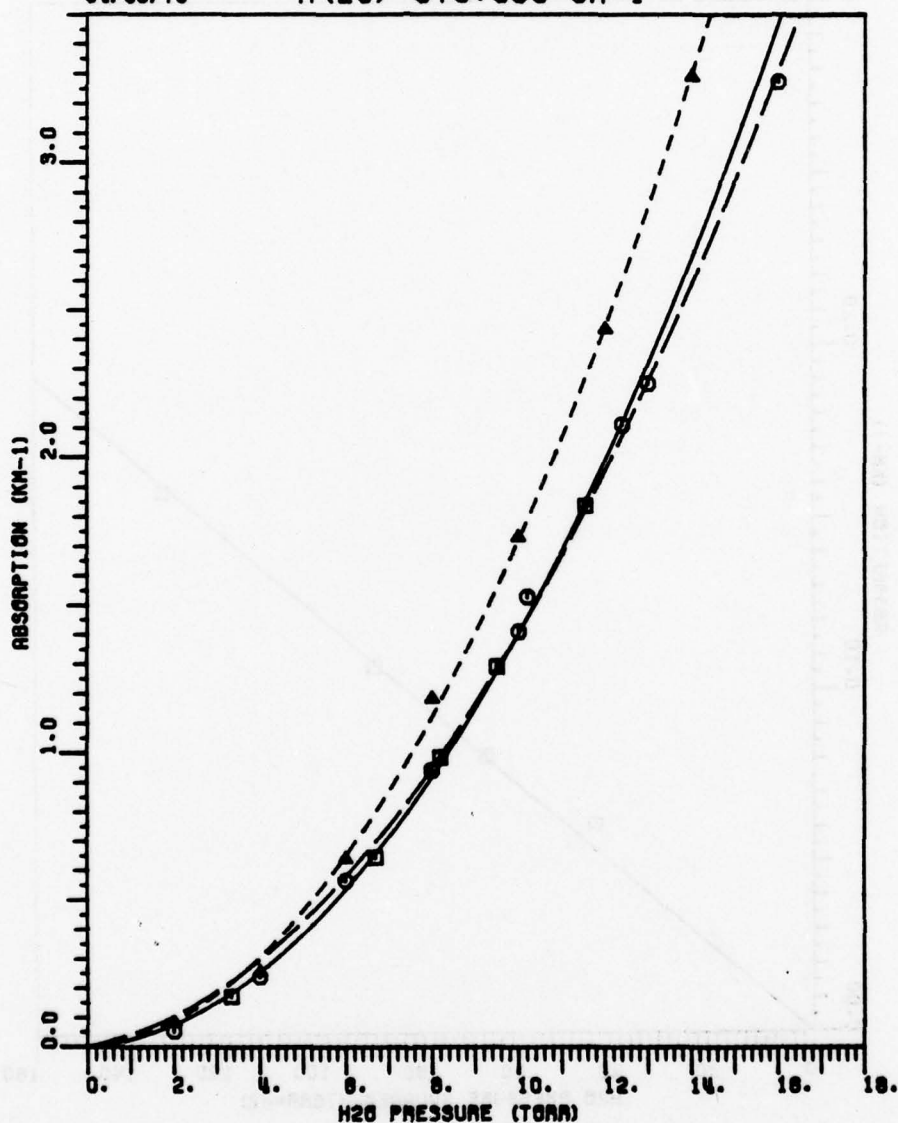


Figure 24. Measured pure water vapor absorption coefficient  
 for the R(20) CO<sub>2</sub> laser line at 975.930 cm<sup>-1</sup> for  
 sample temperatures of 18°C indicated by  
 the symbol  $\square$ , 21.5°C indicated by  
 the symbol  $\circ$  and 28°C indicated  
 by the symbol  $\Delta$ .

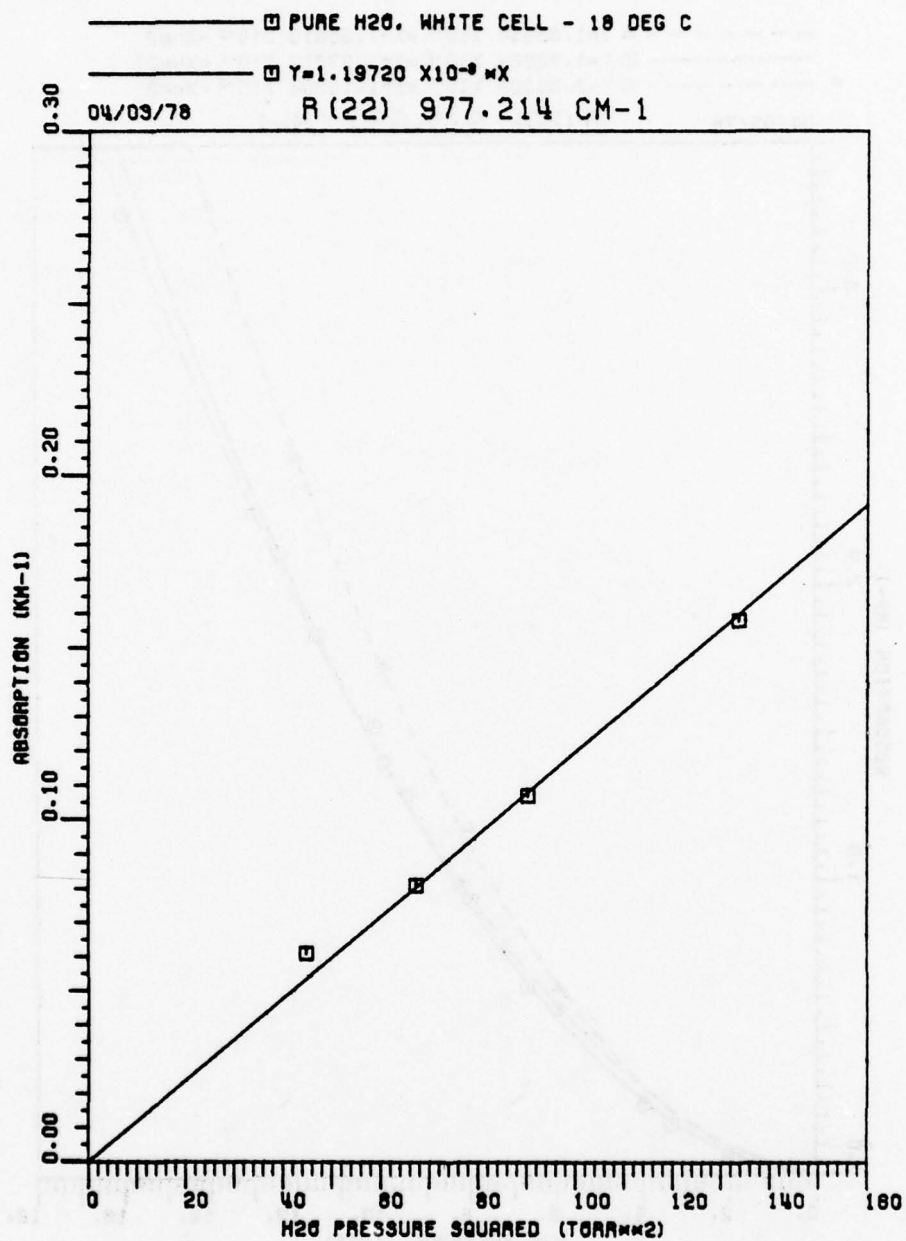


Figure 25. Measured pure water vapor absorption coefficient for the R(22) CO<sub>2</sub> laser line at 977.214 cm<sup>-1</sup> for a sample temperature of 18°C.

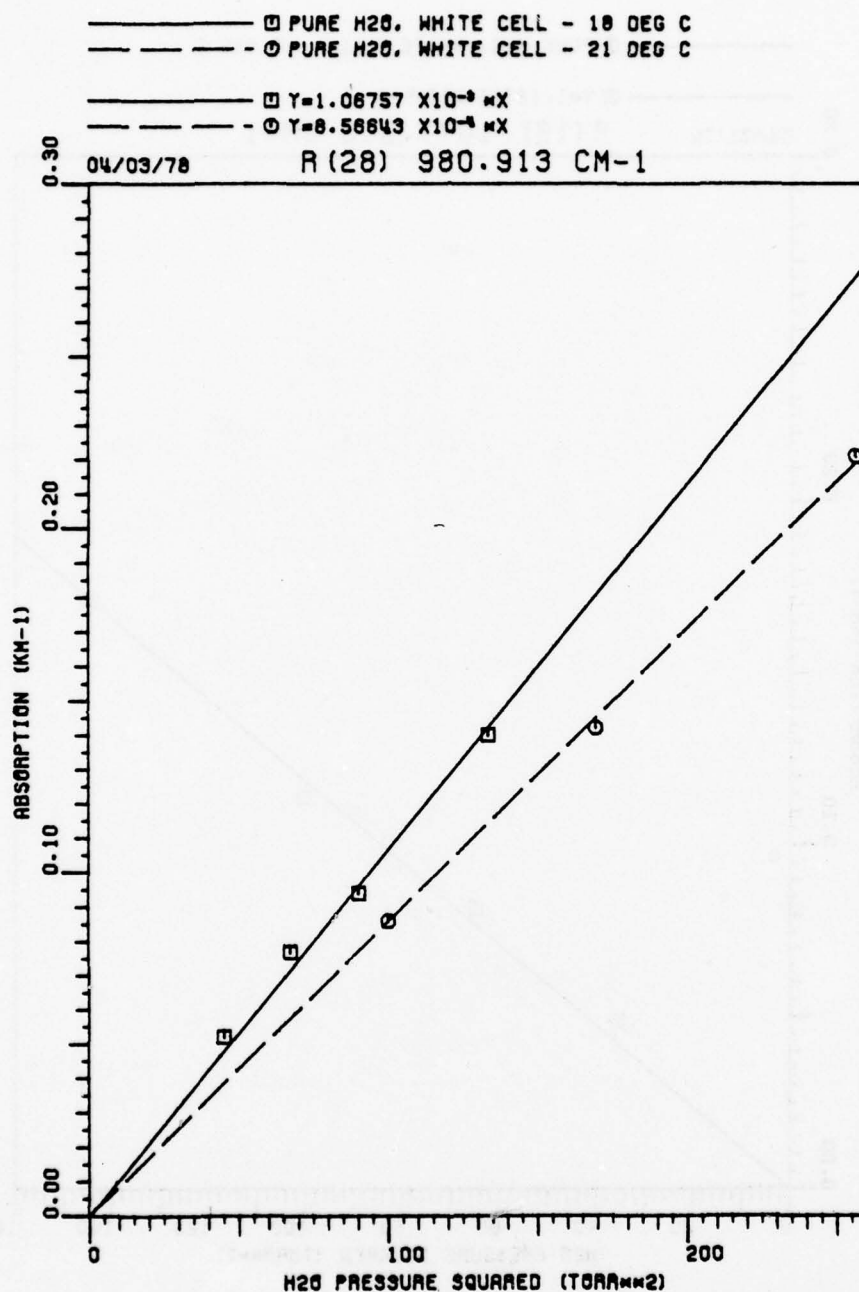


Figure 26. Measured pure water vapor absorption coefficient for the R(28) CO<sub>2</sub> laser line at 980.913 cm<sup>-1</sup> for sample temperatures of 18°C indicated by the symbol □ and 21°C indicated by the symbol ○.

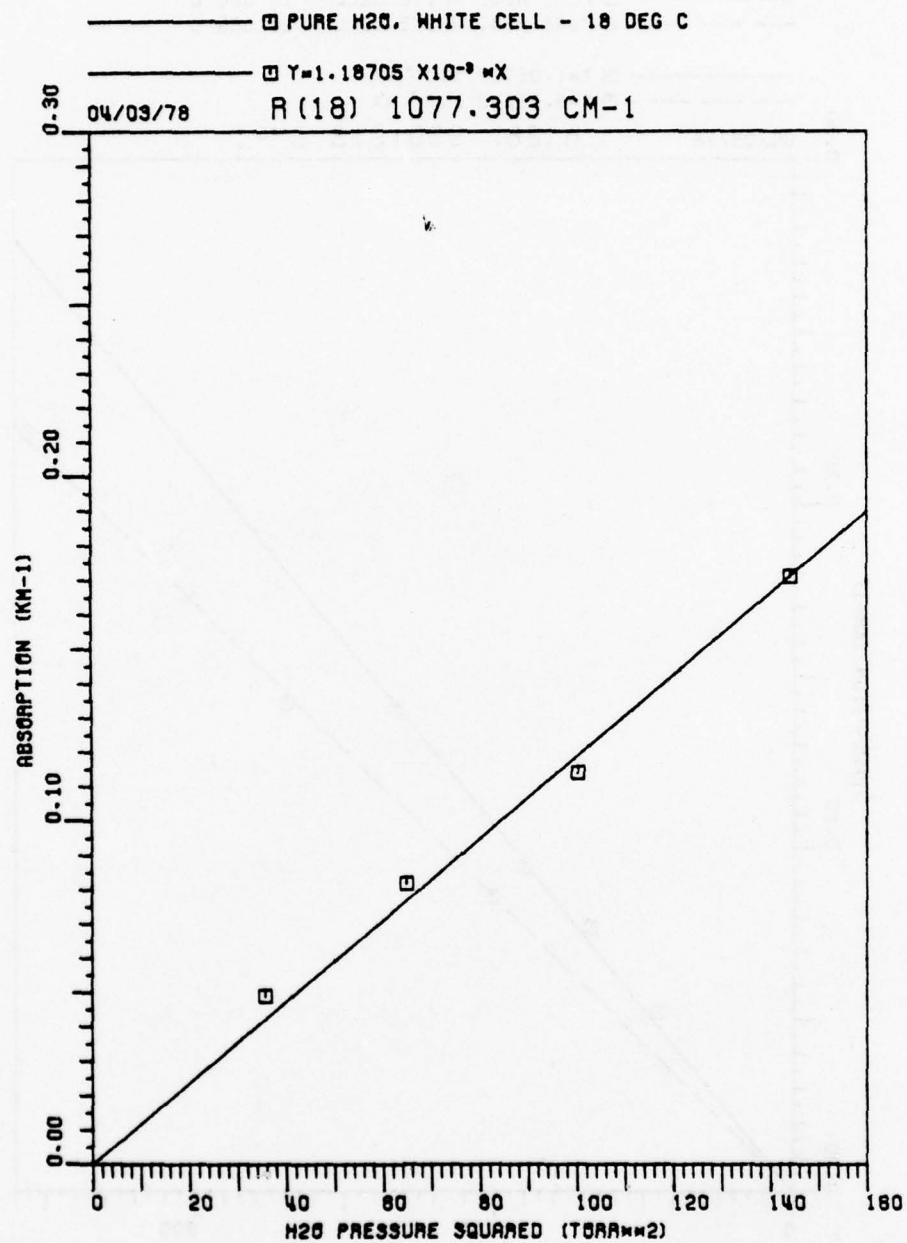


Figure 27. Measured pure water vapor absorption coefficient  
 for the R(18) CO<sub>2</sub> laser line at 1077.303 cm<sup>-1</sup> for  
 a sample temperature of 18°C.



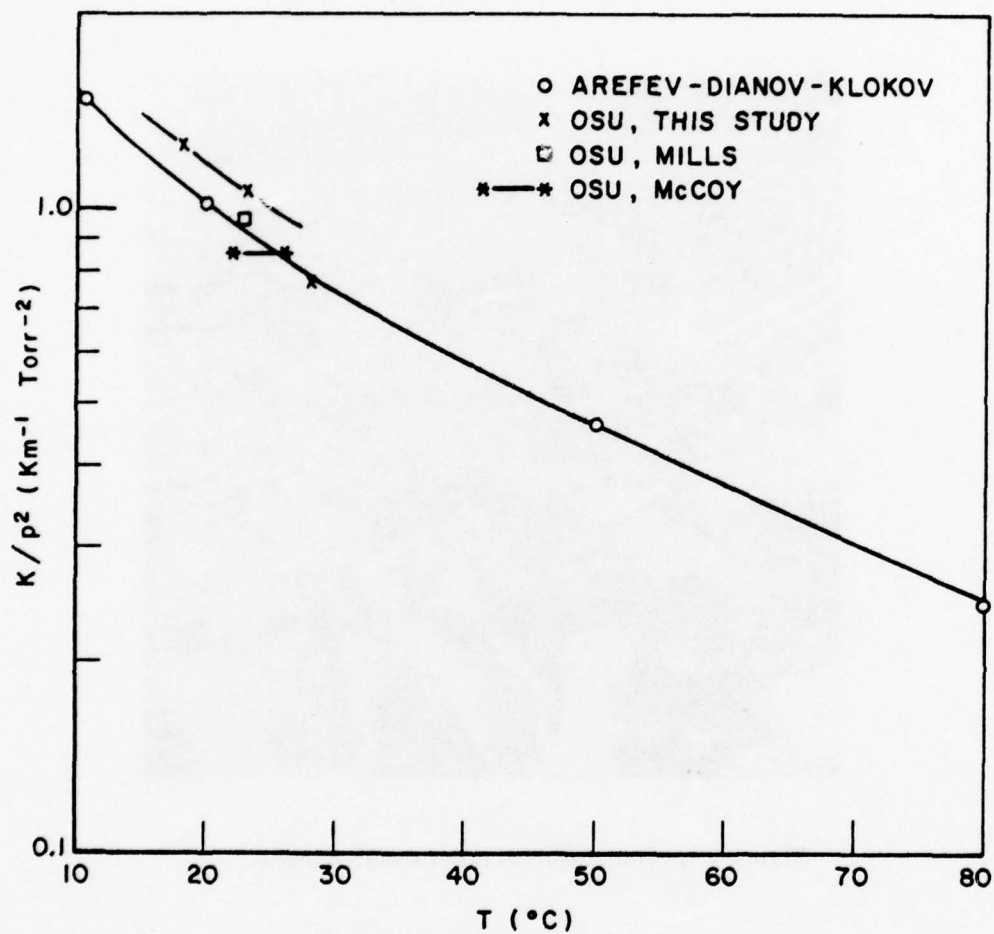


Figure 28. Comparison for P(20)  $944.194 \text{ cm}^{-1}$  of pure water vapor absorption measurements.

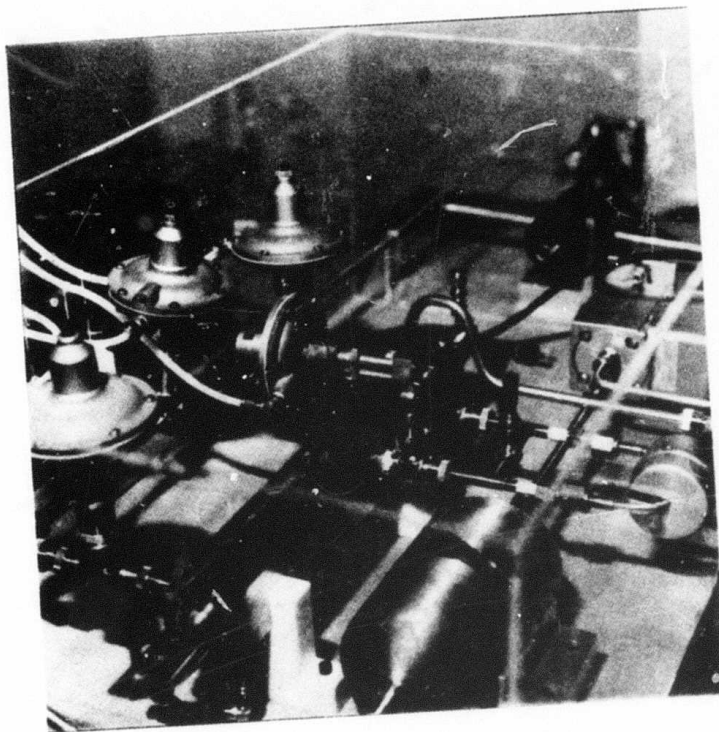
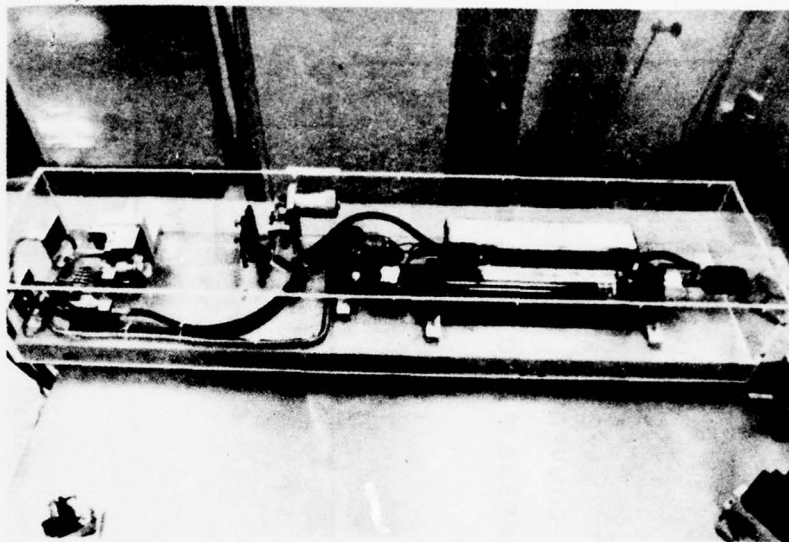
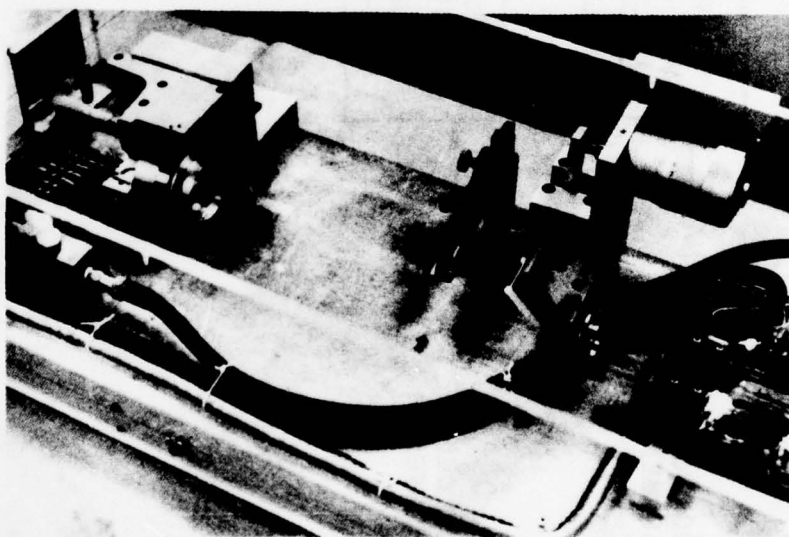


Figure 29. The stainless steel spectrophone.



(a)



(b)

Figure 30. Modified CO<sub>2</sub> laser.

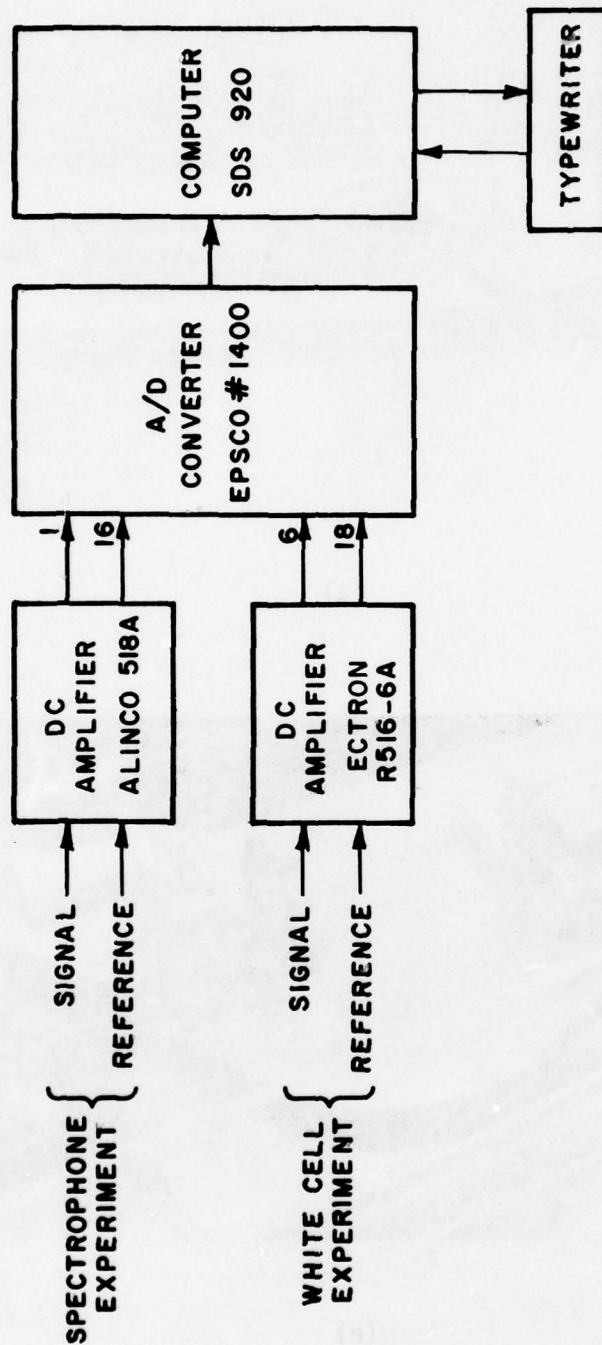


Figure 31. Block diagram of data acquisition system.



Pure H<sub>2</sub>O  
White Cell

o	ID	18°C		22°C		28°C		Figs.
		A	B	A	B	A	B	
936.804	P(28)	1.43E-3		1.09E-3				22
944.194	P(20)	1.20E-3		1.07E-3		7.73E-4		23
975.930	R(20)	1.33E-2	1.27E-2	3.05E-2	1.10E-2	1.36E-2	1.59E-2	24
977.214	R(22)	1.20E-3						25
980.913	R(28)	1.07E-3		8.57E-4				26
1077.303	R(18)	1.19E-3						27

Least square coefficients for pure H<sub>2</sub>O measurements

Table II

T (°K)	k (km <sup>-1</sup> )	Sources & Comments
295	$k=1.067 \times 10^{-3} p_a^2$	OSU, this study, may have systematic error (see text)
301	$k=0.773 \times 10^{-3} p_a^2$	OSU, this study
296 (estimated)	$k=.838 \times 10^{-3} p_a^2$	OSU, Mills, RADC-TR-75-288
295-299	$k=.967 \times 10^{-4} p_a^2$	OSU, McCoy, Appl Optics 8, 1471, (1969), temperature uncertain
284	$k=1.462 \times 10^{-3} p_a$	USSR, Arefev & Dianov-Klovov,
293	$k=1.048 \times 10^{-3} p_a^2$	Optics & Spectroscopy 42, 5, p 488 (translation).
323	$k=0.466 \times 10^{-3} p_a^2$	
353	$k=0.242 \times 10^{-3} p_a^2$	

Pure water vapor absorption coefficients for the P(20) laser line (944.194 cm<sup>-1</sup>).  $p_a$  is in Torr.

Table III

The pressure signal is processed by a lock-in amplifier, Princeton Applied Research Corporation, PAR Model 128A, which synchronously detects and integrates the pressure signal. The reference signal for the lock-in amplifier is obtained from an infrared diode-photo transistor pair that is mounted on a mechanical chopper. This chopper provides 100% modulation of the laser beam at a frequency of 8 Hz. The time constant of the lock-in amplifier was set at 10 sec to match the response of the power meter used in measuring laser power. The output signal from the lock-in amplifier, which has a range of  $\pm 1$  volt, is connected to a signal channel D.C. amplifier (set at X10 gain) of the data system.

An electronic thermometer,, Stow Lab Model 911 PL, was employed to monitor the temperature of the sample gas; the sensor for this instrument is mounted on the spectrophone in a small hole located near the center of the long chamber. The partial pressure of water vapor in the spectrophone was measured with an EG & G industrial dew point hygrometer, model 992. This instrument has an accuracy of  $\pm 0.5^\circ\text{F}$  for dew points in the range from  $-60^\circ\text{F}$  to  $120^\circ\text{F}$ . Figure 32 shows a block diagram of the instrumentation associated with the spectrophone experiment.

The gas handling manifold used in these experiments is constructed of stainless steel tubing and bellows seal valves that were thoroughly cleaned and out-gassed. Water vapor samples were introduced from a glass test tube containing triple distilled water, that is supplied in a glass container. The total pressure of the sample gas was measured with a Wallace and Tiernan model 62B-4D-0800 mechanical pressure gauge having a range of 0 to 800 Torr and an accuracy of 0.8 Torr.

Water vapor samples were mixed for at least 20 minutes. During this time, the dew point was continuously monitored by the EG & G hygrometer. Adequate mixing of the samples was observed to be extremely critical<sup>9</sup>; insufficient mixing apparently left relatively high concentrations of water vapor at the ends of the spectrophone, causing erroneous measurements. This problem was especially noticeable in samples with water vapor partial pressures greater than 10 Torr and precautions were taken to avoid this situation. Following the completion of absorption measurements, high relative humidity samples were recirculated for an additional ten minutes and a second set of measurements performed as a check on uniform mixing of the gas.

Calibration of the spectrophone with White cell measurements introduces a second and equally fundamental question. Accurate White cell measurements are most easily obtained for highly absorbing samples, i.e., with low transmittance; whereas the spectrophone is primarily intended for low level absorption studies. For this work calibration is based on  $\text{H}_2\text{O}$  absorption at the R(20) laser line ( $975.930\text{ cm}^{-1}$ ). This frequency is located within the halfwidth of a strong water line so that the absorption is quite strong, being on the order of  $1.0\text{ km}^{-1}$  at a  $\text{H}_2\text{O}$  partial pressure of 10. Torr. All of the other lines considered here are located in the wings of water vapor lines where the absorption is on the order of  $0.1\text{ km}^{-1}$  at 10 Torr so the following question must be answered - Is the calibration based on measurements at the R(20) line accurate for other lines where the absorption signal is an order of magnitude smaller; i.e., is the instrument response (pressure signal) linear with respect to absorption by the sample gas?

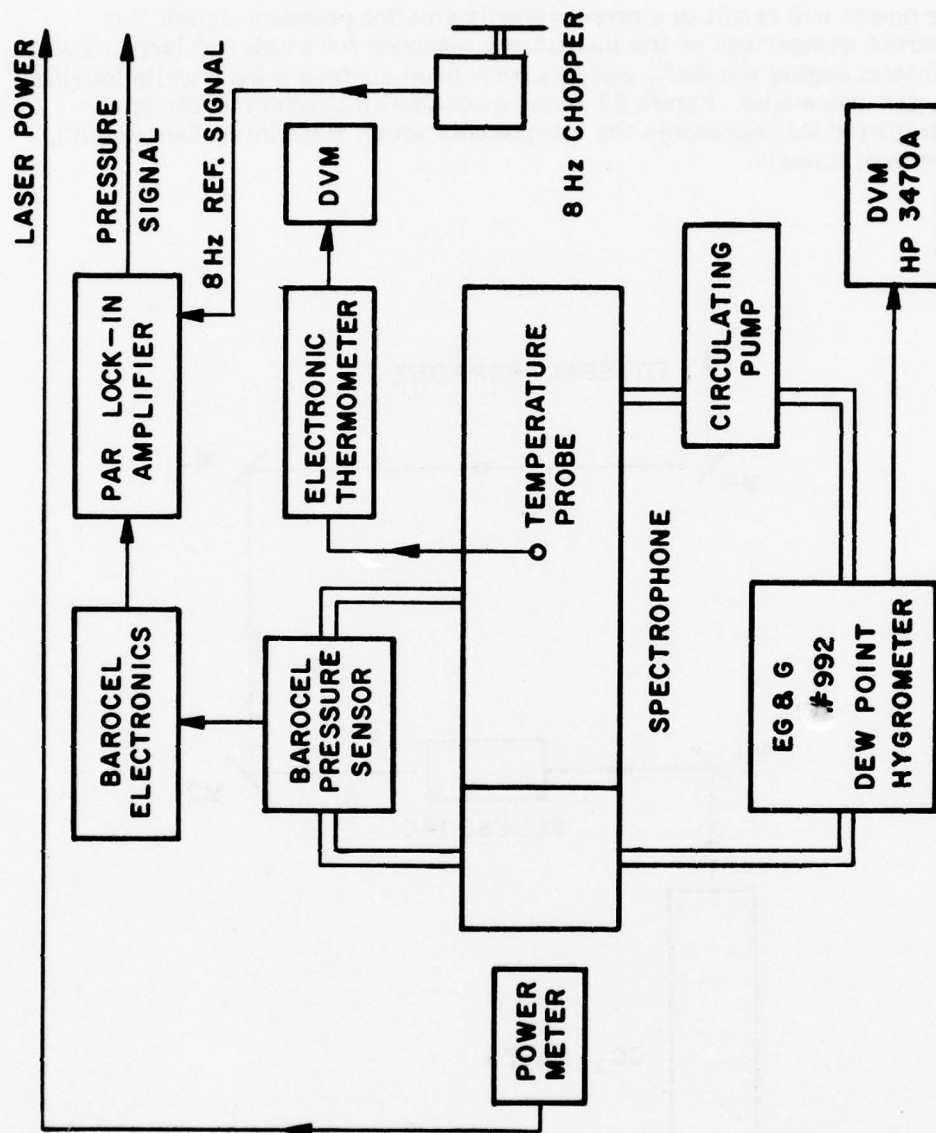


Figure 32. Block diagram of spectrophone instrumentation.

To determine whether the spectrophone response is linear an experiment was performed using a  $\text{BaF}_2$  wedge to replace a conventional mirror and thus reduce the laser power incident on the spectrophone. The idea is that reduced laser power will result in a proportionally smaller pressure signal; this permits a direct comparison of the instrument response for small and large signals by simply interchanging the  $\text{BaF}_2$  wedge with a front surface mirror while leaving the sample gas unchanged. Figure 33 shows a schematic diagram of the pertinent optics; mirror M3 represents the components which were interchanged using kinematic mirror mounts.

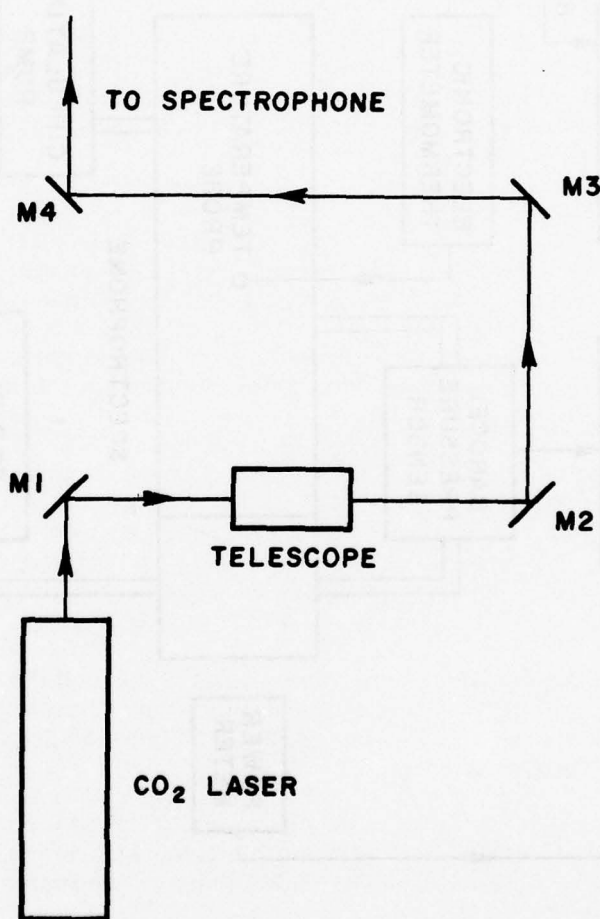


Figure 33. Schematic diagram of optics for spectrophone linearity experiment.



The experiment consisted of introducing an arbitrary amount of absorber,  $\text{CO}_2$ , in this case, into the spectrophone and measuring the response at both full and reduced laser power levels. The reduced power level was obtained as described above by replacing mirror M3 with a  $\text{BaF}_2$  wedge. Full power is defined as that observed with a conventional mirror located at M3. Figure 34 shows a plot of normalized spectrophone signal (pressure signal divided by laser power) at full laser power vs normalized spectrophone signal at reduced laser power with absorber concentration as a parameter. Linear response for this instrument implies that, independent of pressure signal magnitude, the normalized response of the spectrophone must be directly proportional to the absorption coefficient of the sample gas. In the above experiment a sample was introduced (with a fixed absorption coefficient) while the magnitude of the pressure signal was discretely altered by varying the laser power. For a linear system the normalized response under the two conditions of reduced and full laser power must be linearly related and as further defined above they must be equal. The plot in Figure 34 verifies that this is the situation. The two normalized responses are related by a linear equation with unit slope and zero intercept.

The results of spectrophone  $\text{H}_2\text{O}$  measurements at 14.3 torr are shown in Figure 35. Where possible a comparison with White cell measurement is shown. For most laser lines there is excellent agreement between the two experiments. A notable exception are the P(22) through P(28) lines in the  $10.4\ \mu\text{m}$  band. One possible explanation for the discrepancies observed at these lines is that a shorter path length was used for these laser frequencies than was employed in all the other White cell water vapor measurements. A shorter path length results in a relatively high transmittance and therefore more uncertainty in the absorption coefficient.

All of the results obtained with the spectrophone are shown in Figures 36-52, 54-62, 65-70, and 72-81. Table IV summarizes the results by presenting the least square curve fit coefficients for each measurement. This table also references the appropriate figure number and thus serves as a convenient index to the data figures. Table IV also gives the temperature at which each measurement was performed.

Also in these figures and in Table IV the White cell data described in the beginning of this section are given for comparison. These figures and the table together with the one-pressure comparison of Figure 35 give a comprehensive picture of the results obtained.

Once a satisfactory calibration has been obtained the spectrophone is a highly reliable and easy to use device. The close agreement between the spectrophone and White cell measurements is a tribute to the patience of the White cell experimenters.

The White cell and spectrophone measurements confirm a non-linear partial pressure dependence which has been characteristic of our results from the earliest measurements of McCoy. We have compared our results with those of Shumate et al.<sup>6</sup> and find generally poor agreement. A detailed discussion will be included in a forthcoming report but the inescapable conclusion is that in spite of the care which Shumate et al. took, the results are unreliable. One should note that

the coefficients of the least square fit are extremely sensitive to small changes in the data; i.e., while the agreement between data points for the two experiments is quite good, the coefficients of the curve fits can differ significantly.

There appears to be excellent agreement between the spectrophone and White cell measurements of  $H_2O$  in artificial air at the R(20),  $975.930\text{ cm}^{-1}$  laser line. However, the spectrophone results at other laser lines indicate a smaller dependence of the absorption coefficient on the concentration of oxygen in the buffer gas than that indicated by White cell measurements. This discrepancy has not yet been resolved.

		760 Torr Air & H <sub>2</sub> O					760 Torr N <sub>2</sub> & H <sub>2</sub> O					White Cell				
		Spectrophone			White Cell		Spectrophone			White Cell		Spectrophone			White Cell	
		A	B	T	Figs.		A	B	T	Figs.		A	B	T	Figs.	
$\nu_o$	ID															
934.894	P(30)						1.32E-3	1.04E-3	24.5	36		2.75E-3	1.19E-3	22.5	37,1	
936.804	P(28)	5.04E-3	6.18E-4	24.0	38		1.63E-3	9.24E-4	24.5	40		2.44E-3	1.10E-3	22.5	41,2	
938.688	P(26)						6.15E-4	9.79E-4	24.5	42		3.80E-3	9.73E-4	22.5	43,3	
940.548	P(24)						6.11E-4	1.01E-3	24.5	44		4.34E-3	9.73E-4	22.5	45,4	
942.383	P(22)						7.25E-4	9.93E-4	24.5	46		5.77E-3	8.64E-4	22.5	47,5	
944.194	P(20)	4.80E-3	6.47E-4	24.0	48		2.39E-3	8.56E-4	23.5	50		1.96E-3	8.76E-4	22.5	51,6	
945.980	P(18)						1.09E-3	9.21E-4	24.5	52		1.25E-3	9.00E-4	22.5	53,7	
947.742	P(16)						4.67E-4	9.09E-4	24.5	54		1.04E-2	4.39E-4	22.5	8	
951.192	P(12)						1.21E-3	9.11E-4	24.5	56		2.35E-3	8.16E-4	22.5	55,9	
957.981	P(10)						3.09E-4	8.67E-4	24.5	58		2.52E-3	8.30E-4	22.5	57,10	
969.140	R(10)						1.32E-2	6.41E-4	24.5	59		1.34E-2	6.01E-4	22.5	60,11	
970.547	R(12)						8.29E-3	1.16E-3	24.5	61						
971.930	R(14)						6.36E-3	7.90E-4	24.5	62						
973.288	R(16)															
974.822	R(18)															
975.930	R(20)	9.71E-2		24.0	63		9.16E-2		22.5	65		6.86E-3	7.19E-4	22.5	12	
977.214	R(22)						4.98E-3	7.80E-4	25.0	66		9.16E-2		22.5	13	
980.913	R(28)	4.42E-3	4.25E-4	24.0	68		1.84E-4	8.58E-4	25.0	70		5.85E-3	7.46E-4	22.5	67,14	
1048.661	P(18)											1.24E-3	7.60E-4	22.5	71,15	
1050.441	P(16)						9.38E-3	2.64E-4	23.5	72		4.22E-3	6.66E-4	22.5	16	
1052.196	P(14)						7.92E-3	3.48E-4	23.5	74		5.54E-3	6.28E-4	22.5	73,17	
1053.924	P(12)						7.25E-3	4.31E-4	23.5	76		5.12E-3	6.61E-4	22.5	75,18	
1073.278	R(12)						3.05E-3	8.52E-4	24.0	77						
1077.303	R(18)						1.51E-3	6.94E-4	24.0	78		4.43E-3	6.54E-4	22.5	79,19	
1079.852	R(22)						1.27E-3	6.92E-4	24.0	80		4.29E-3	7.35E-4	22.5	20	
1081.087	R(24)						4.98E-4	7.66E-4	24.0	81		4.15E-3	5.71E-4	22.5	21	
1082.296	R(26)															

Table IV

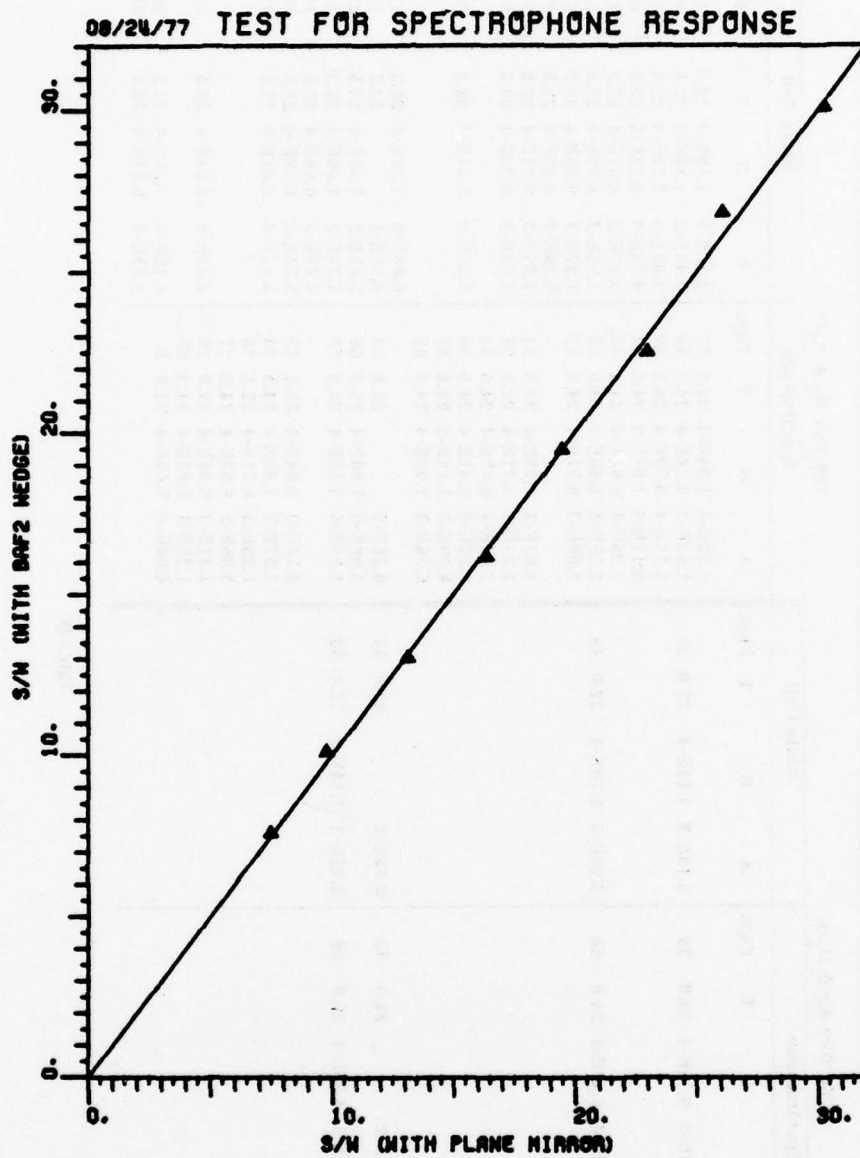


Figure 34. Plot of normalized response at reduced laser power vs normalized response at "full" power.



□ 14.3 Torr H<sub>2</sub>O in N<sub>2</sub> Spectrophone  
 ▲ 14.3 Torr H<sub>2</sub>O in N<sub>2</sub> White Cell

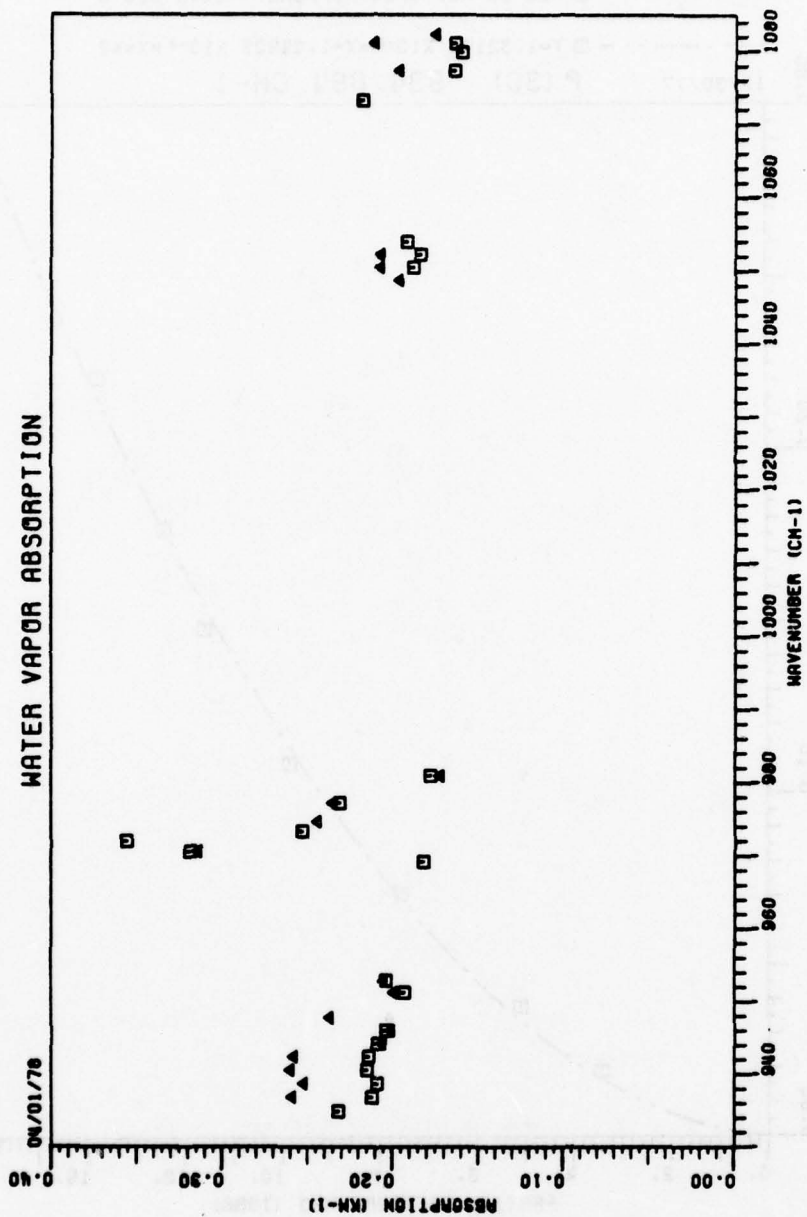


Figure 35. Comparison of White cell and spectrophone measurements at 14.3 Torr H<sub>2</sub>O.  
 760 Torr total pressure(N<sub>2</sub>) for 23<sup>±</sup>1°C for 22 CO<sub>2</sub> laser lines.



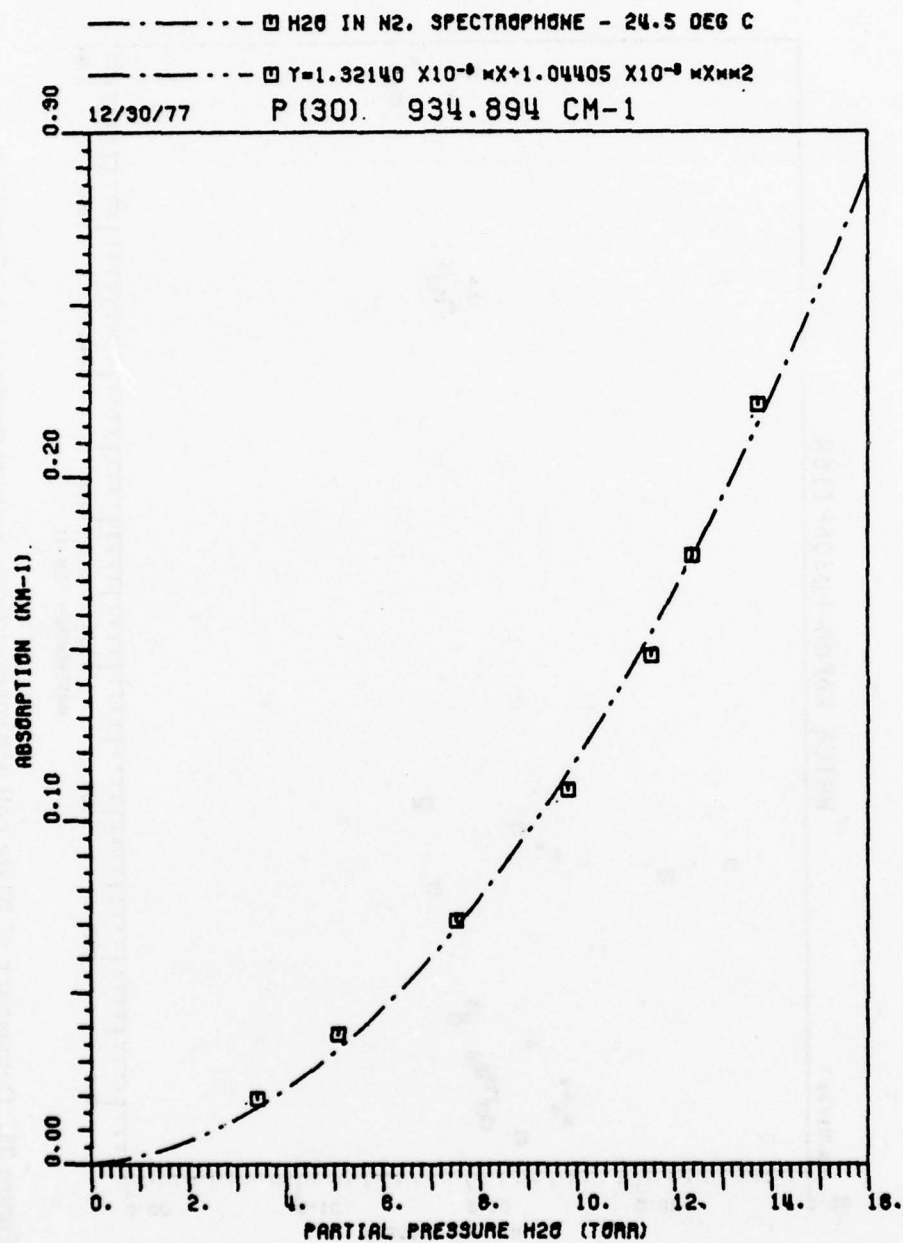


Figure 36. Spectrophone measurement, 760 Torr N<sub>2</sub> and H<sub>2</sub>O, P(30) 934.894 cm<sup>-1</sup> CO<sub>2</sub> laser line, T=24.5°C.

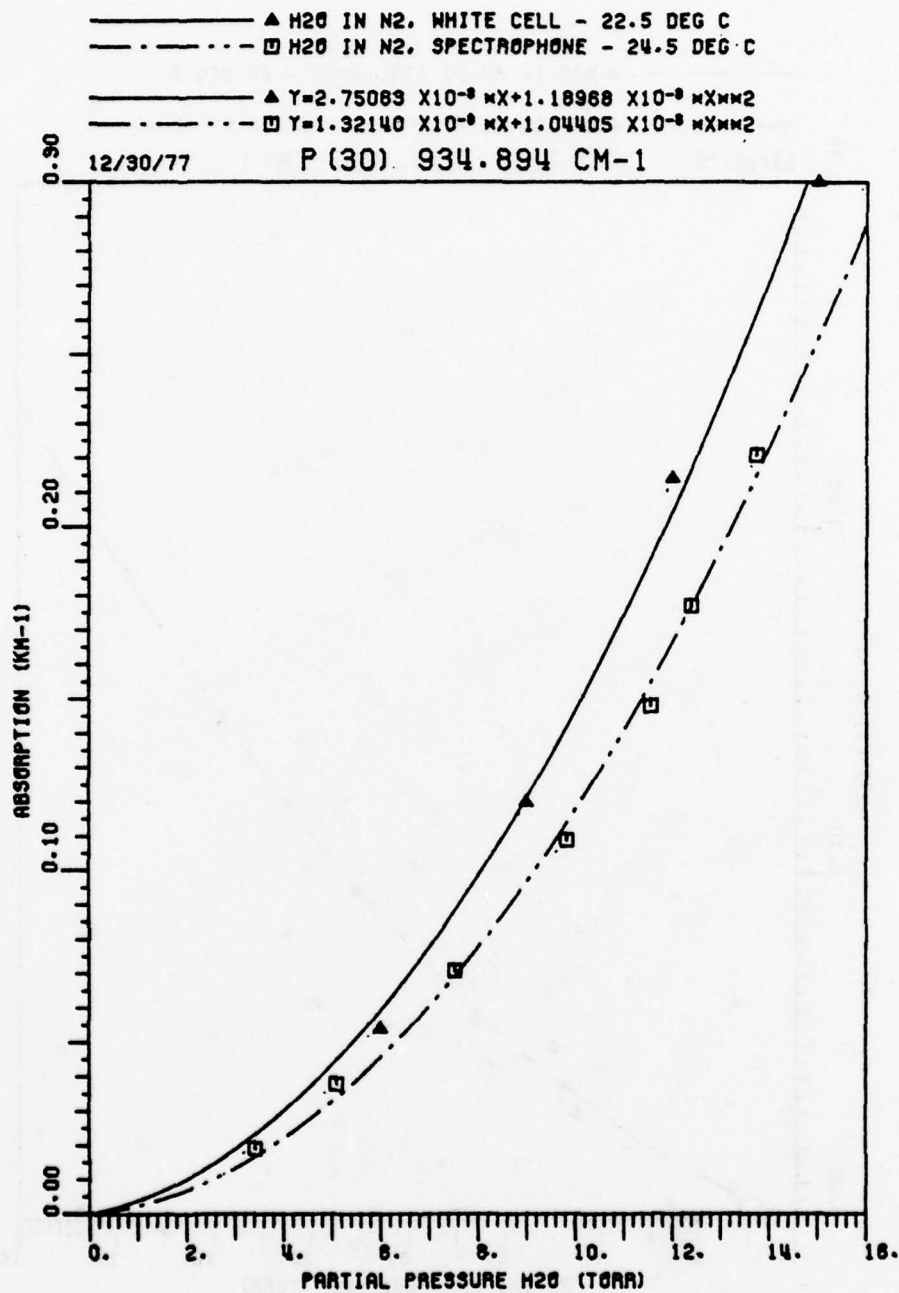


Figure 37. Comparison of spectrophone and White cell measurements, 760 Torr N<sub>2</sub> and H<sub>2</sub>O at P(30) 934.894 cm<sup>-1</sup> CO<sub>2</sub> laser line. temperatures as noted.

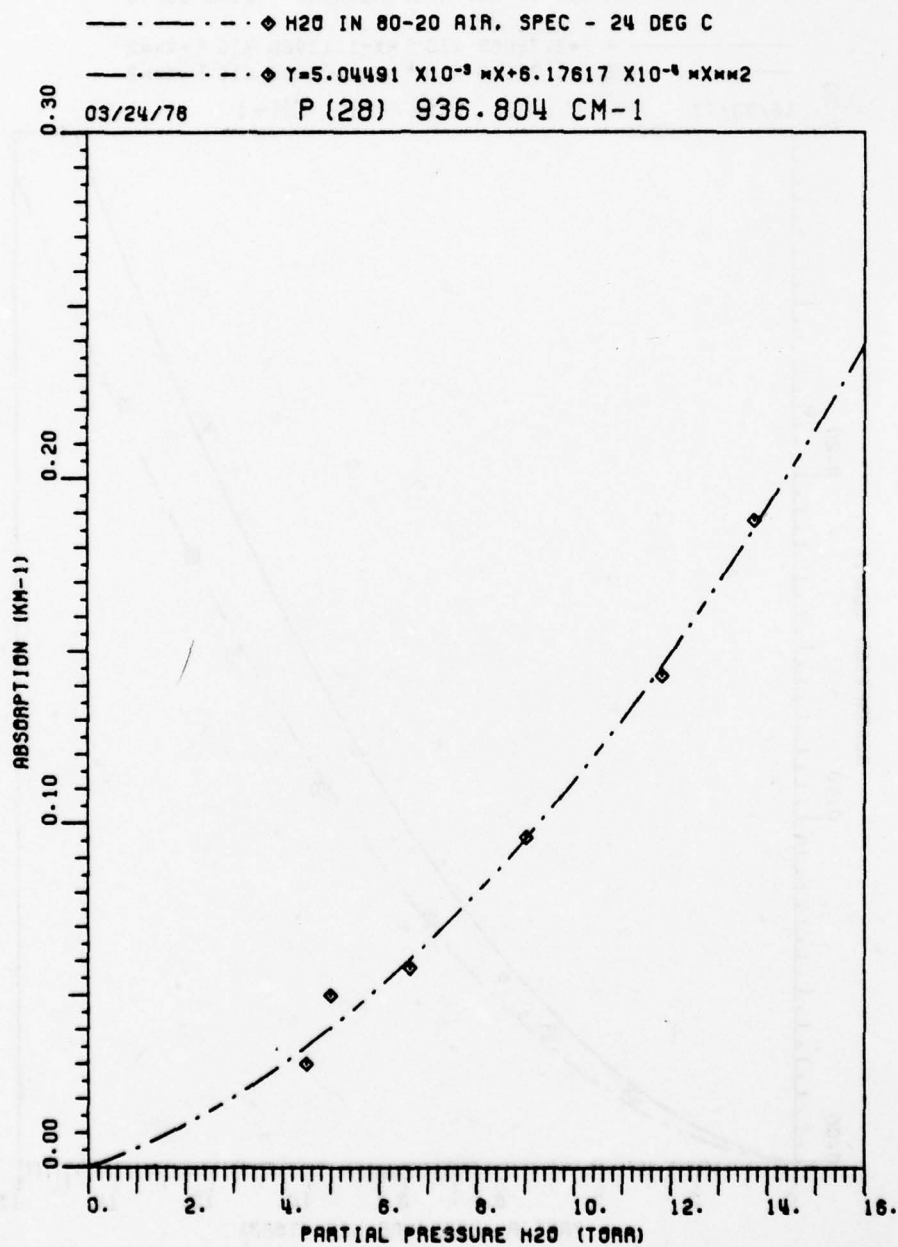


Figure 38. Spectrophone measurements, 760 Torr air and H<sub>2</sub>O,  
 P(28) 936.804 cm<sup>-1</sup> CO<sub>2</sub> laser line, T=24°C.

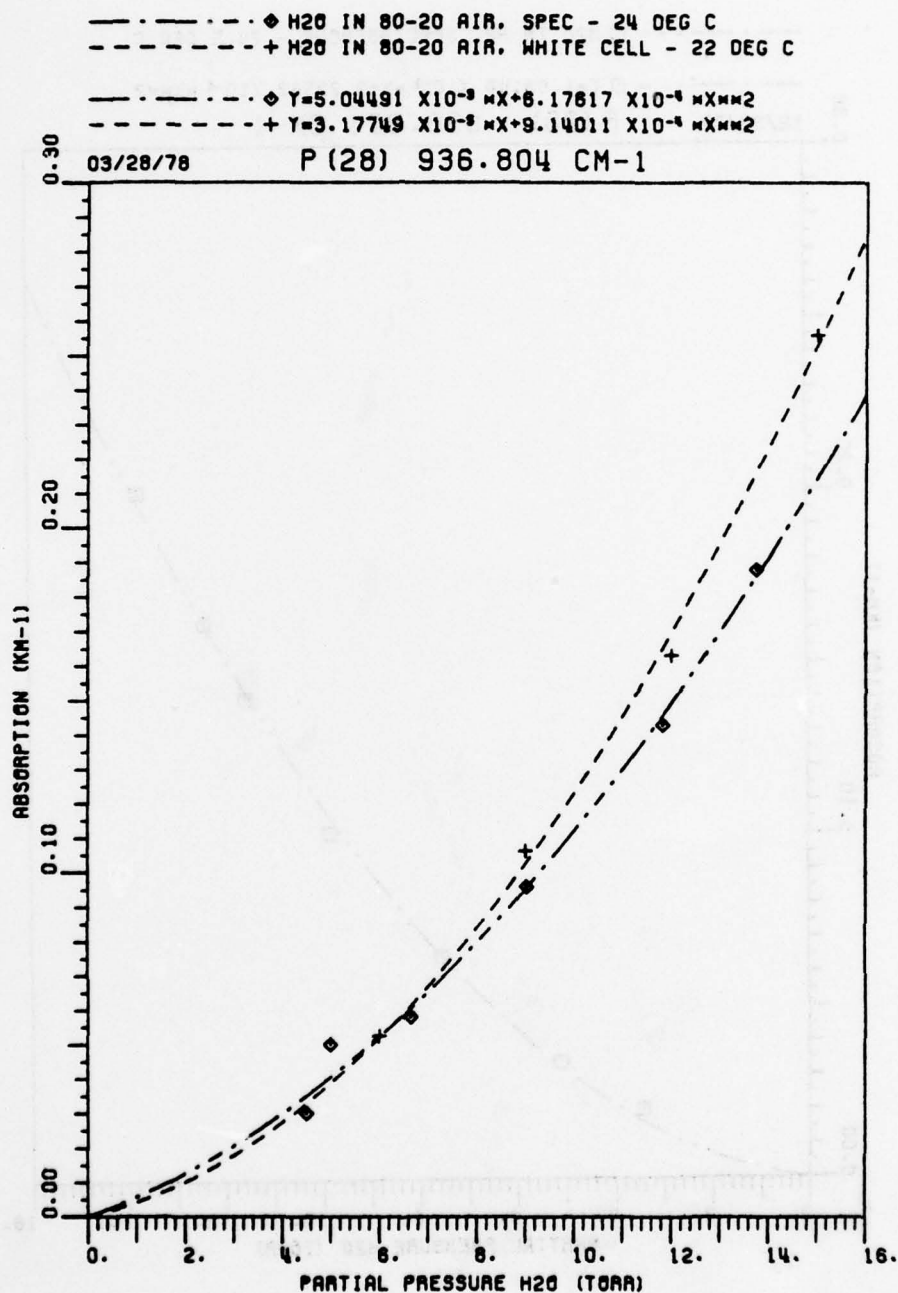


Figure 39. Comparison of White cell and spectrophone measurements, 760 Torr air and H<sub>2</sub>O, P(28) 936.804 cm<sup>-1</sup> temperatures as noted.

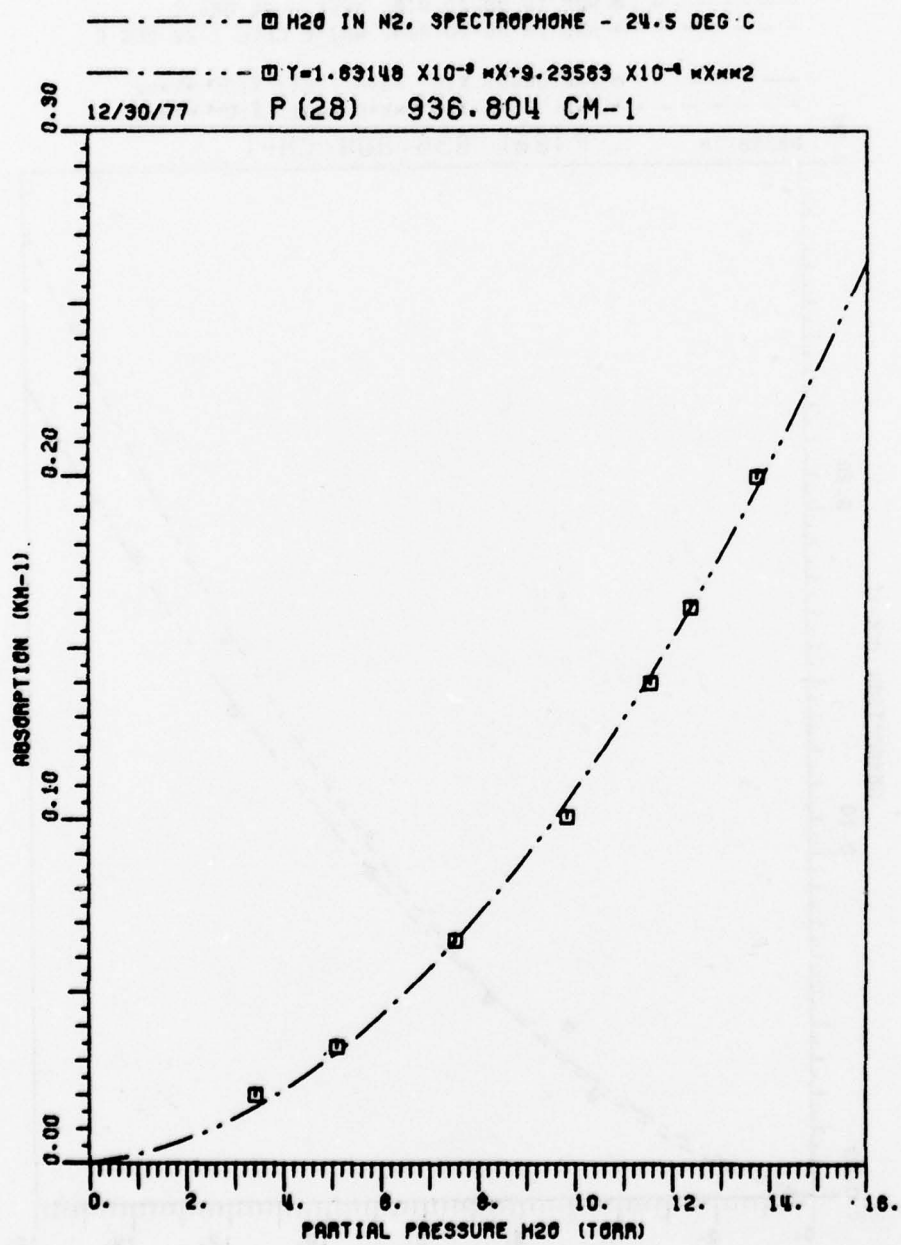


Figure 40. Spectrophone measurement, 760 Torr N<sub>2</sub> and H<sub>2</sub>O,  
P(28) 936.804 cm<sup>-1</sup>, T=24.5°C.



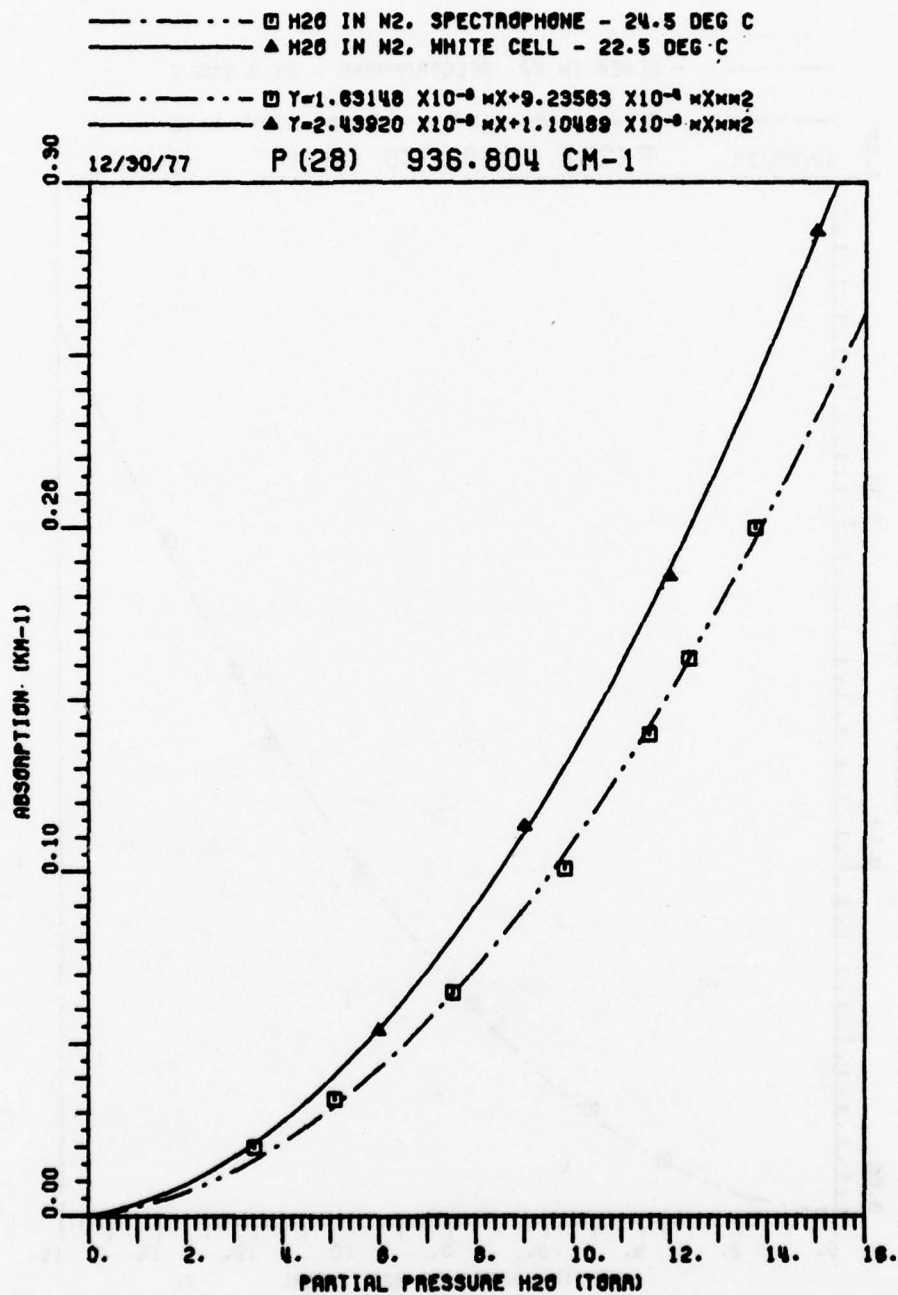


Figure 41. Comparison of spectrophone and White cell measurements, P(28) 936.804  $\text{cm}^{-1}$ , temperatures as noted, 760 Torr  $\text{N}_2\text{O}$  and  $\text{H}_2\text{O}$ .

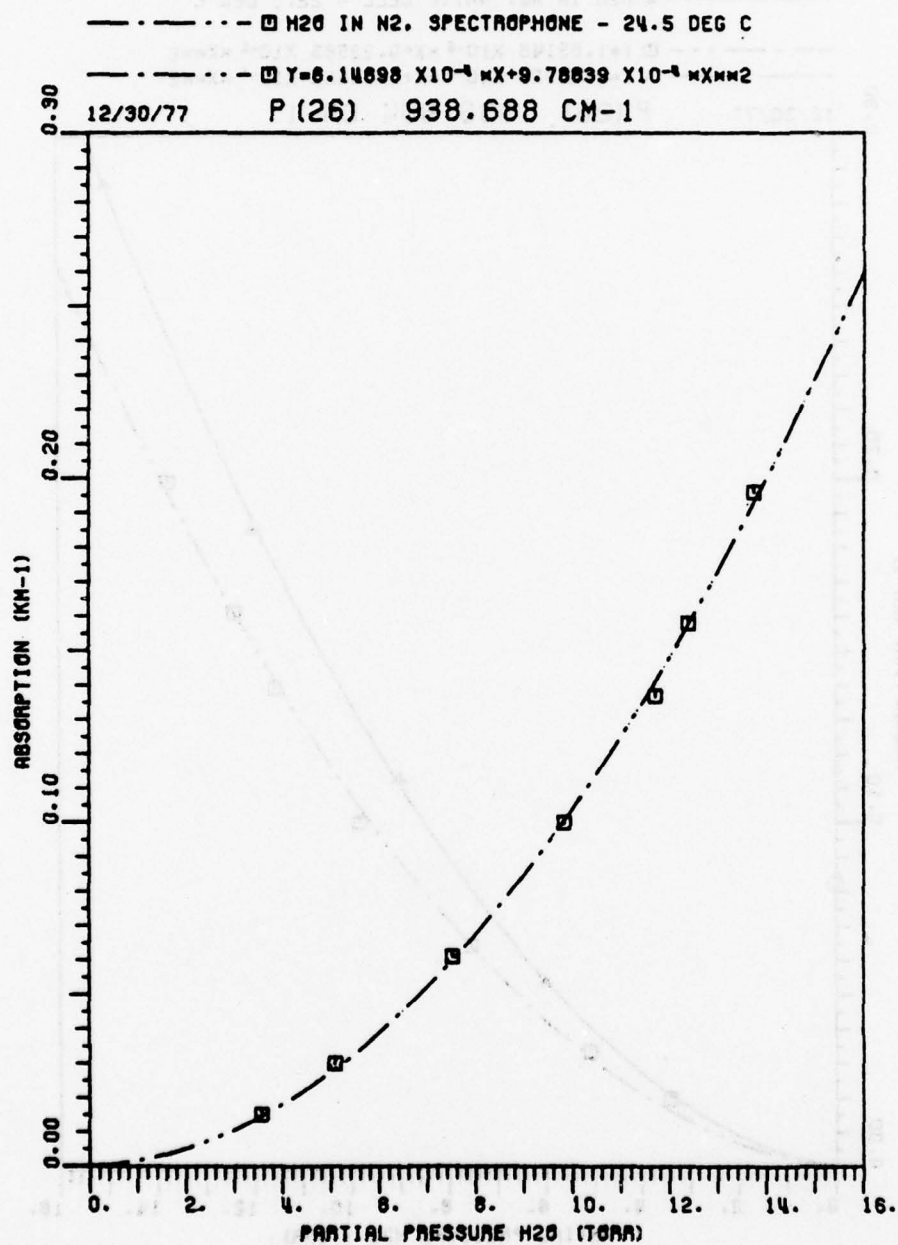


Figure 42. Spectrophone measurement, 760 Torr N<sub>2</sub> and H<sub>2</sub>O,  
 T=24.5°C, P(26) 938.688 cm<sup>-1</sup>.

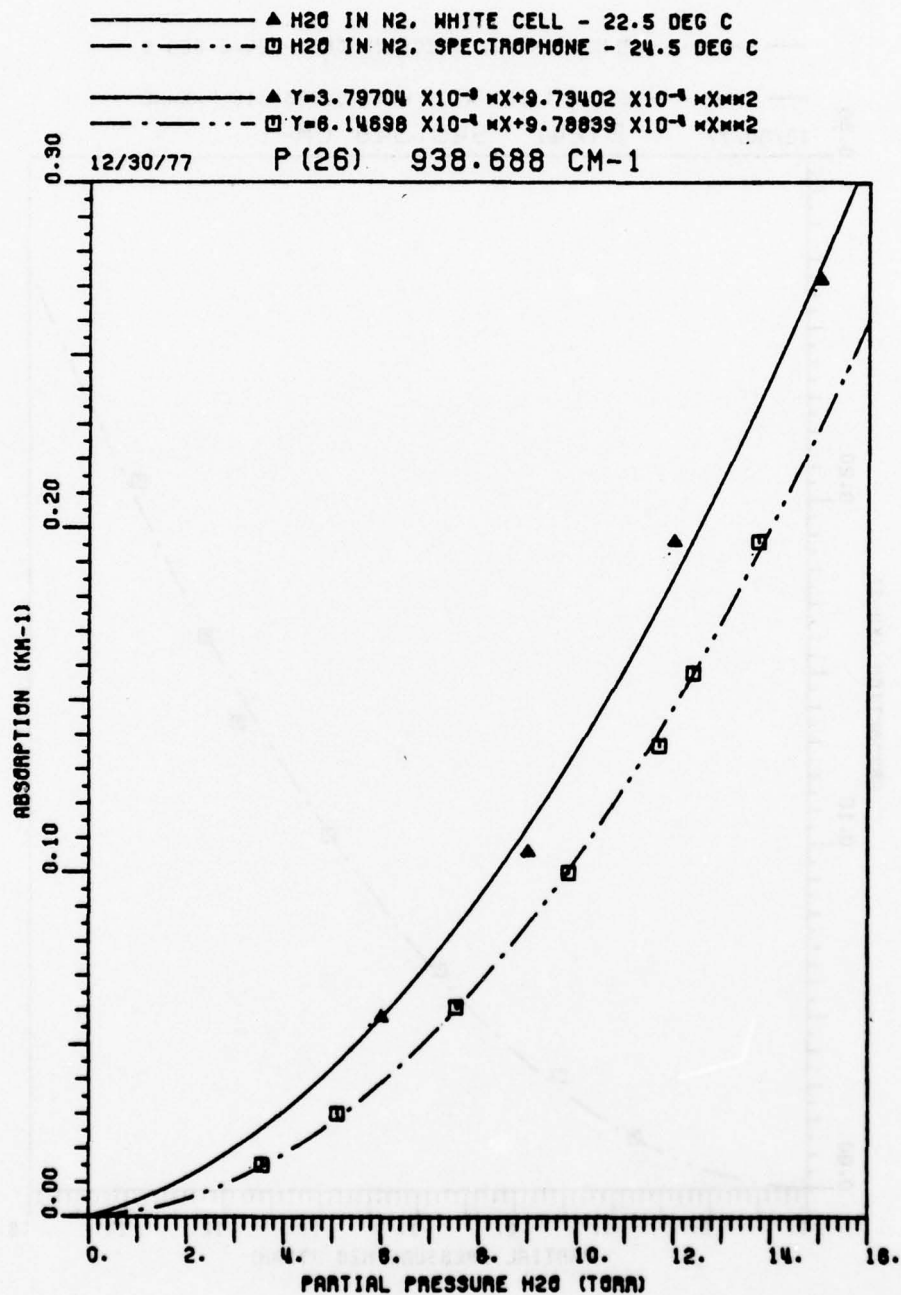


Figure 43. Comparison of White cell and spectrophone measurements, 760Torr N<sub>2</sub> and H<sub>2</sub>O, temperatures as noted, P(26) 938.688 cm<sup>-1</sup>.

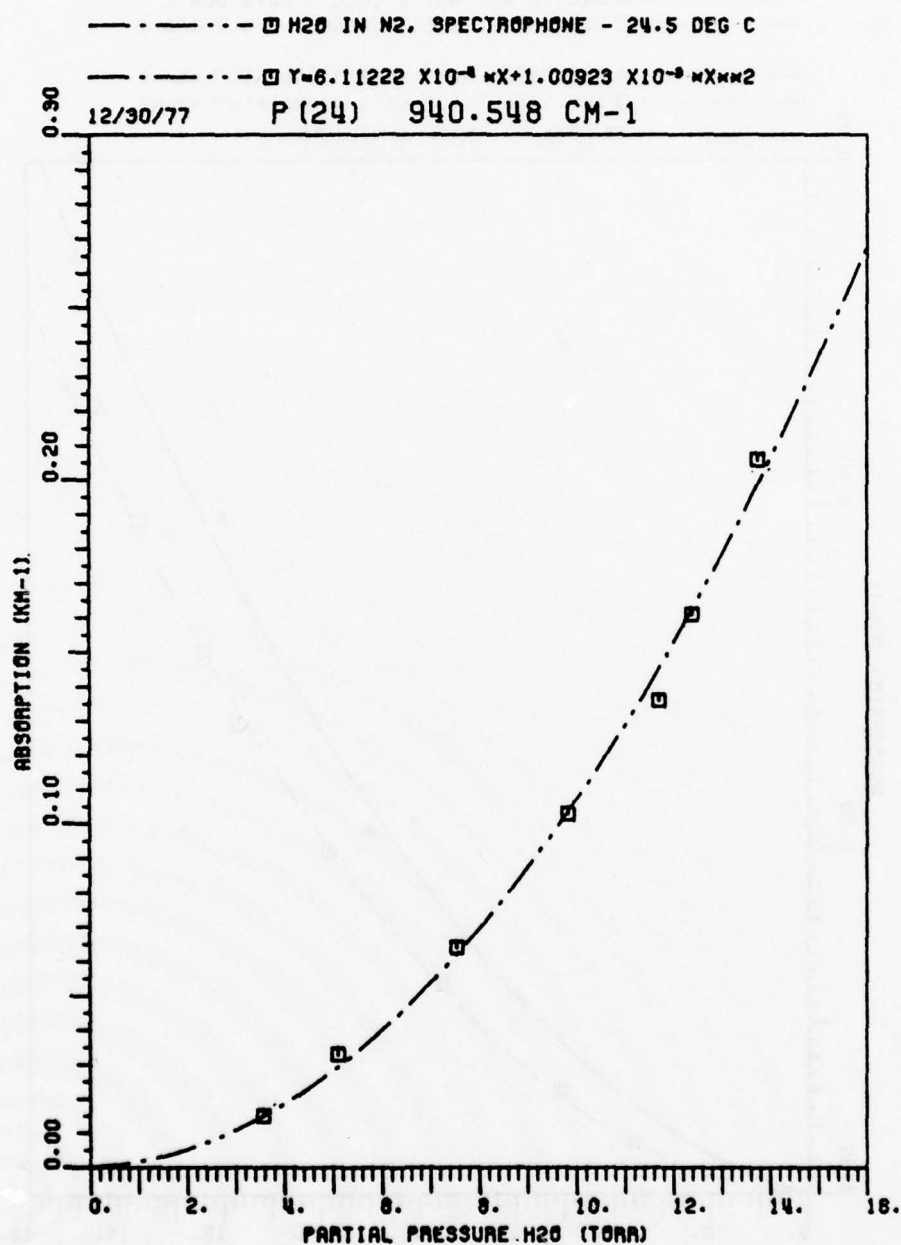


Figure 44. Spectrophone measurement, 760 Torr N<sub>2</sub> and H<sub>2</sub>O,  
 T=24.5°C, P(24) 940.548 cm<sup>-1</sup>.

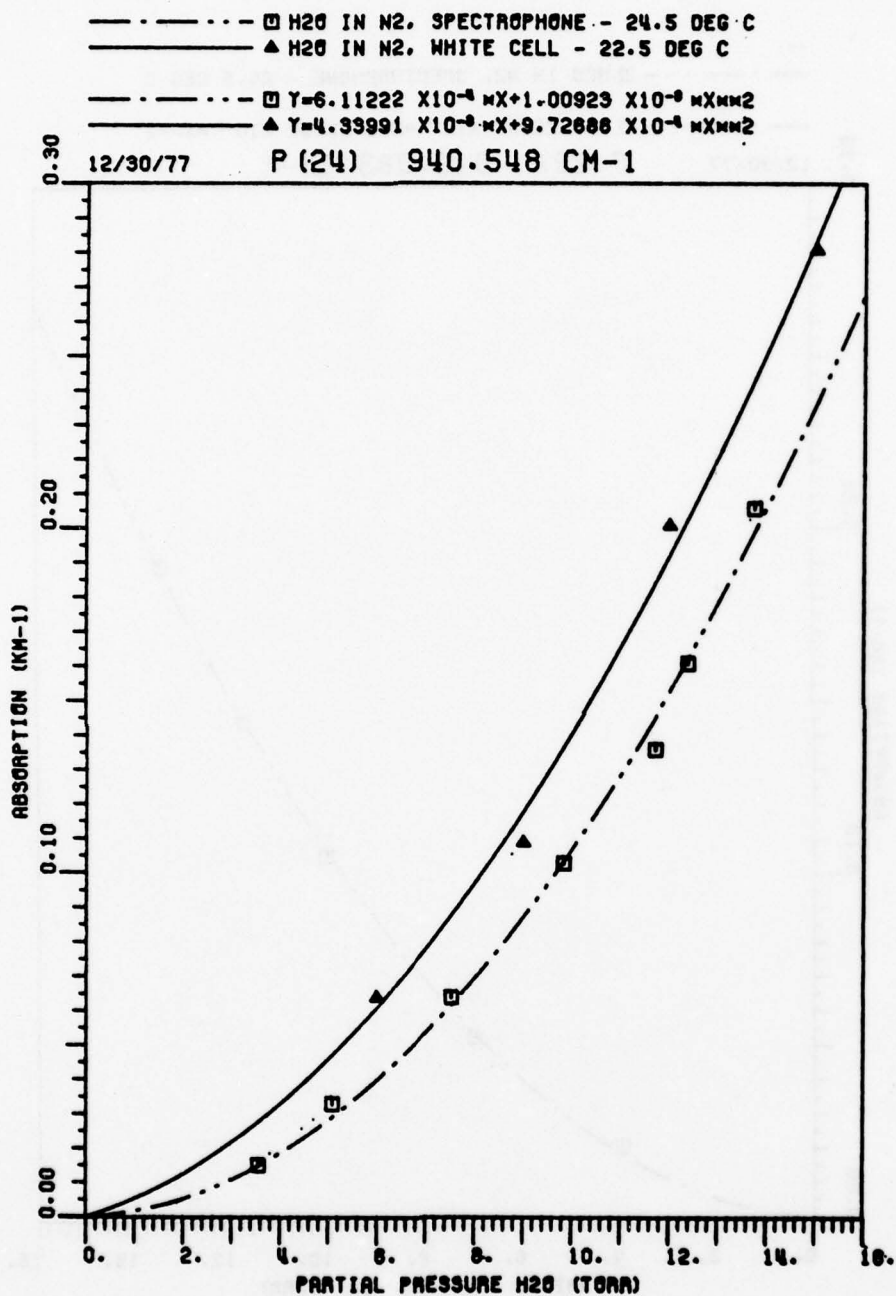


Figure 45. Comparison of White cell and spectrophone measurements, 760 Torr N<sub>2</sub> and H<sub>2</sub>O, temperatures as noted, P(24) 940.548 cm<sup>-1</sup>.



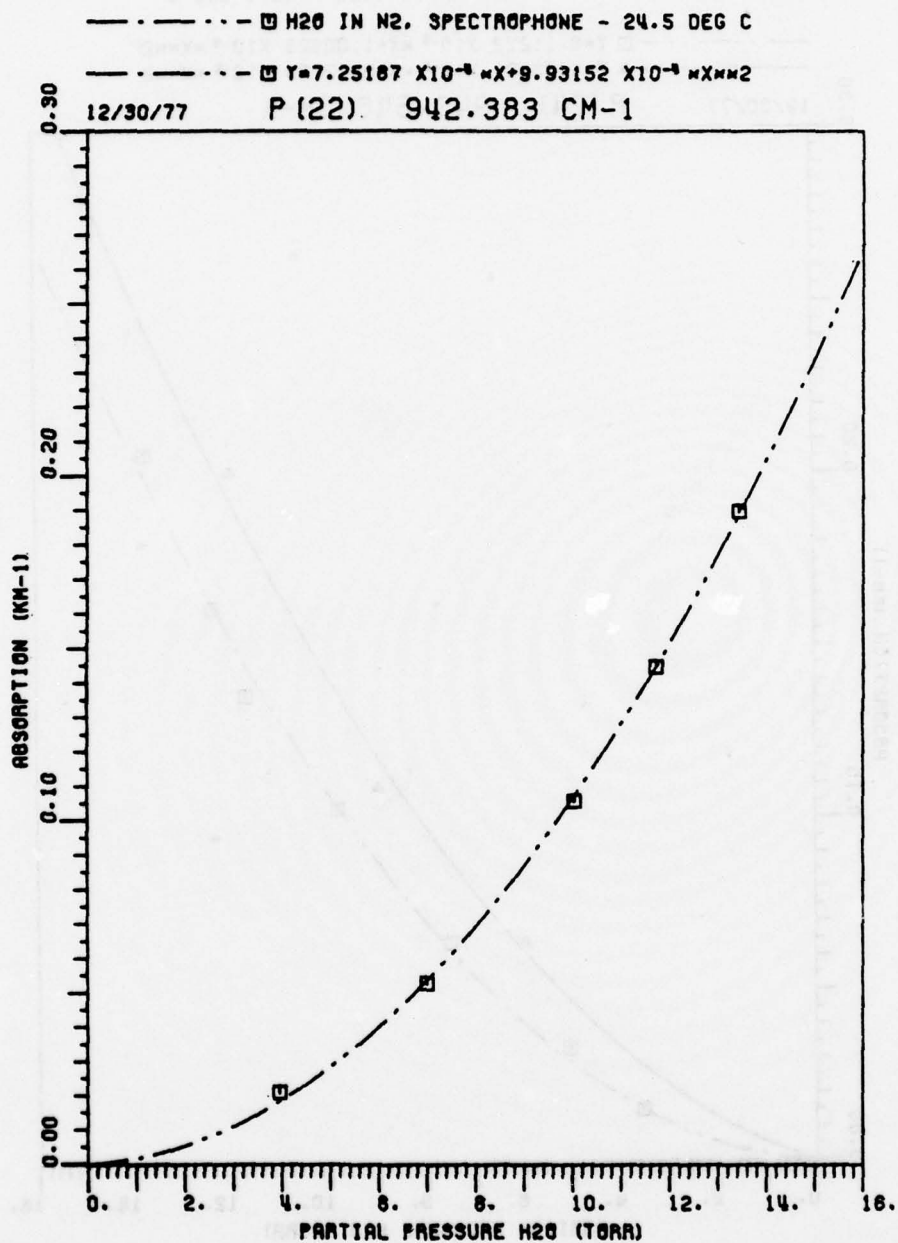


Figure 46. Spectrophone measurement, 760 Torr N<sub>2</sub> and H<sub>2</sub>O, T=24.5°C, P(22) 942.383 cm<sup>-1</sup>.

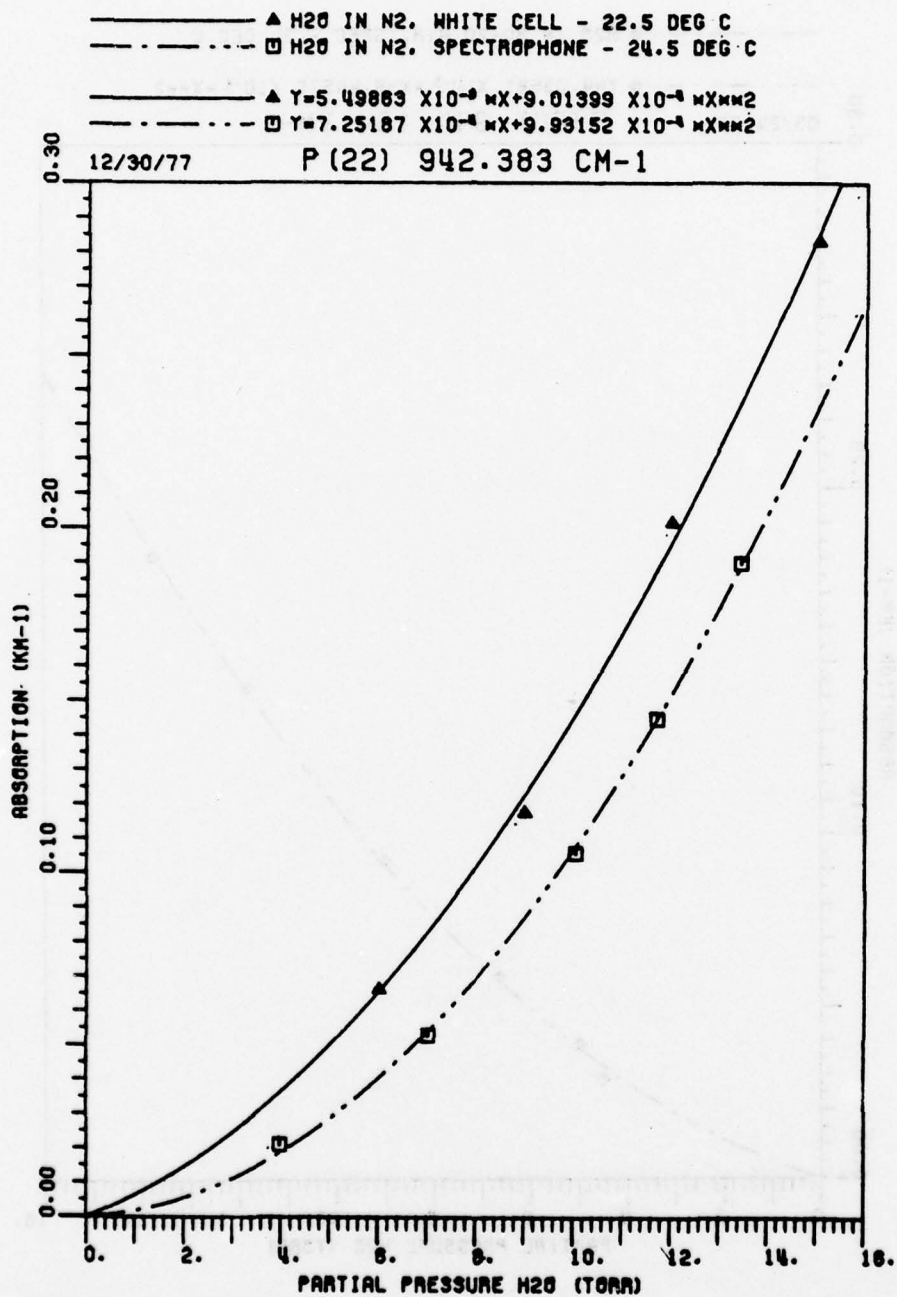


Figure 47. Comparison of White cell and spectrophone measurements, 760 Torr N<sub>2</sub> and H<sub>2</sub>O, temperatures as noted, P(22) 942.383 cm<sup>-1</sup>.

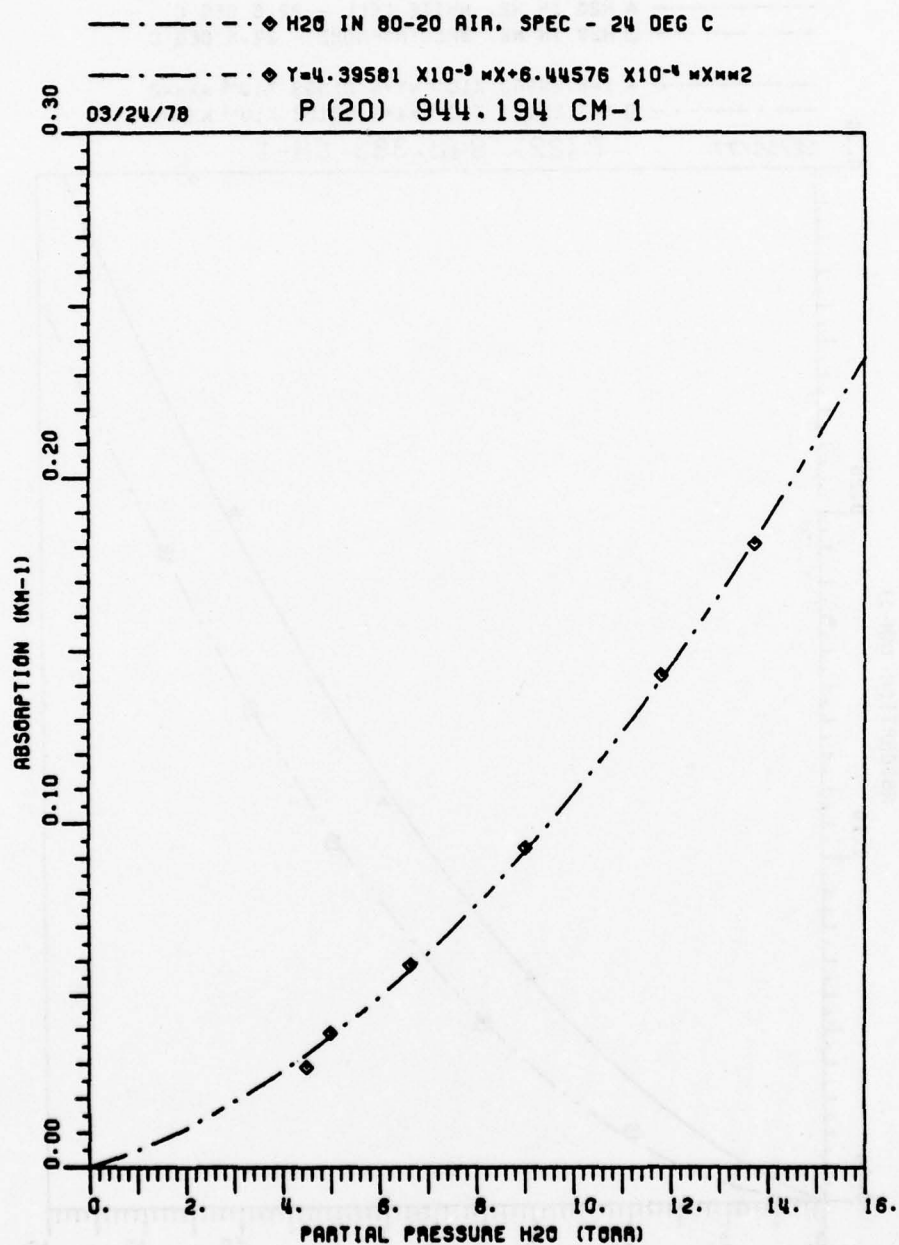


Figure 48. Spectrophone measurement, 760 Torr air and H<sub>2</sub>O 24°C, P(20) 944.194 cm<sup>-1</sup>.

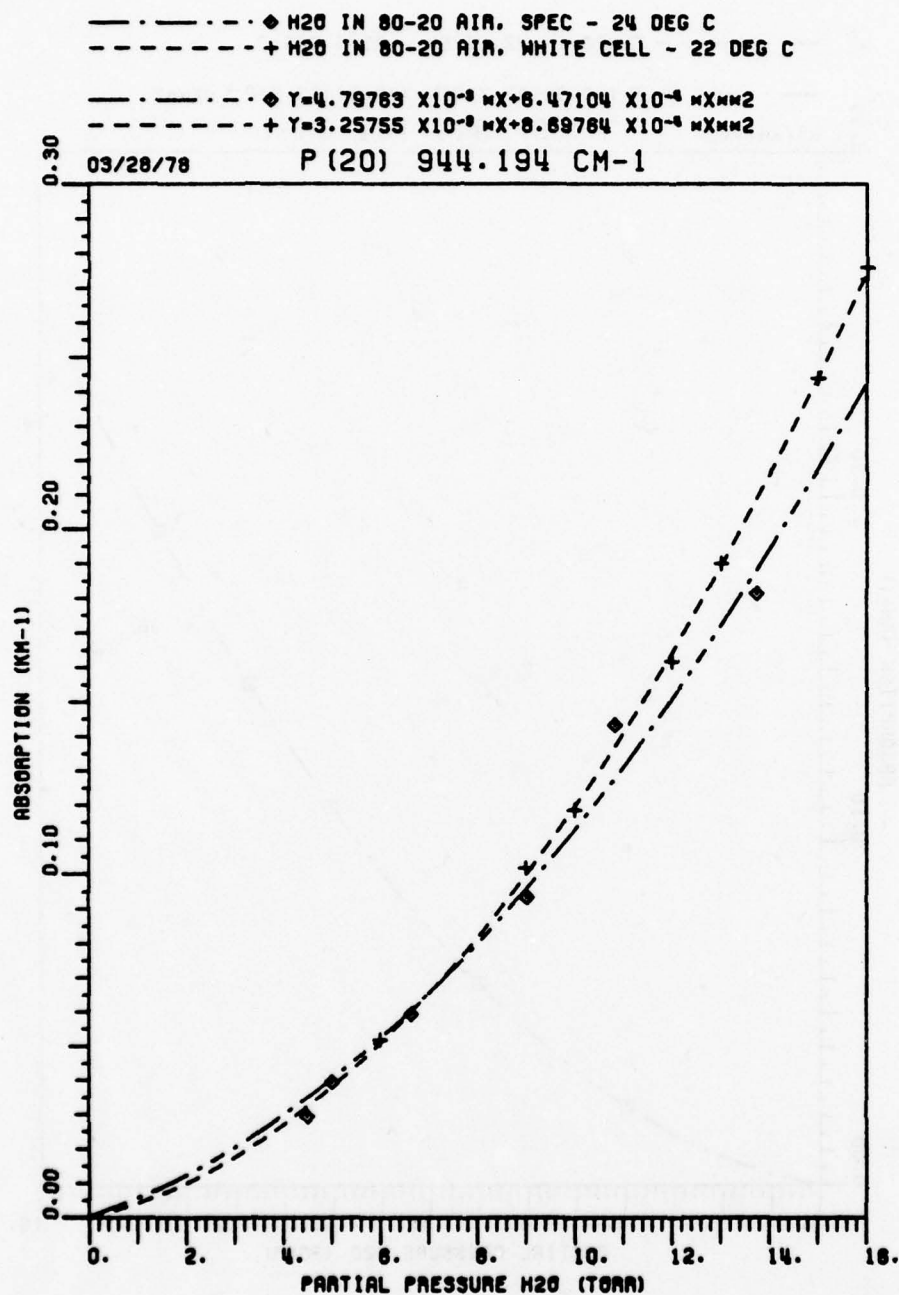


Figure 49. Comparison of White cell and spectrophone measurements, 760 Torr air and H<sub>2</sub>O, temperatures as noted, P(20) 944.194 cm<sup>-1</sup>.

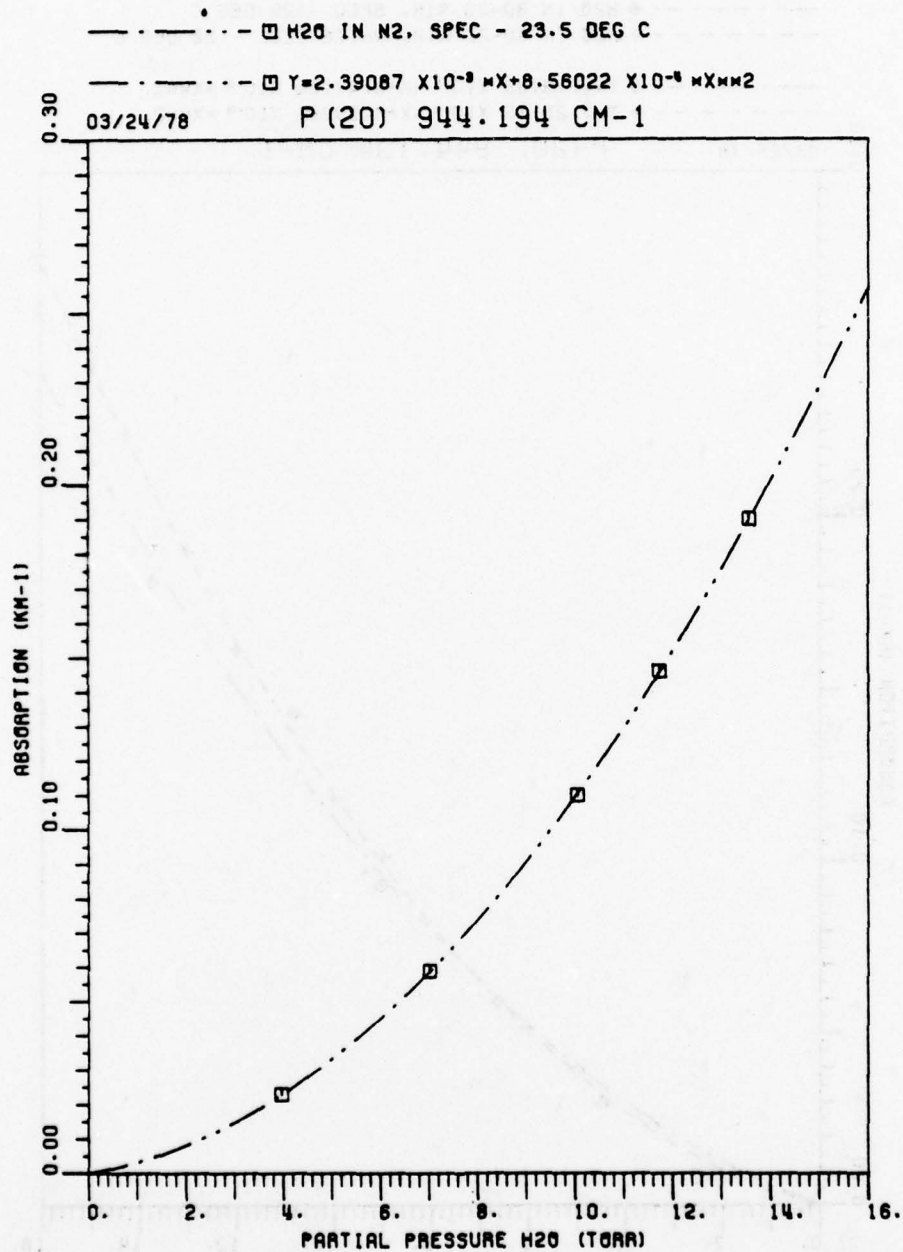


Figure 50. Spectrophone measurement, 760 Torr  $N_2$  and  $H_2O$ ,  
 $P(20) 944.194 \text{ cm}^{-1}$ .



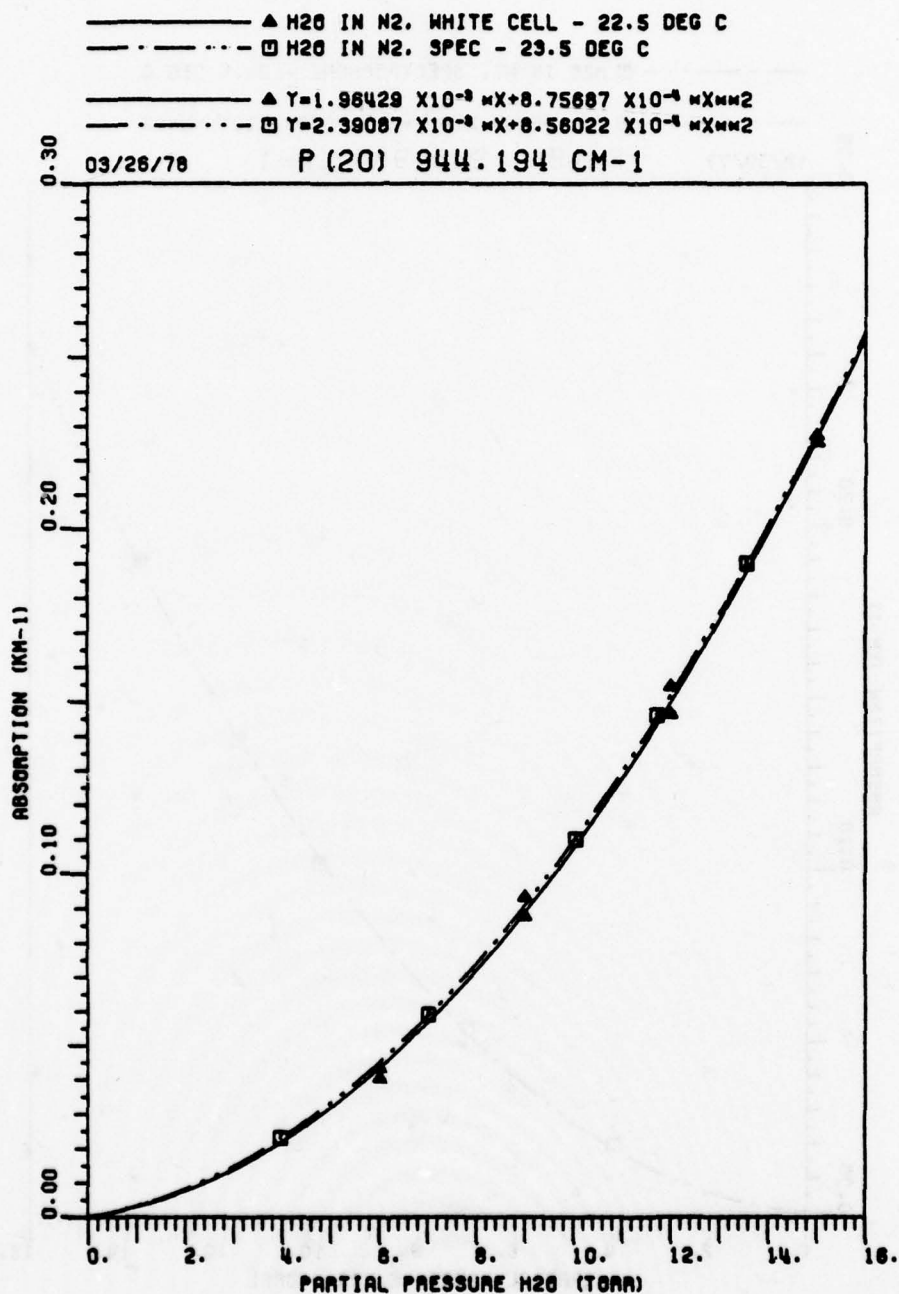


Figure 51. Comparison of spectrophotometer and White cell measurements, 760 Torr N<sub>2</sub> and H<sub>2</sub>O, P(20) 944.194 cm<sup>-1</sup>.

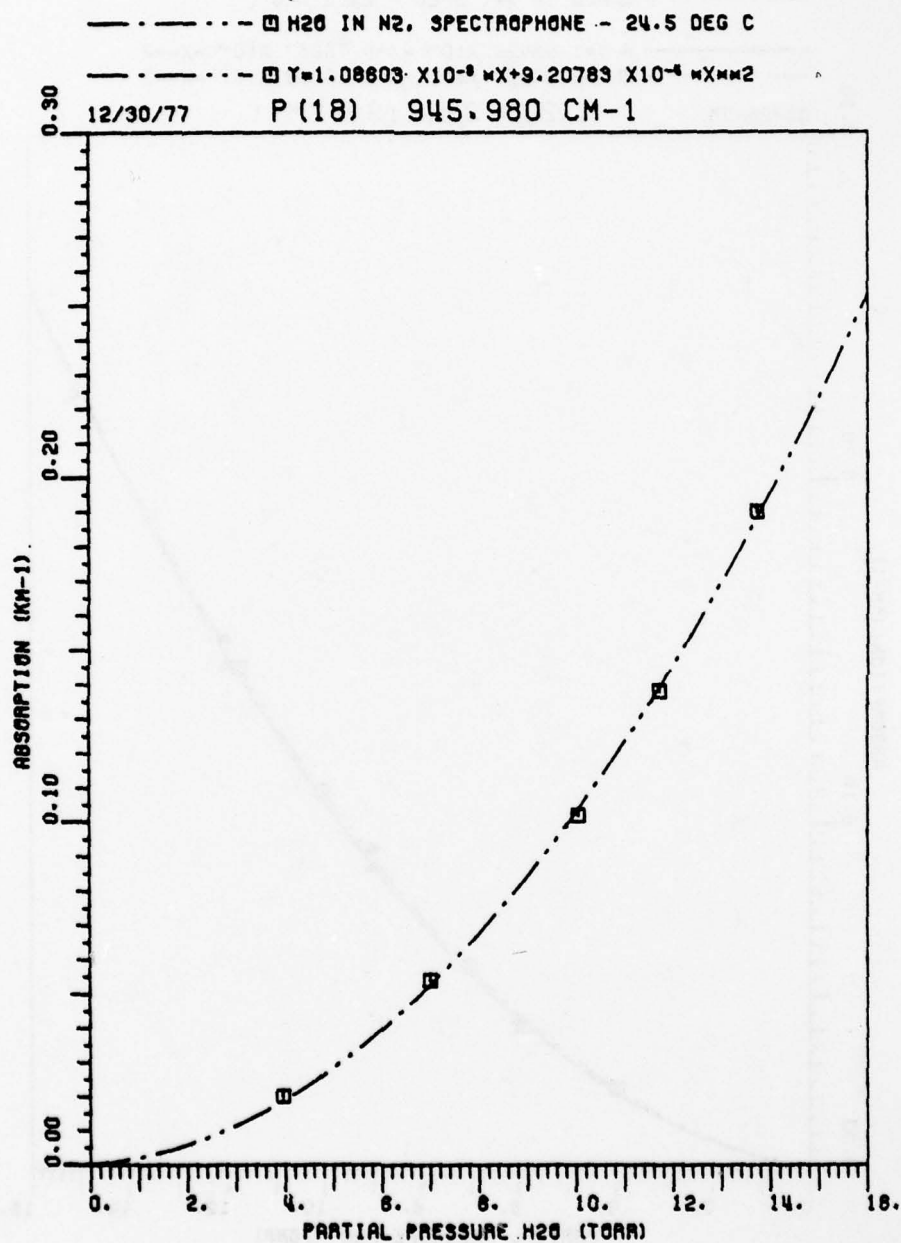


Figure 52. Spectrophone measurement, 760 Torr N<sub>2</sub> and H<sub>2</sub>O,  
 T=24.5°C, P(18) 945.980 cm<sup>-1</sup>.

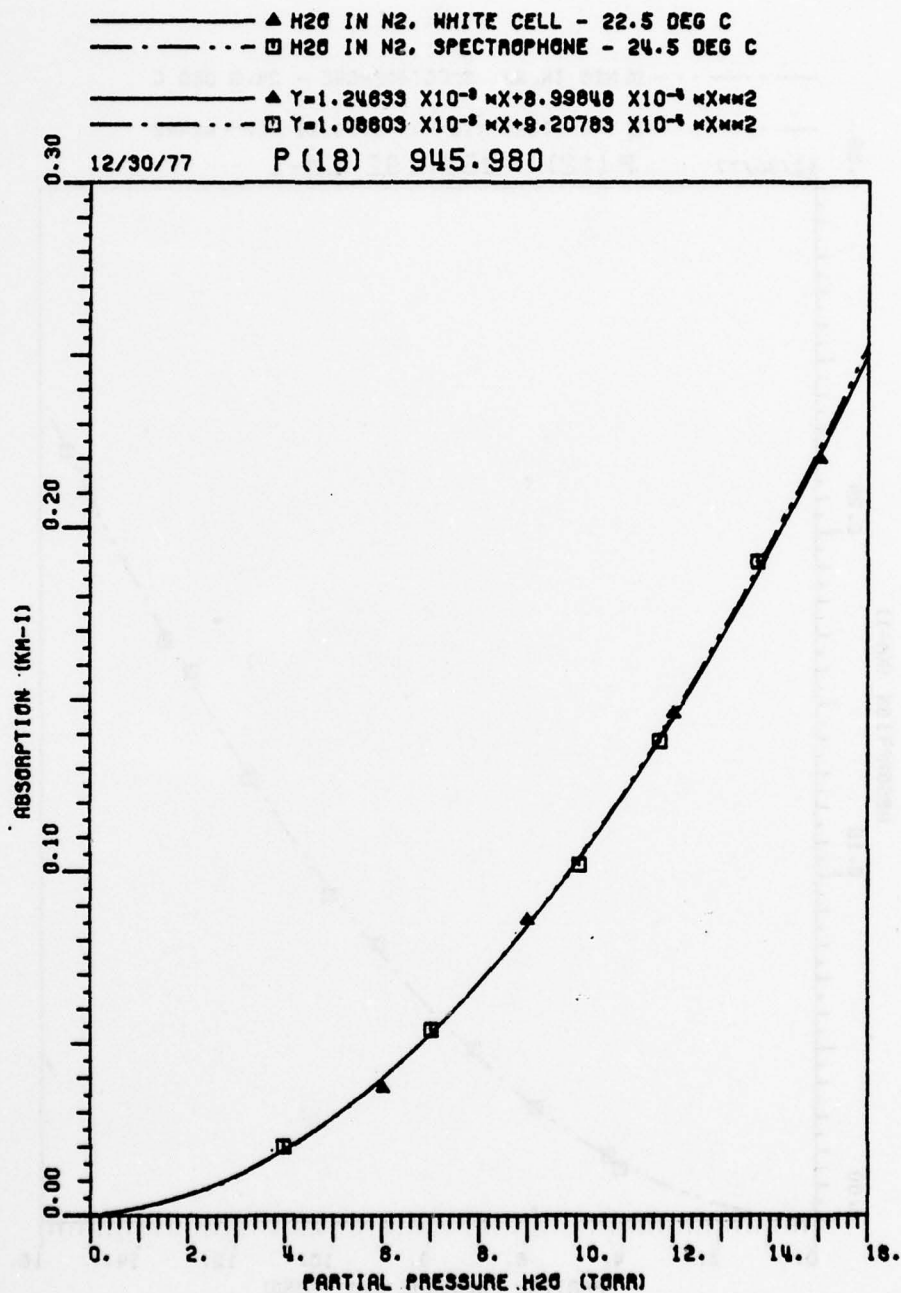


Figure 53. Comparison of White cell and spectrophone measurements, 760 Torr N<sub>2</sub> and H<sub>2</sub>O, temperatures as noted, P(18) 945.980 cm<sup>-1</sup>.

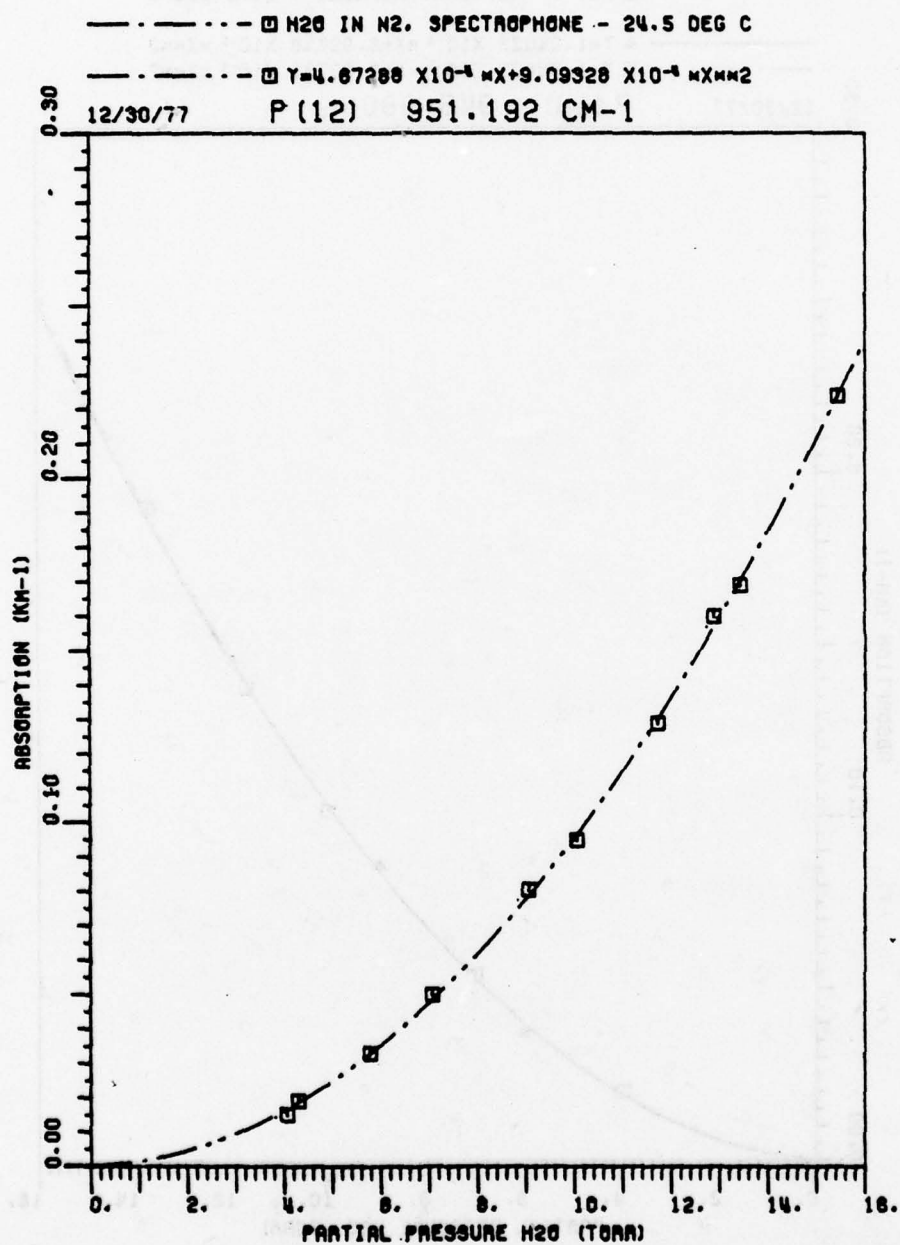


Figure 54. Spectrophone measurement, 760 Torr N<sub>2</sub> and H<sub>2</sub>O,  
 T=24.5°C, P(12) 951.192 cm<sup>-1</sup>.

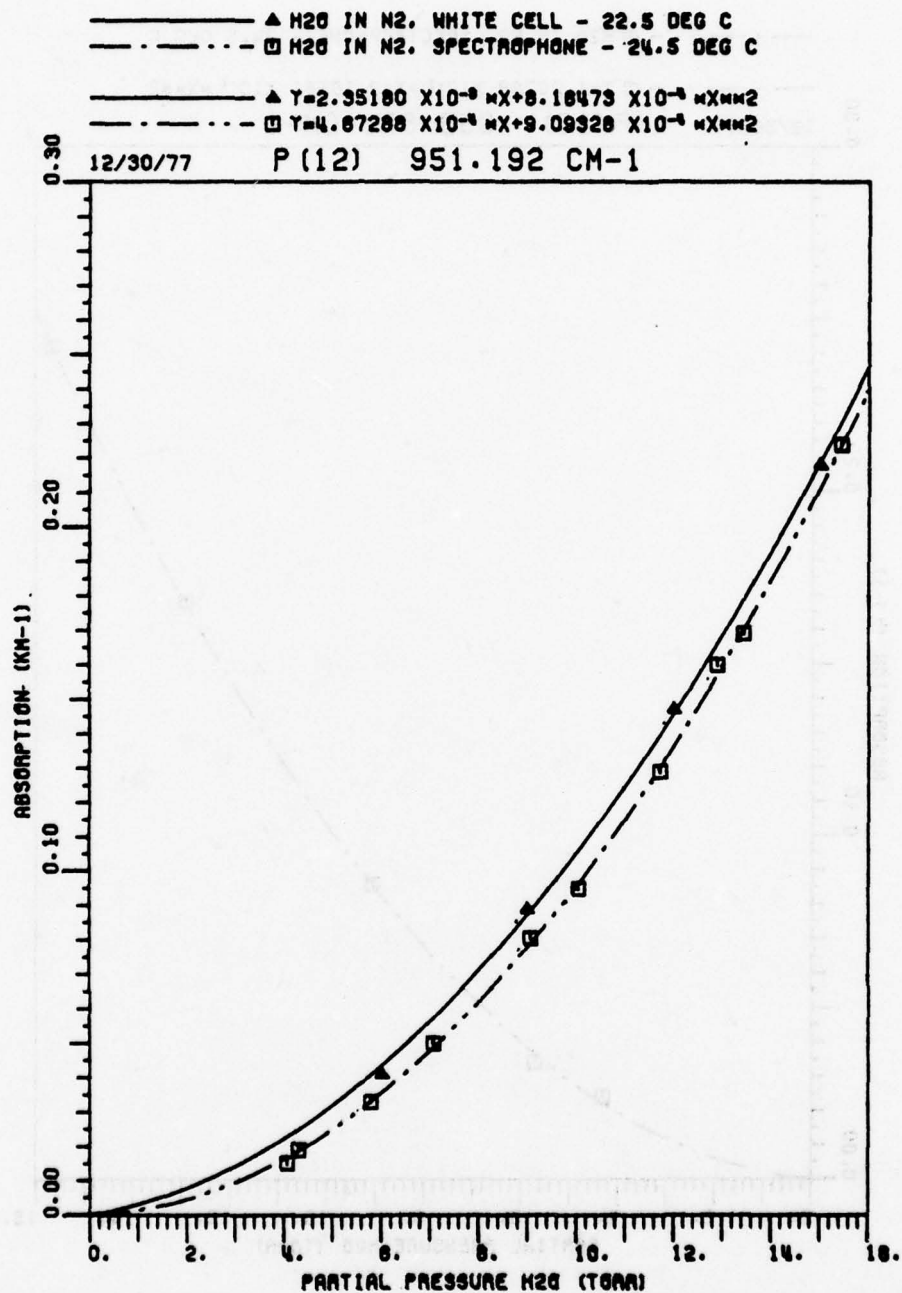


Figure 55. Comparison of White cell and spectrophone measurement, 760 Torr N<sub>2</sub> and H<sub>2</sub>O, temperatures as noted, P(12) 951.192 cm<sup>-1</sup>.



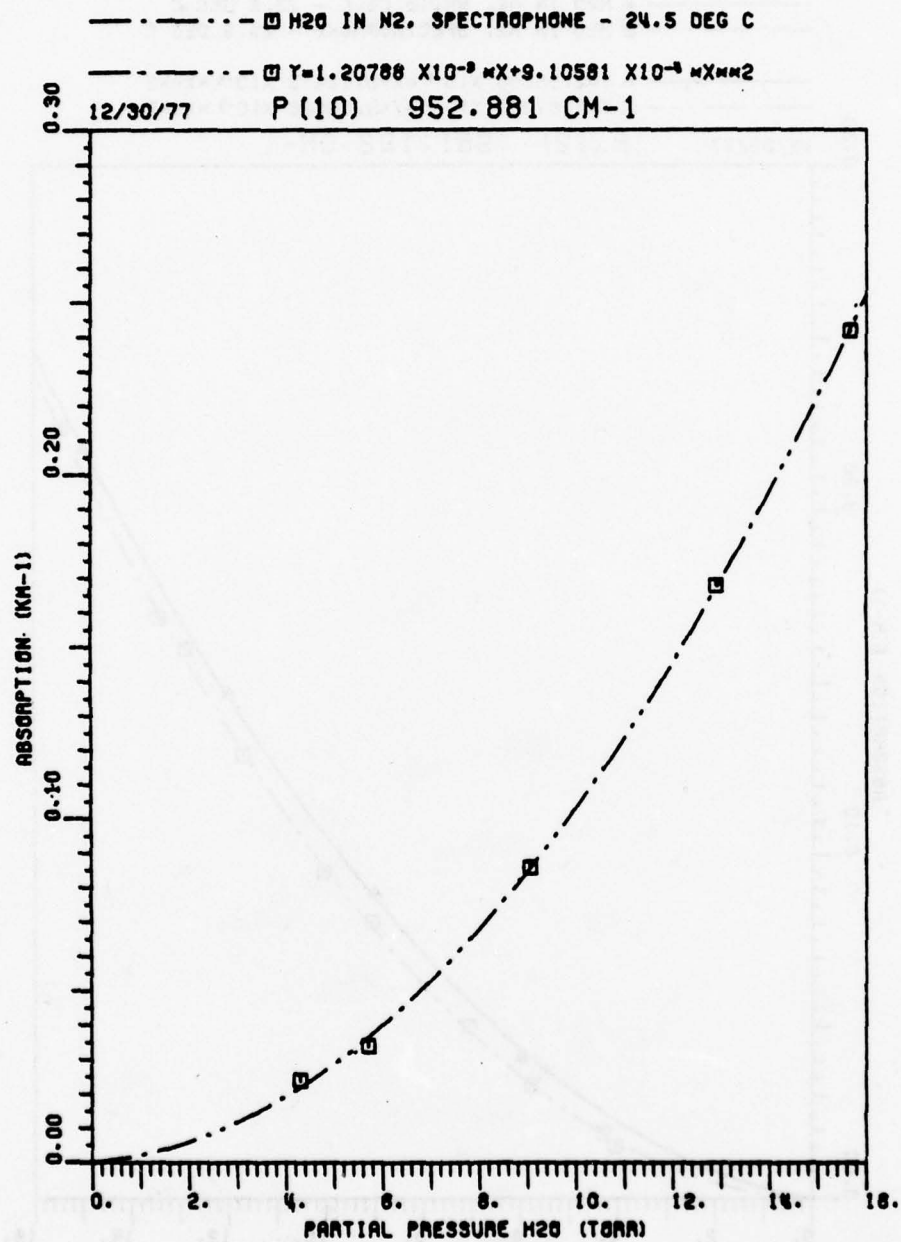


Figure 56. Spectrophone measurement, 760 Torr N<sub>2</sub> and H<sub>2</sub>O,  
 T=24.5°C, P(10) 952.881 cm<sup>-1</sup>.

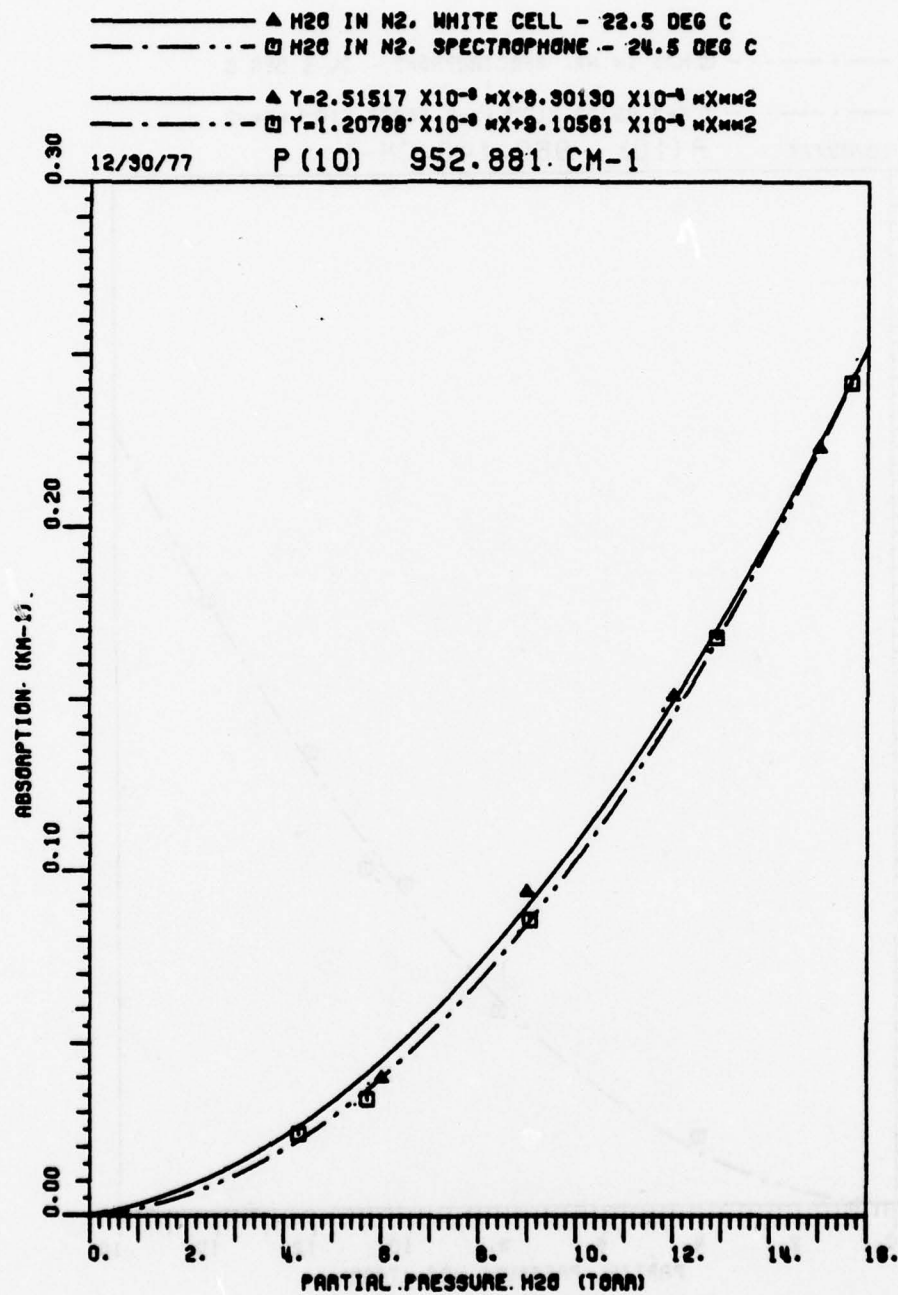


Figure 57. Comparison of White cell and spectrophone measurements, 760 Torr N<sub>2</sub> and H<sub>2</sub>O, temperatures as noted, P(10) 952.881 cm<sup>-1</sup>.

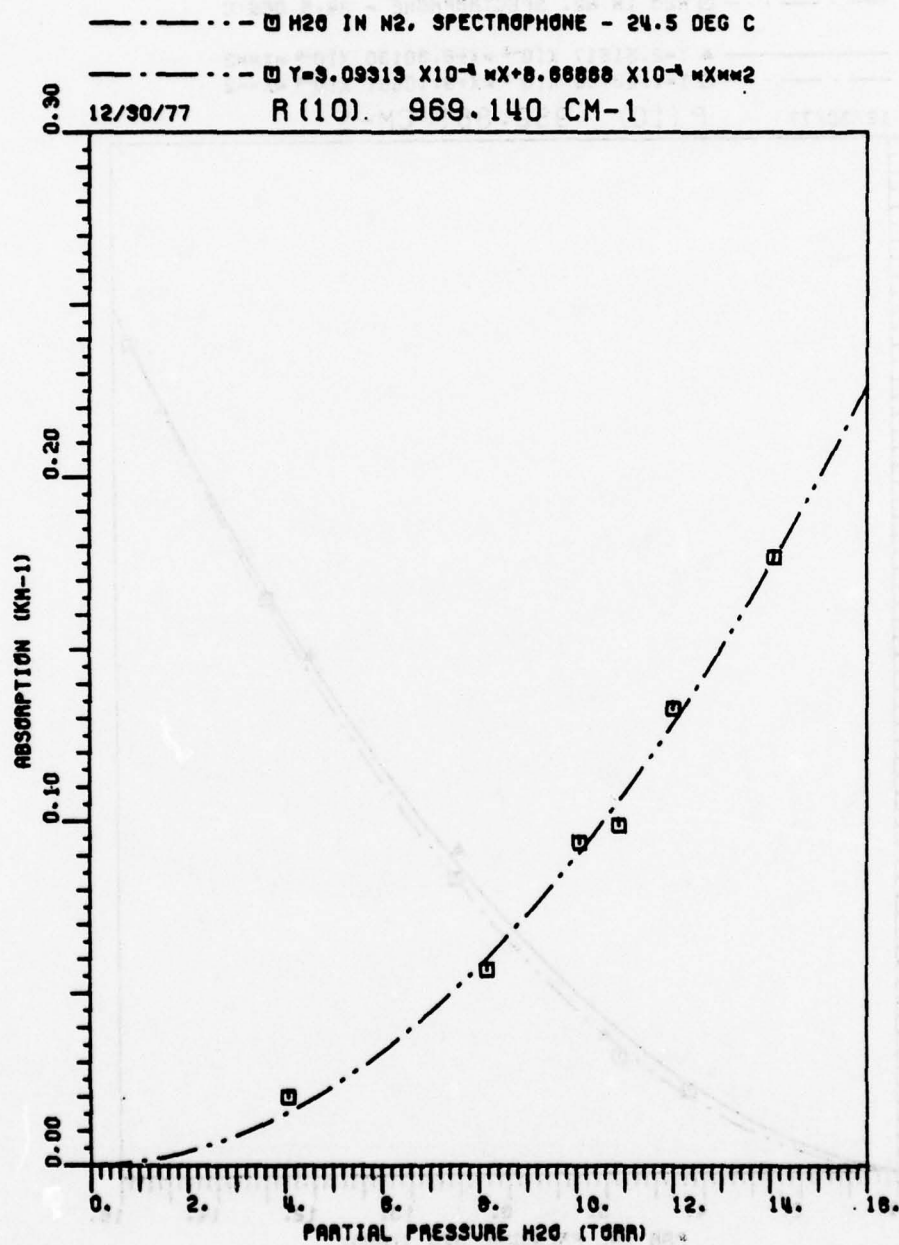


Figure 58. Spectrophone measurement, 760 Torr N<sub>2</sub> and H<sub>2</sub>O broadened,  
 T=24.5°C, R(10) 969.140 cm<sup>-1</sup>.

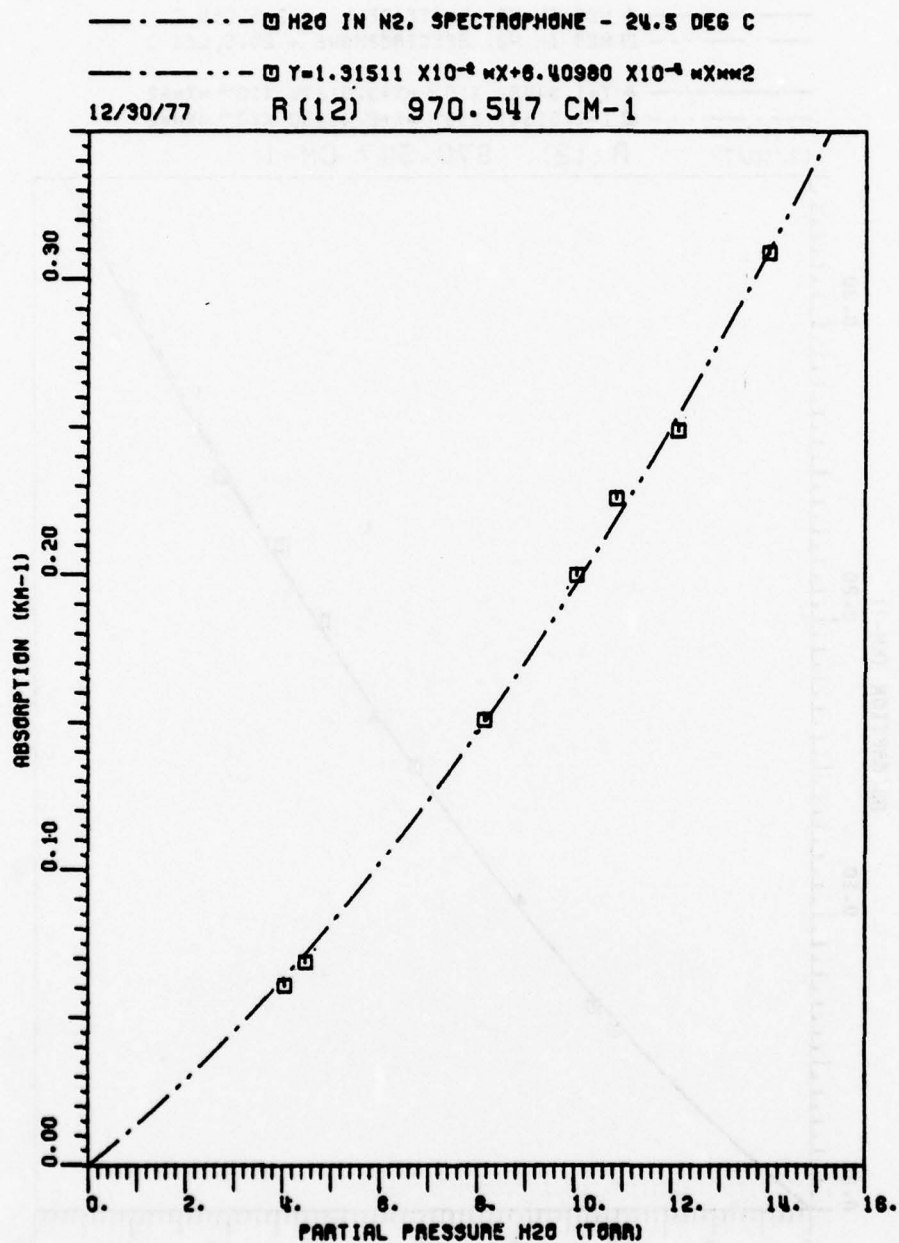


Figure 59. Spectrophone measurement, 760 Torr  $\text{N}_2$  and  $\text{H}_2\text{O}$ ,  
 $T=24.5^\circ\text{C}$ ,  $R(12) 970.547 \text{ cm}^{-1}$ .

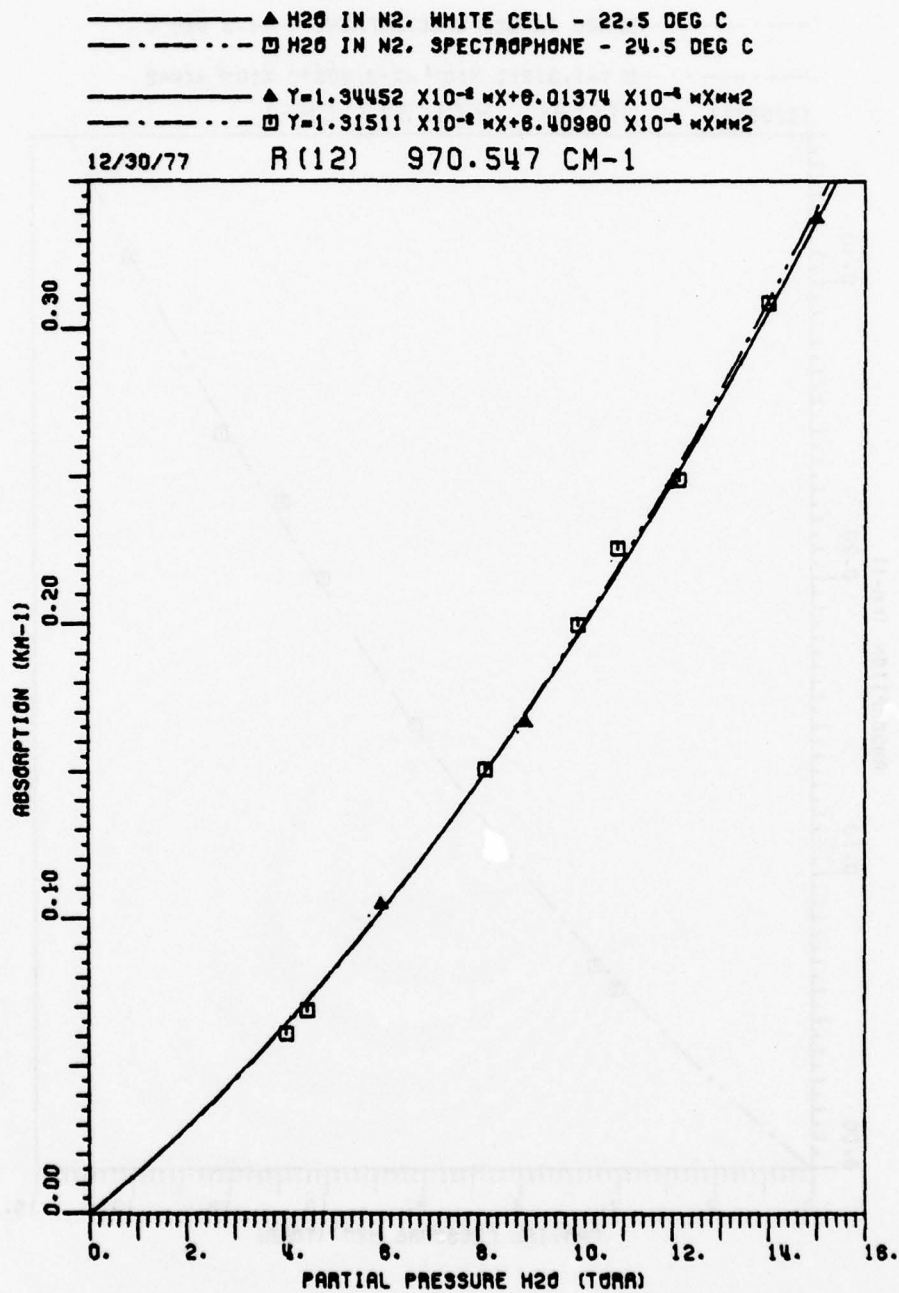


Figure 60. Comparison of White cell and spectrophone measurements, 760 Torr N<sub>2</sub> and H<sub>2</sub>O, temperatures as noted, R(12) 970.547 cm<sup>-1</sup>.



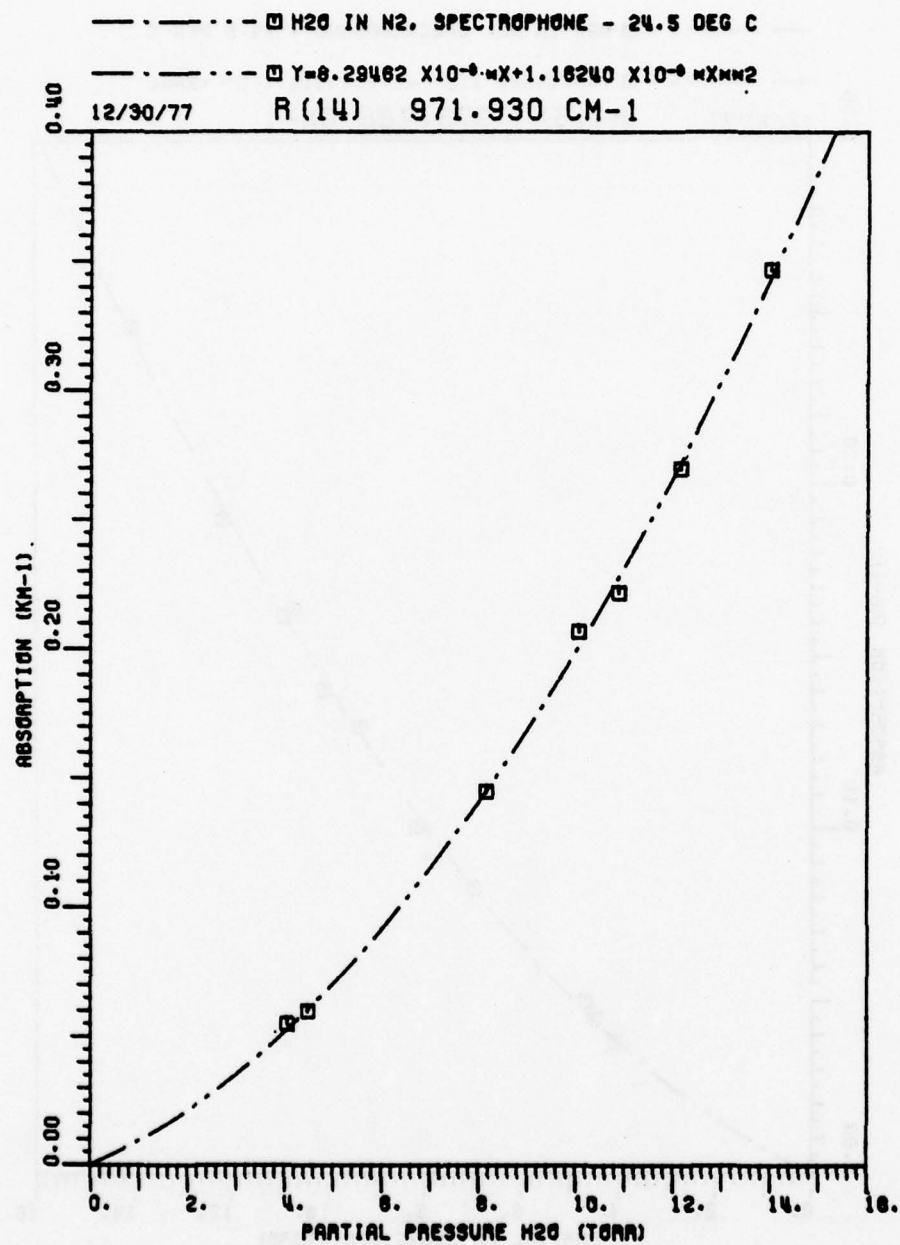


Figure 61. Spectrophone measurement 760 Torr N<sub>2</sub> and H<sub>2</sub>O,  
 T=24.5°C, R(14) 971.930 cm<sup>-1</sup>.

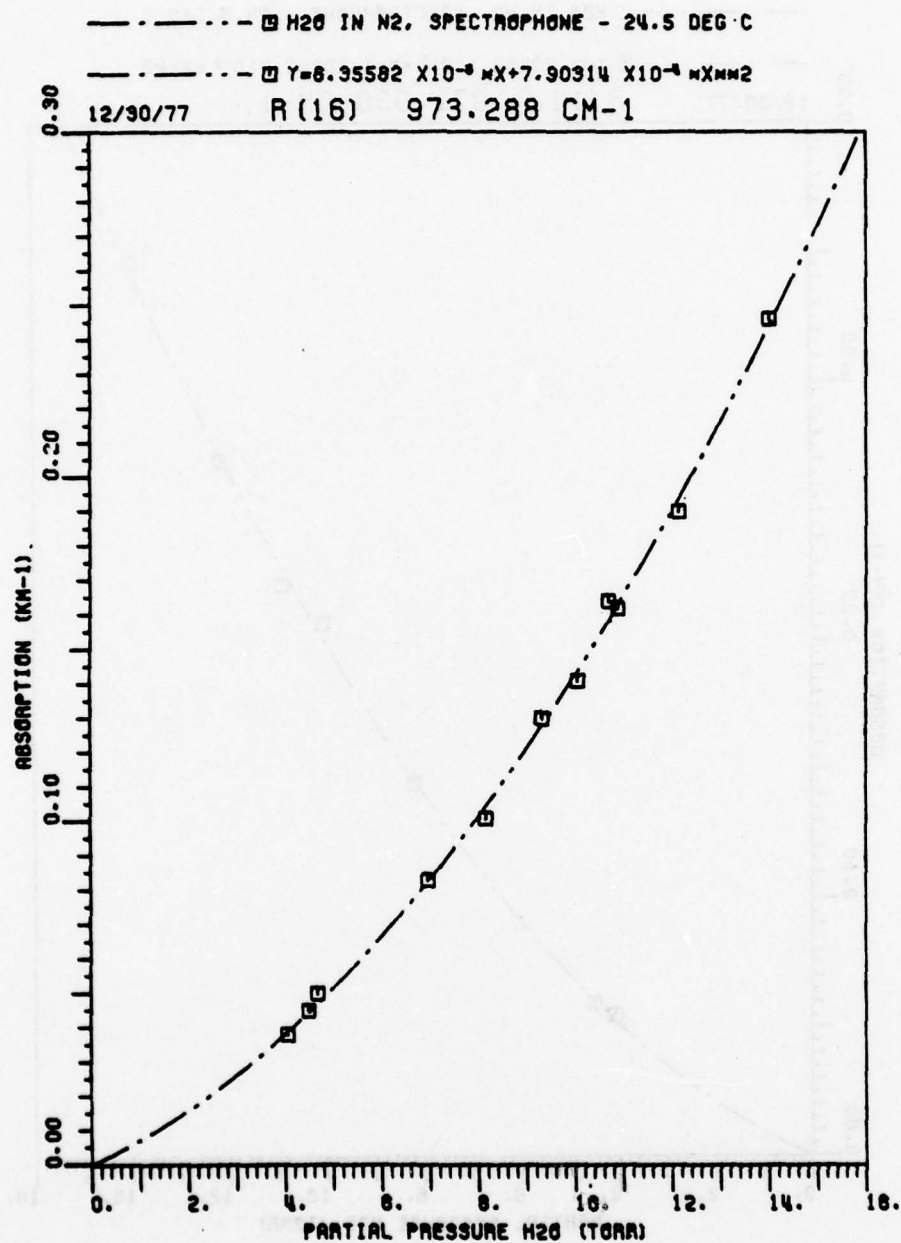


Figure 62. Spectrophone measurement, 760 Torr N<sub>2</sub> and H<sub>2</sub>O, T=24.5°C, R(16) 973.288 cm<sup>-1</sup>.

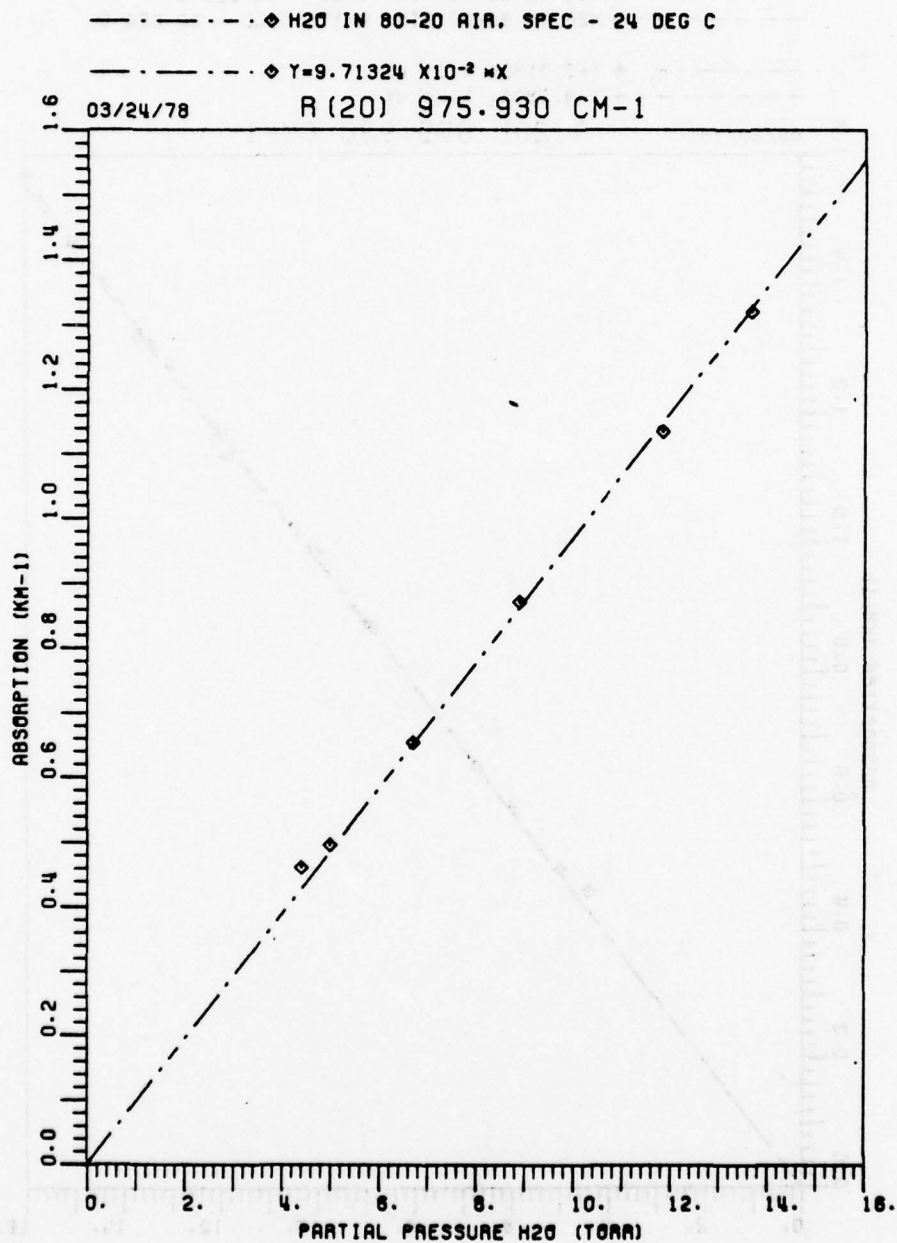


Figure 63. Spectrophone measurement, 760 Torr air and H<sub>2</sub>O,  
 T=24°C, R(20) 975.930 cm<sup>-1</sup>.

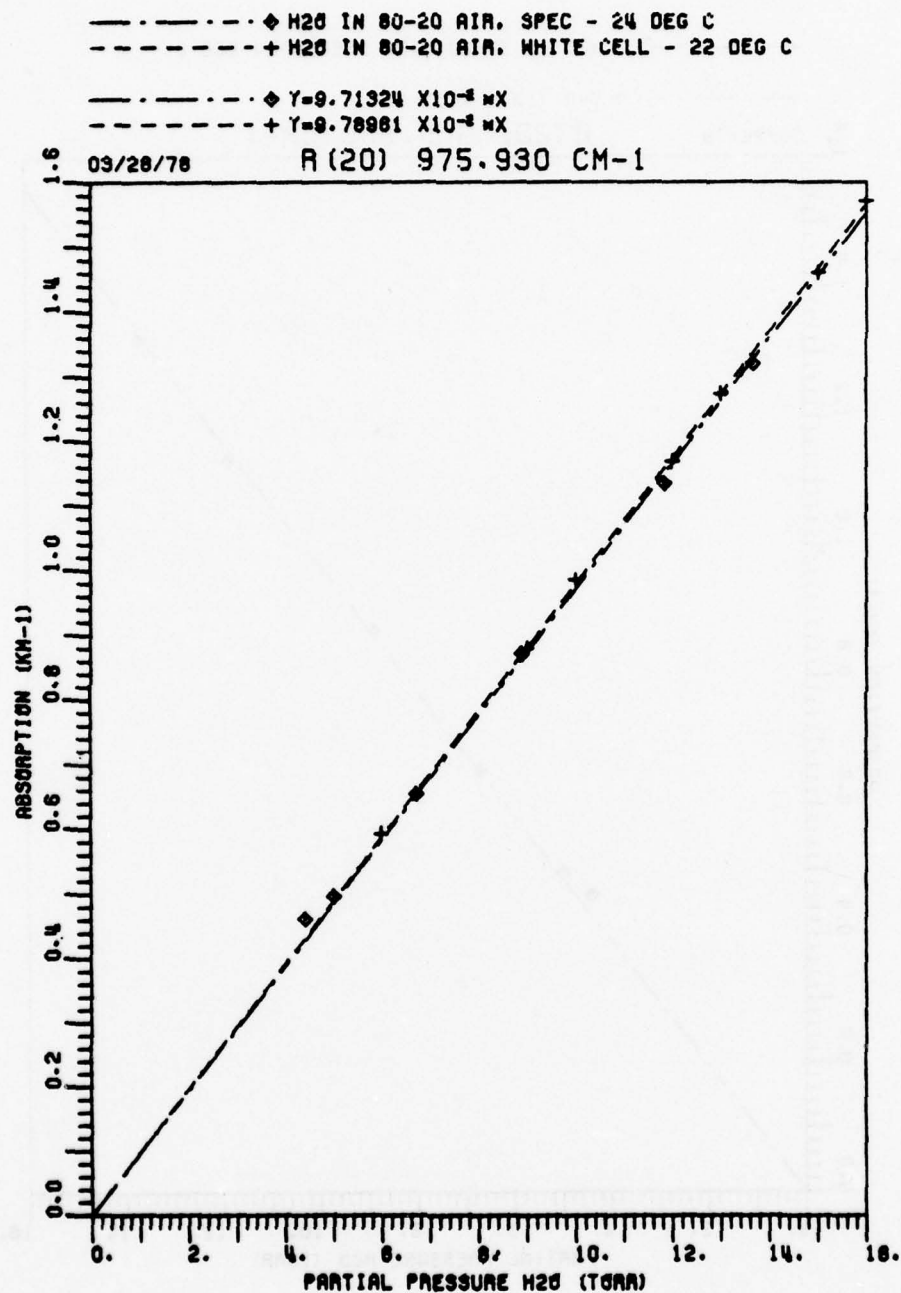


Figure 64. Comparison of White cell and spectrophone measurements, 760 Torr air and H<sub>2</sub>O, temperatures as noted, R(20) 975.930 cm<sup>-1</sup>.

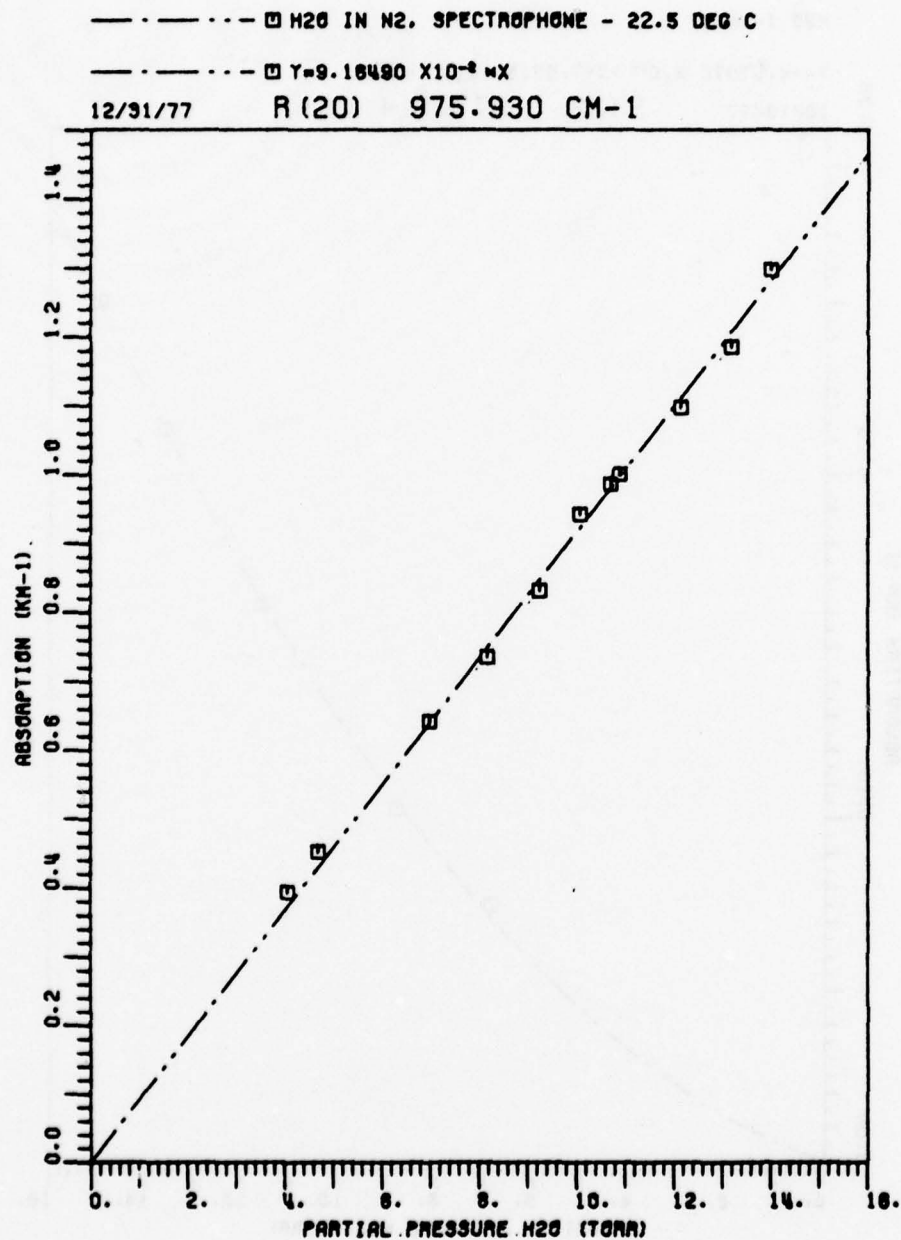


Figure 65. Spectrophone measurement, 760 Torr N<sub>2</sub> and H<sub>2</sub>O,  
 T=22.5°C, R(20) 975.930 cm<sup>-1</sup>.



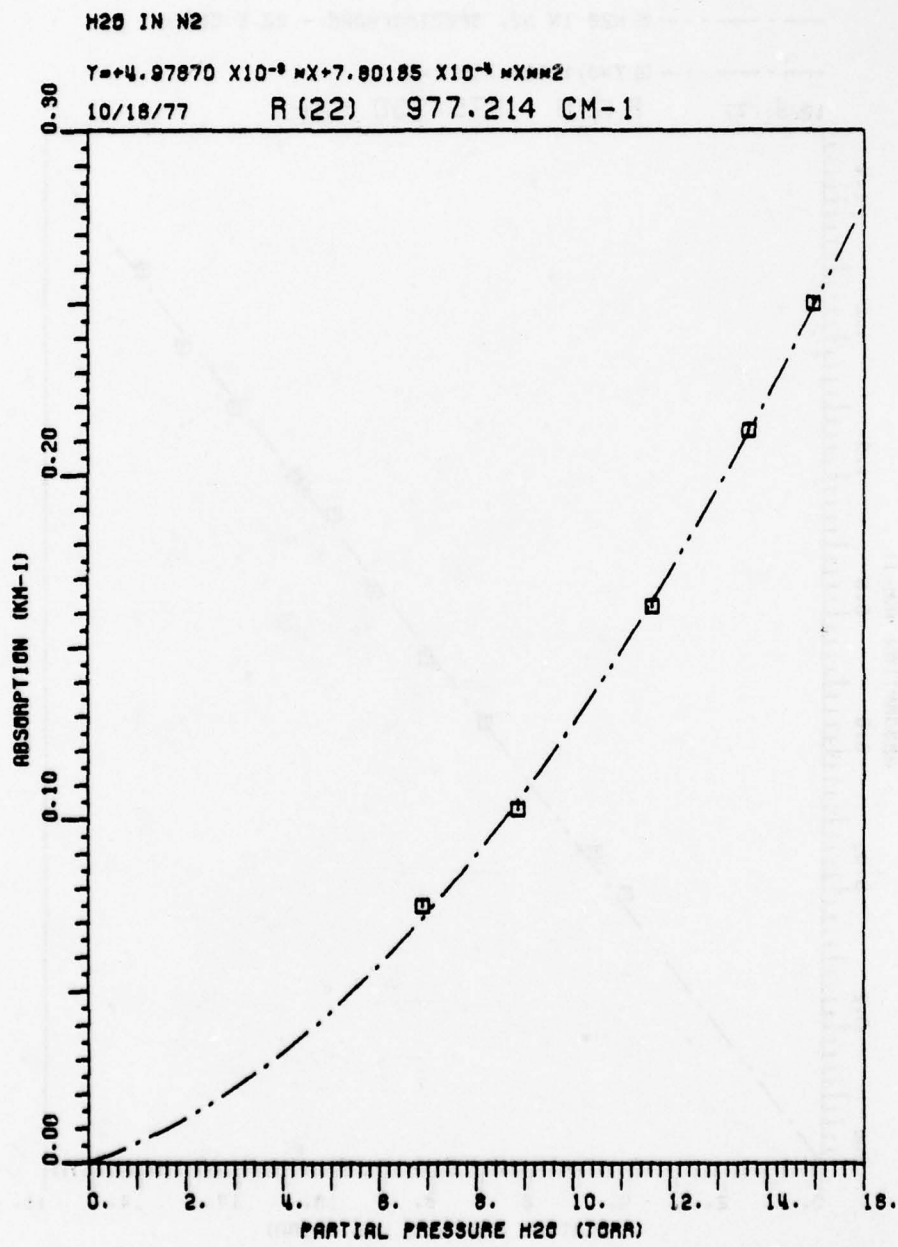


Figure 66. Spectrophone measurement, 760 Torr N<sub>2</sub> and H<sub>2</sub>O,  
T=24.5°C, R(22) 977.214 cm<sup>-1</sup>.

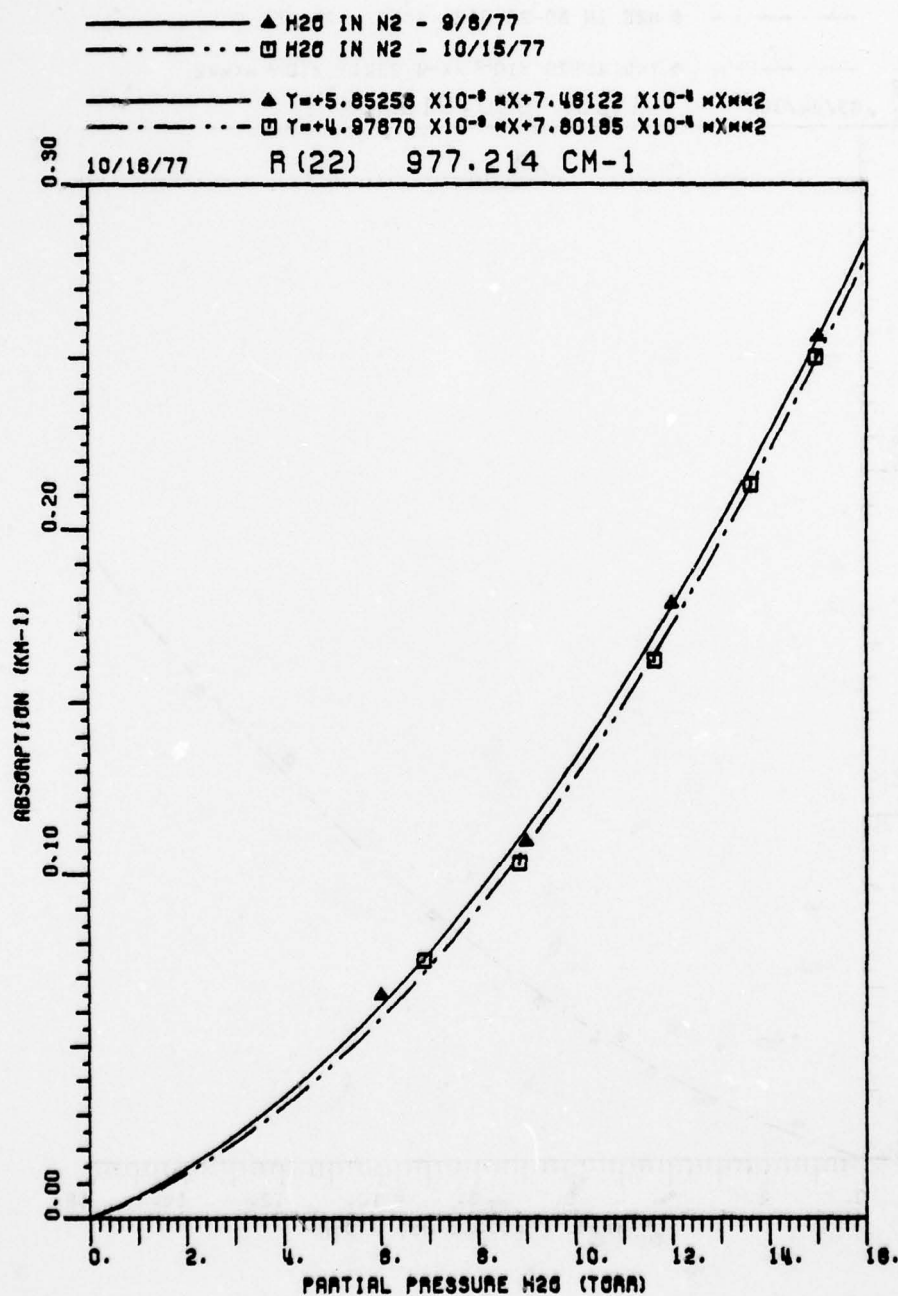


Figure 67. Comparison of White cell and spectrophone measurements, 760 Torr N<sub>2</sub> and H<sub>2</sub>O, R(22) 977.214 cm<sup>-1</sup>.

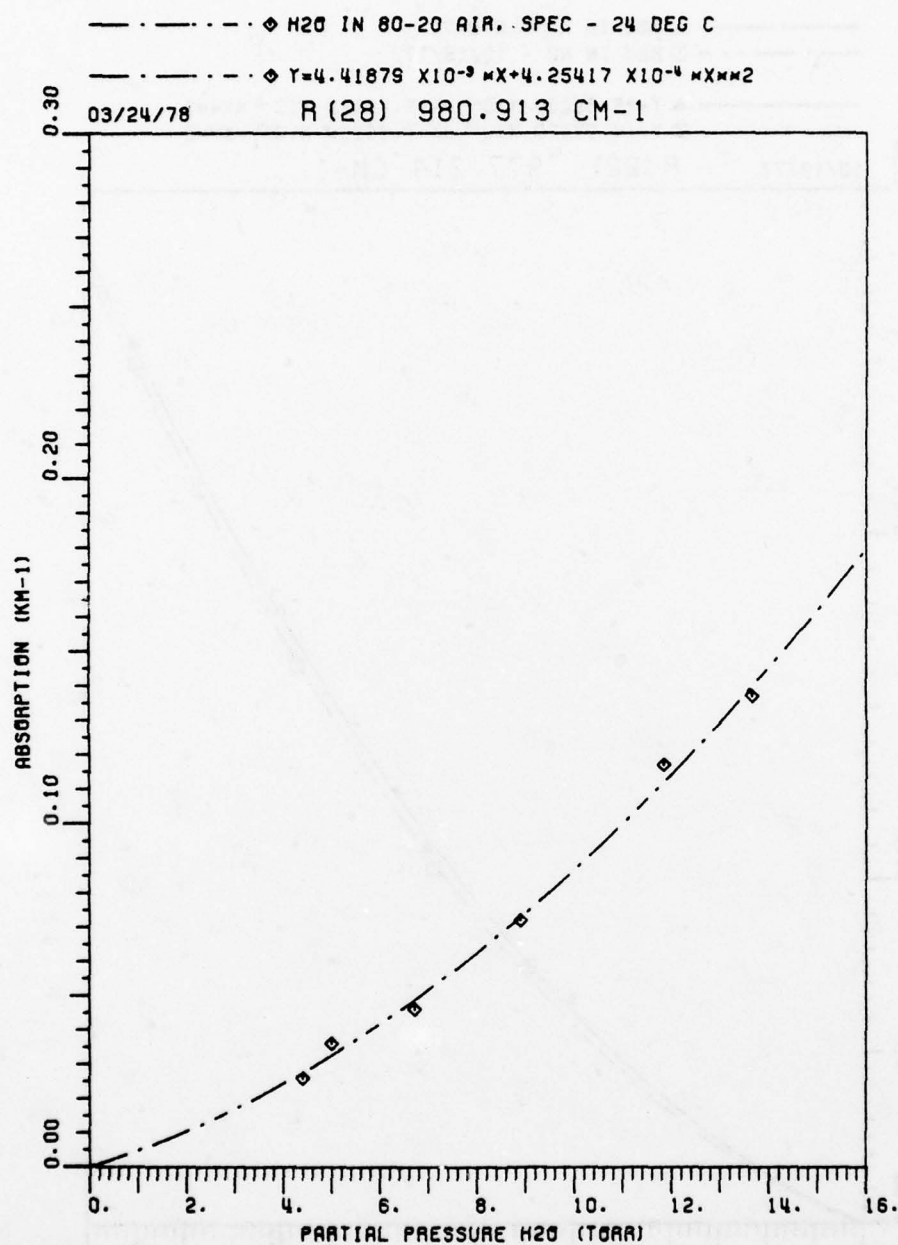


Figure 68. Spectrophone measurement, 760 Torr air and H<sub>2</sub>O, R(28) 980.913 cm<sup>-1</sup>.

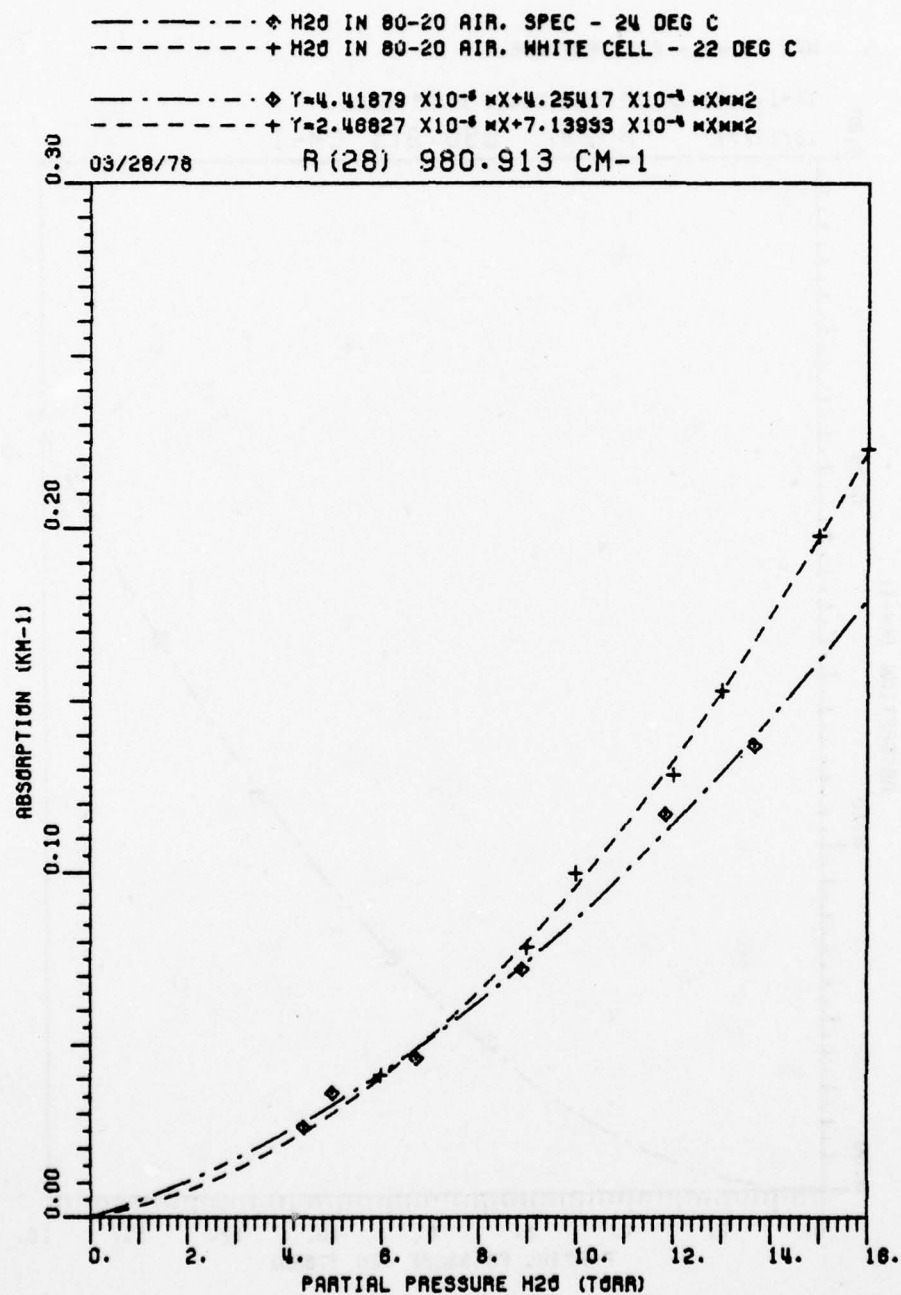


Figure 69. Comparison of White cell and spectrophone, 760 Torr air and H<sub>2</sub>O, temperatures as noted, R(28) 980.913 cm<sup>-1</sup>.

# H2O IN N2 - SPECTROPHONE

$$Y = +1.04034 \times 10^{-3} \text{ MX} + 8.58417 \times 10^{-5} \text{ MXMM}^2$$

10/17/77 R(28) 980.913 CM-1

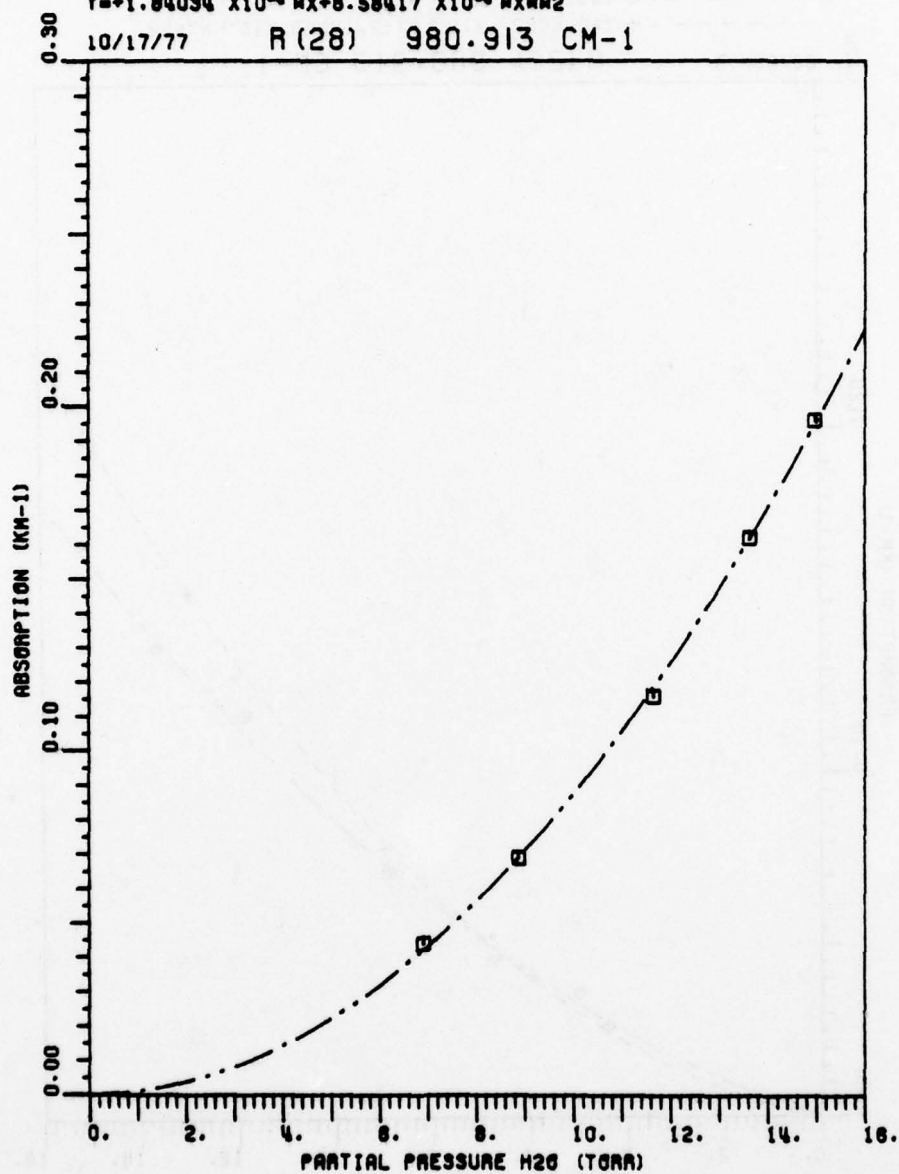


Figure 70. Spectrophone measurement, 760 Torr N<sub>2</sub> and H<sub>2</sub>O,  
T=25, R(28) 980.913 cm<sup>-1</sup>.



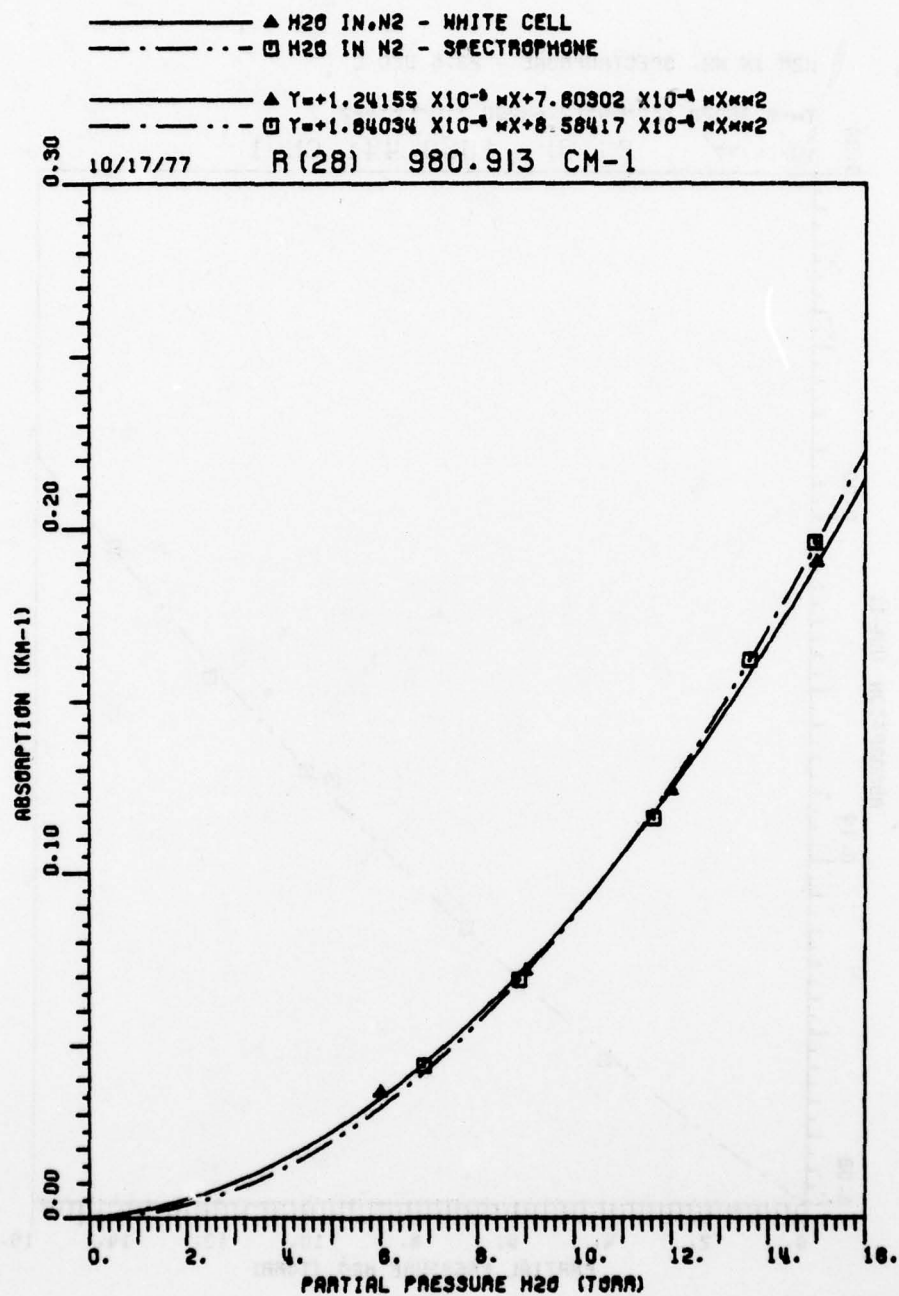


Figure 71. Comparison of White cell and spectrophone measurements, 760 Torr N<sub>2</sub> and H<sub>2</sub>O, R(28), T=25 980.913 cm<sup>-1</sup>.

H2O IN N2. SPECTROPHONE - 23.5 DEG C

$$Y = +9.38028 \times 10^{-6} X + 2.64290 \times 10^{-6} X^2$$

10/16/77 P (16) 1050.441 CM-1

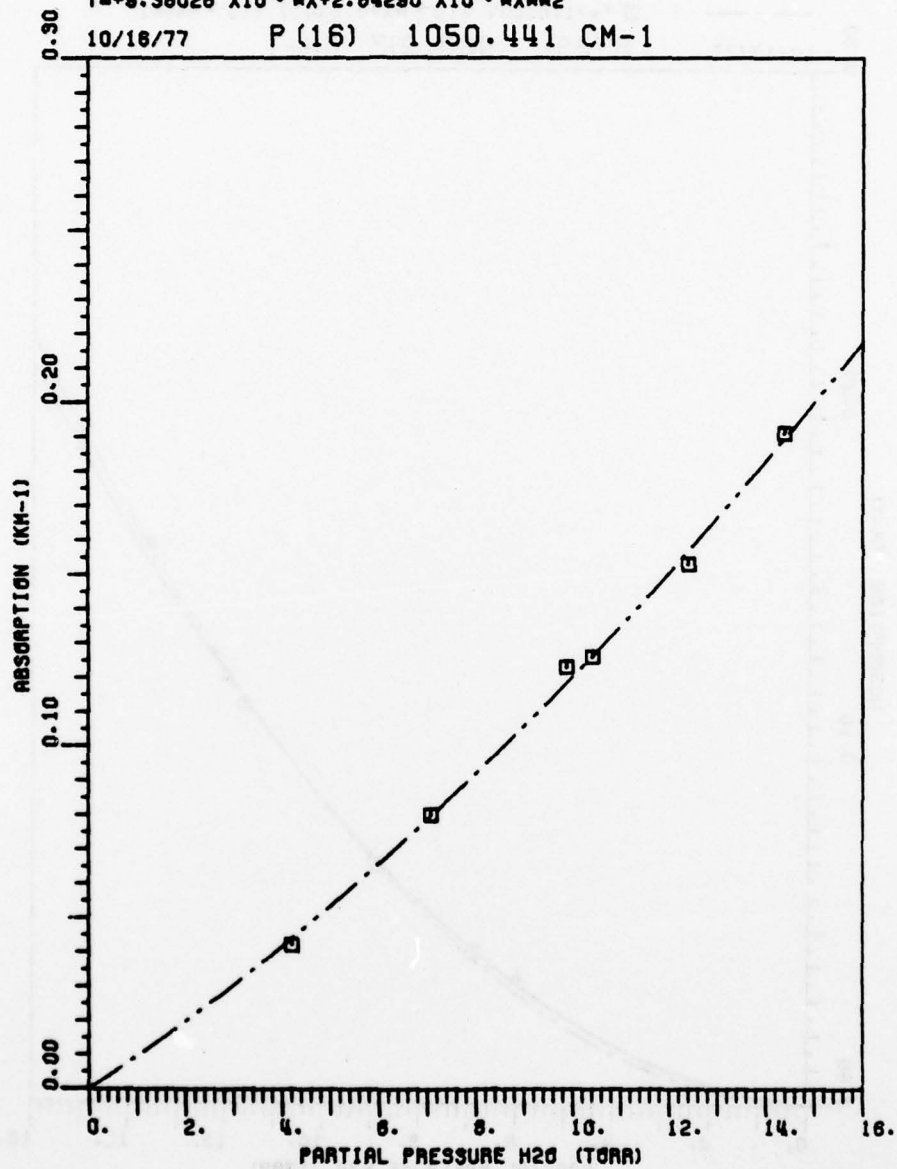


Figure 72. Spectrophone measurement, 760 Torr N<sub>2</sub> and H<sub>2</sub>O,  
T=23.5°C, P(16) 1050.441 cm<sup>-1</sup>

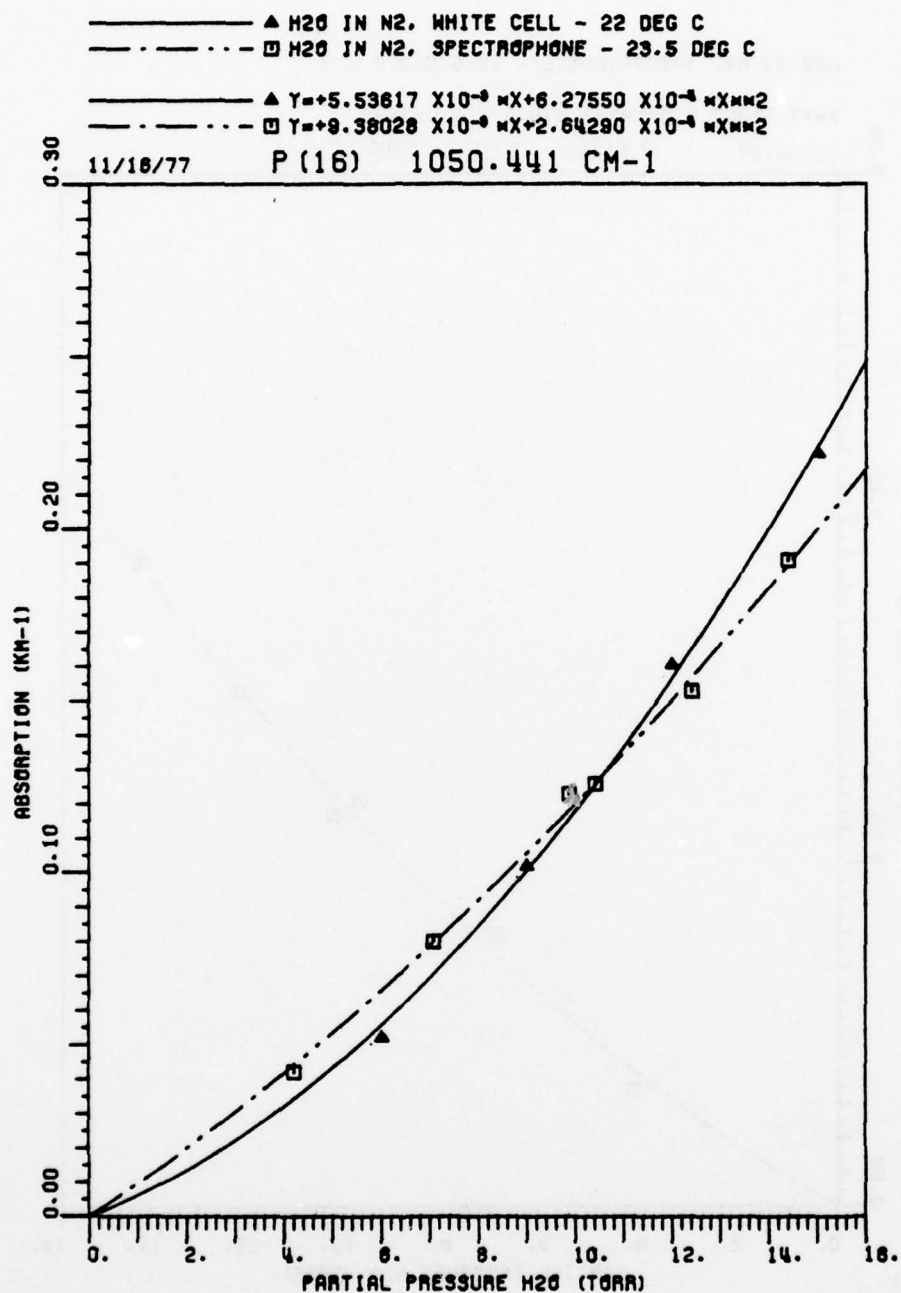


Figure 73. Comparison of White cell and spectrophone measurements, 760 Torr N<sub>2</sub> and H<sub>2</sub>O, T=23.5°C, P(16) 1050.441 cm<sup>-1</sup>.

H2O IN N2, SPECTROPHONE - 23.5 DEG C

$$Y = +7.91507 \times 10^{-3} X + 3.47979 \times 10^{-3} X^2$$

11/16/77 P (14) 1052.196 CM-1

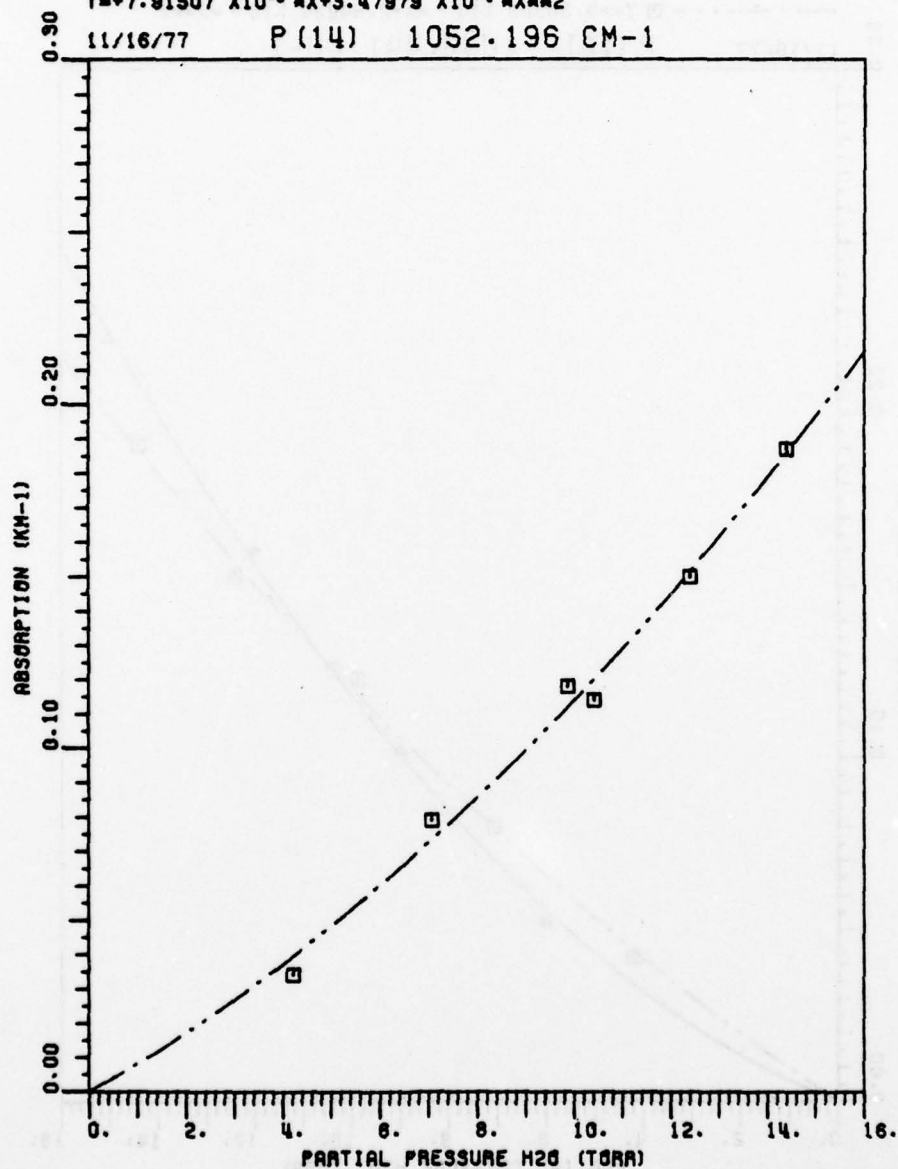


Figure 74. Spectrophone measurement, 760 Torr N<sub>2</sub> and H<sub>2</sub>O,  
T=23.5°C, P(14) 1052.196 cm<sup>-1</sup>.

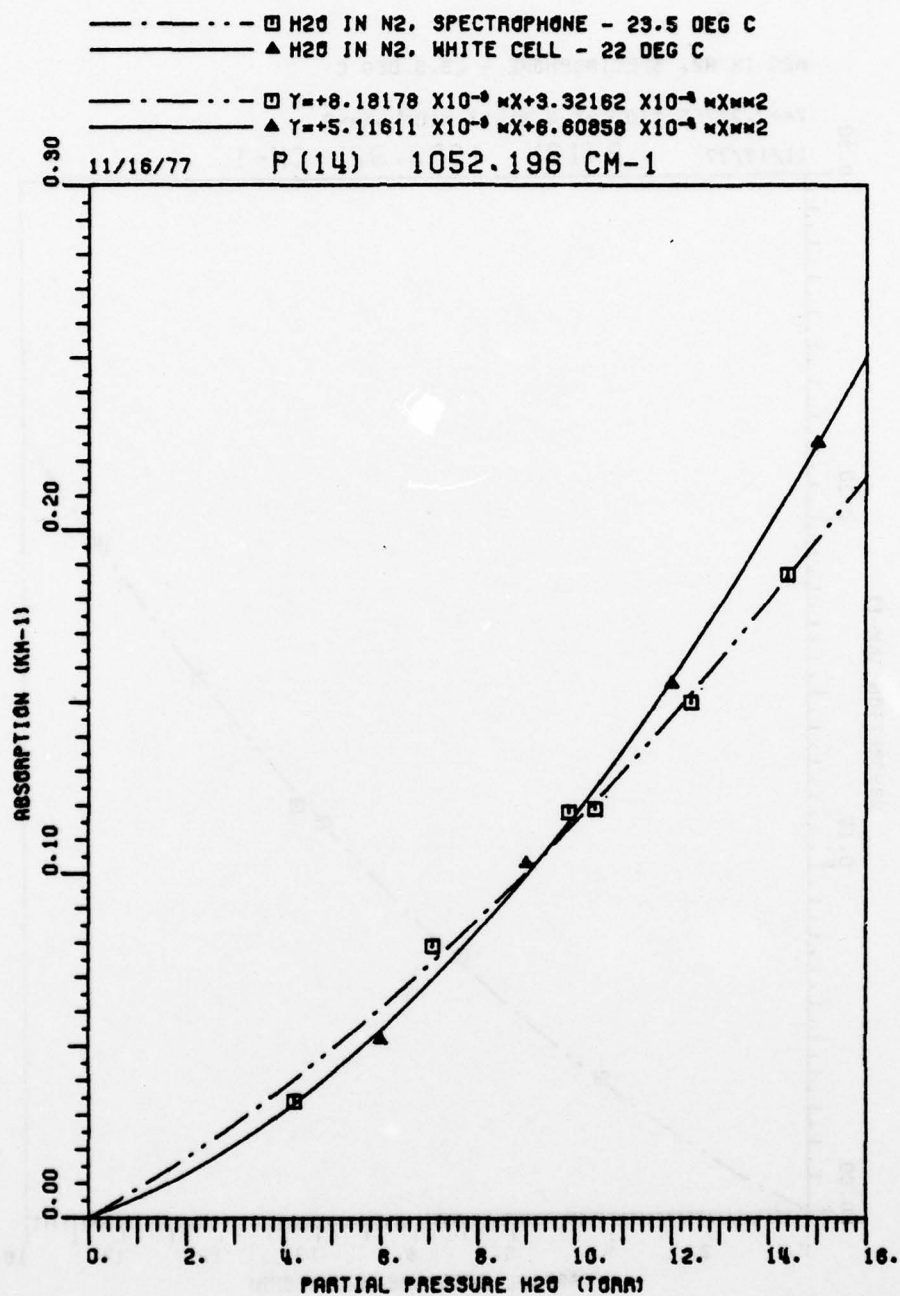


Figure 75. Comparison of White cell and spectrophone measurements, 760 Torr N<sub>2</sub> and H<sub>2</sub>O, T=23.5°C, P(14) 1052.196 cm<sup>-1</sup>.



H2O IN N2. SPECTROPHONE - 23.5 DEG C

$$Y = +7.24755 \times 10^{-3} X + 4.31413 \times 10^{-3} X^2$$

11/18/77 P (12) 1053.924 CM-1

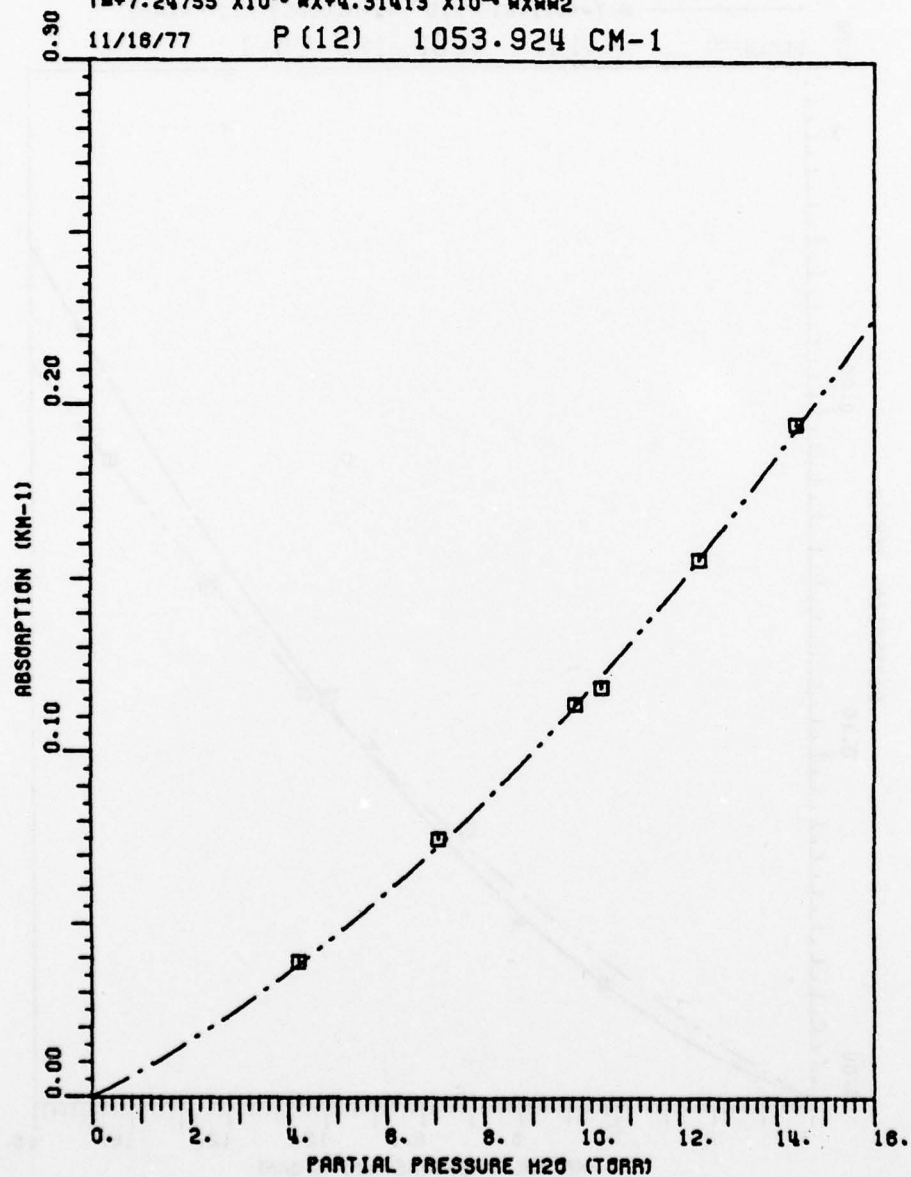


Figure 76. Spectrophone measurement, 760 Torr N<sub>2</sub> and H<sub>2</sub>O,  
T=23.5°C, P(12) 1053.924 cm<sup>-1</sup>.

H2O IN N2. SPECTROPHONE - 24 DEG C

$$Y = 3.05358 \times 10^{-3} X + 8.52058 \times 10^{-4} X^2$$

12/29/77 R(12) 1073.278 CM-1

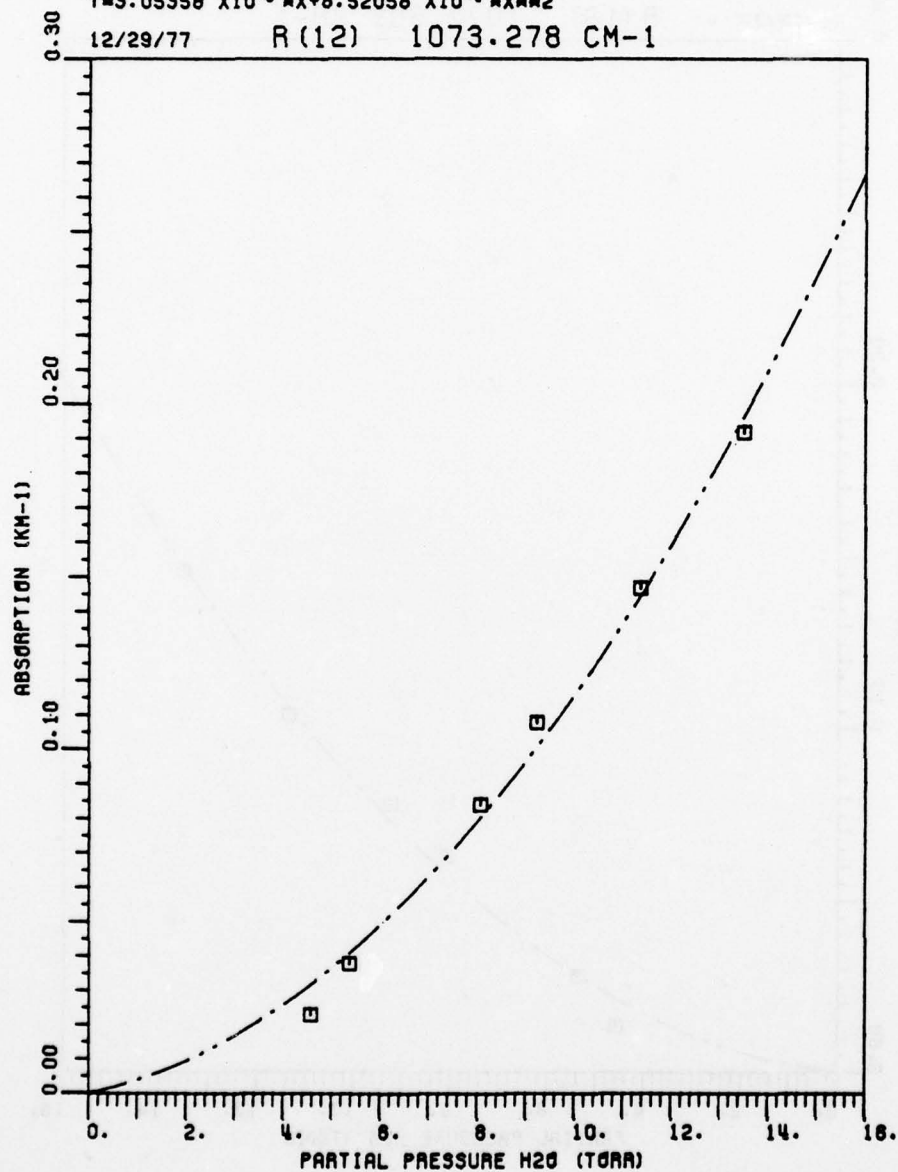


Figure 77. Spectrophone measurement, 760 Torr N<sub>2</sub> and H<sub>2</sub>O,  
T=24°C, R(12) 1073.278 cm<sup>-1</sup>.

H2O IN N2. SPECTROPHONE - 24 DEG C

$$Y = +1.51226 \times 10^{-3} X + 8.94418 \times 10^{-4} X^2$$

10/16/77 R (18) 1077.303 CM-1

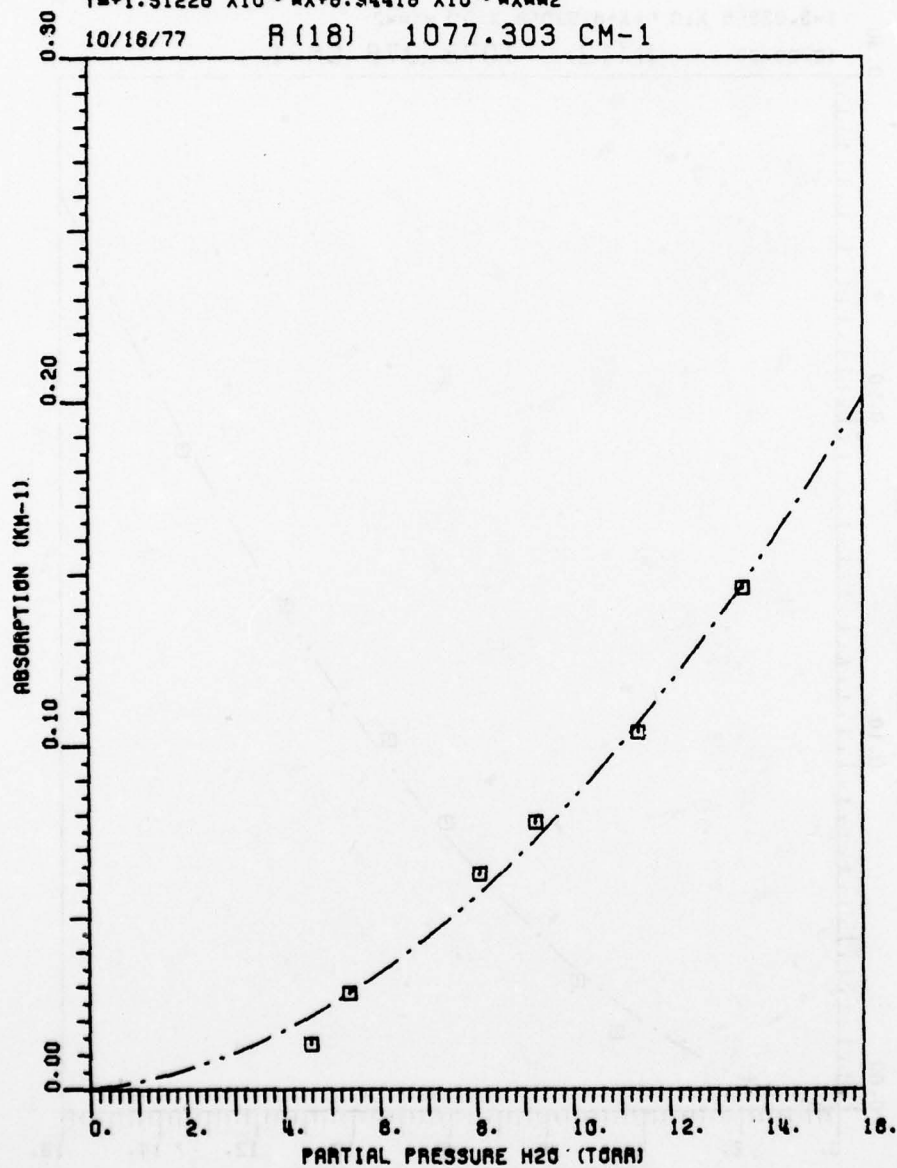


Figure 78. Spectrophone measurement, 760 Torr N<sub>2</sub> and H<sub>2</sub>O,  
T=24°C, R(18) 1077.303 cm<sup>-1</sup>.

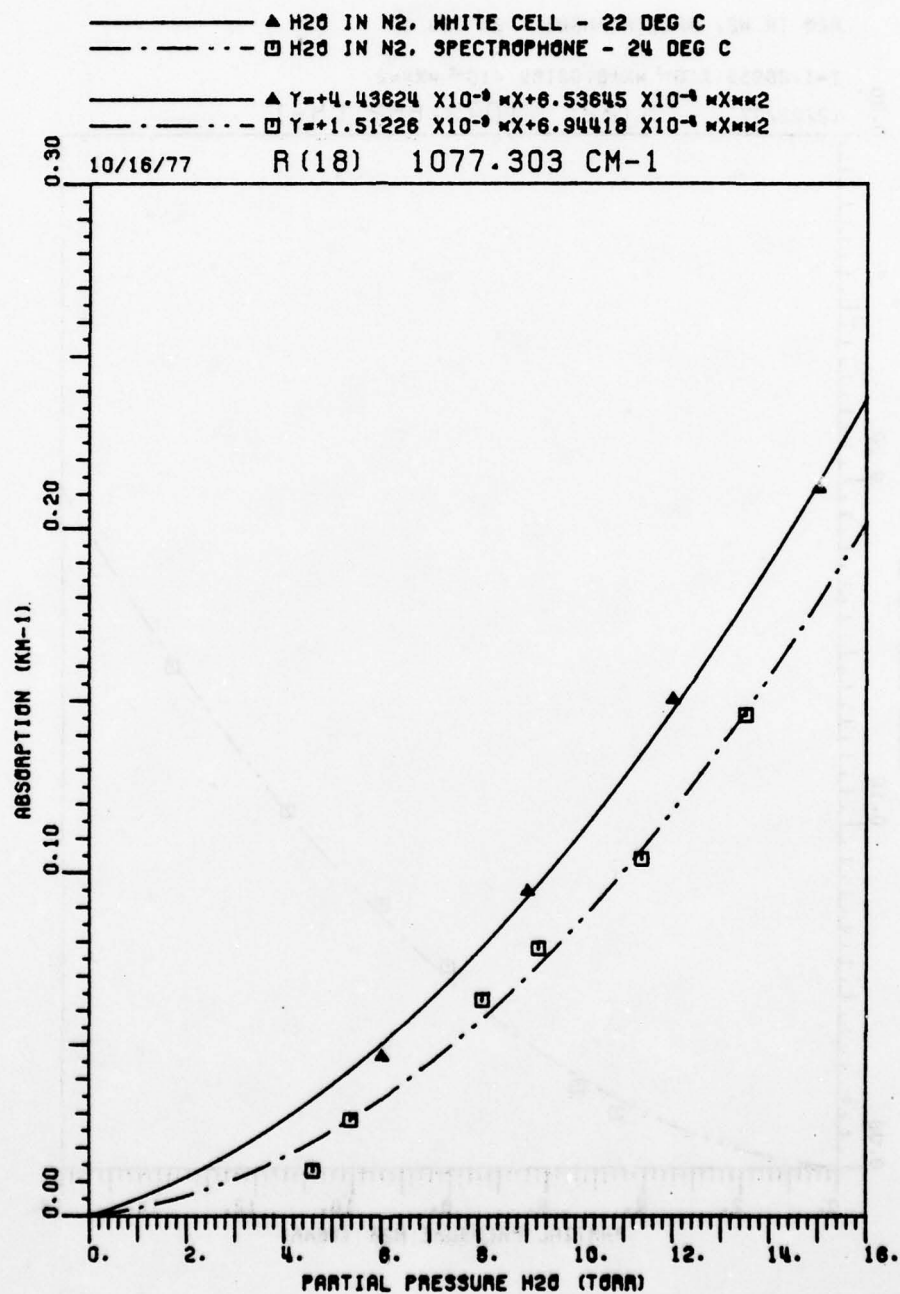


Figure 79. Comparison of White cell and spectrophone measurements, temperatures as noted, N<sub>2</sub> and H<sub>2</sub>O, R(18) 1077.303 cm<sup>-1</sup>.

H2O IN N2, SPECTROPHONE - 24 DEG C

$$Y = 1.28935 \times 10^{-5} X + 6.92194 \times 10^{-5} X^2$$

12/29/77 R(22) 1079.852 CM-1

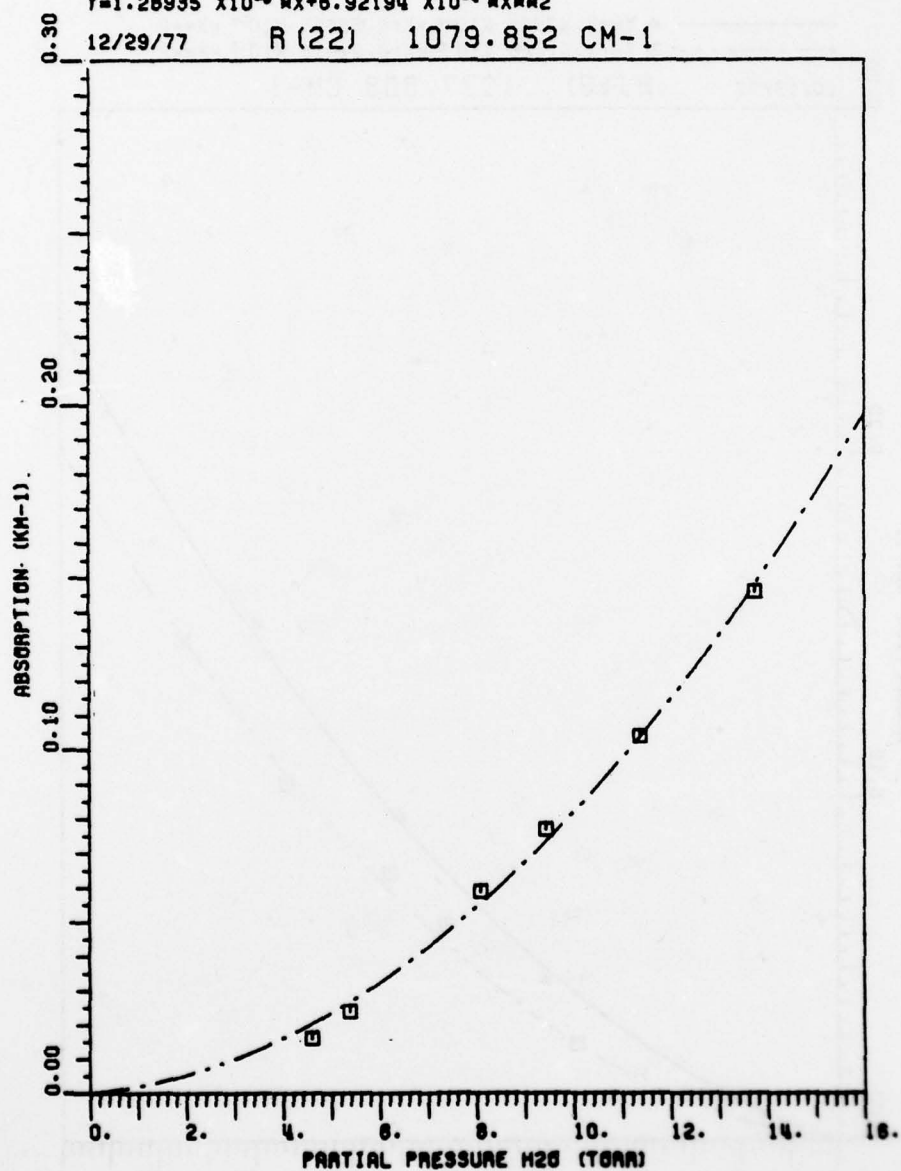


Figure 80. Spectrophone measurement,  $N_2$  and  $H_2O$ ,  
 $T=24^{\circ}C$ ,  $R(22)$  1079.852  $cm^{-1}$ .



H<sub>2</sub>O IN N<sub>2</sub>. SPECTROPHONE - 24 DEG C

$$Y = 4.97635 \times 10^{-3} X + 7.89288 \times 10^{-4} X^2$$

12/29/77 R(24) 1081.087 CM-1

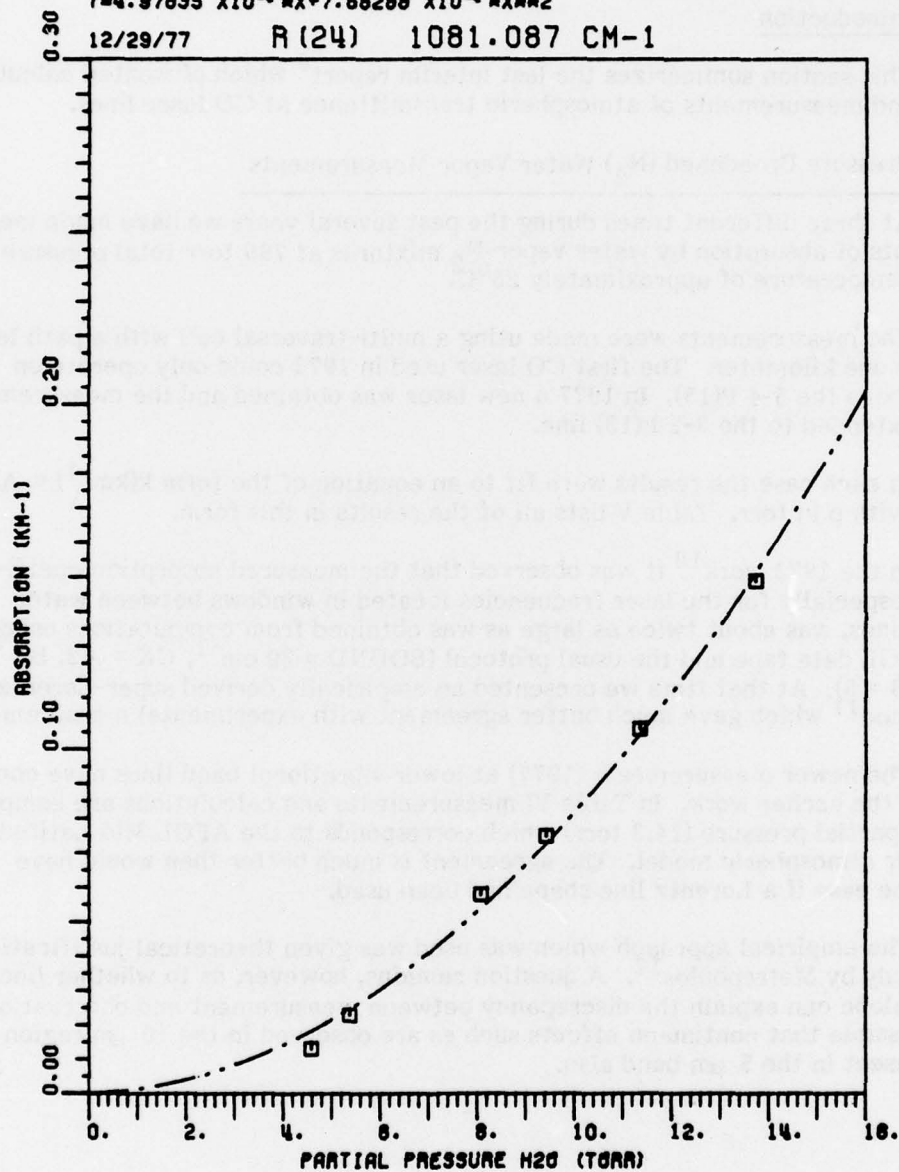


Figure 81. Spectrophone measurement,  $N_2$  and  $H_2O$ ,  
 $T=24^\circ C$ ,  $R(24)$  1081.087  $cm^{-1}$ .

## SECTION II

### WATER VAPOR ABSORPTION MEASUREMENTS USING A CO LASER

#### A. Introduction

This section summarizes the last interim report<sup>9</sup> which presented calculations and measurements of atmospheric transmittance at CO laser lines.

#### B. Pressure Broadened (N<sub>2</sub>) Water Vapor Measurements

At three different times during the past several years we have made measurements of absorption by water vapor-N<sub>2</sub> mixtures at 760 torr total pressure and a temperature of approximately 23°C.

The measurements were made using a multi-traversal cell with a path length of near one kilometer. The first CO laser used in 1973 could only operate on lines above the 5-4 P(15). In 1977 a new laser was obtained and the measurements were extended to the 3-2 P(13) line.

In each case the results were fit to an equation of the form  $k(\text{km}^{-1}) = Ap + Bp^2$  with  $p$  in torr. Table V lists all of the results in this form.

In the 1973 work<sup>10</sup> it was observed that the measured absorption coefficient, especially for the laser frequencies located in windows between water vapor lines, was about twice as large as was obtained from computations using the AFGL data tape and the usual protocol (BOUND = 20 cm<sup>-1</sup>, CX = .62, BX = 1.5, B = 5). At that time we presented an empirically derived super-Lorentz line shape<sup>11</sup> which gave much better agreement with experimental measurements.

The newer measurements (1977) at lower vibrational band lines have confirmed the earlier work. In Table VI measurements and calculations are compared at one partial pressure (14.3 torr) which corresponds to the AFGL Mid Latitude Summer atmospheric model. The agreement is much better than would have been the case if a Lorentz line shape had been used.

The empirical approach which was used was given theoretical justification in a study by Metropoulos<sup>12</sup>. A question remains, however, as to whether line shape alone can explain the discrepancy between measurement and observation. It is possible that continuum effects such as are observed in the 10 μm region are present in the 5 μm band also.

Group I (1973)

Line	Iden.	Wavenumber	Experimental Absorption Coefficient Equation
11-10	P(12)	1837.430	$(12.19)p + (.023)p^2$
10-9	P(14)	1854.927	$(3.26E-1)p + (2.83E-3)p^2$
9-8	P(16)	1872.231	$(1.18)p + (.0135)p^2$
	P(14)	1880.343	$(2.03E-1)p + (4.03E-3)p^2$
8-7	P(14)	1905.836	$(2.96E-1)p + (3.46E-3)p^2$
7-6	P(15)	1927.296	$(1.78E-1)p + (2.20E-3)p^2$
	P(14)	1931.405	$(1.31E-1)p + (1.24E-3)p^2$
6-5	P(16)	1948.727	$(1.50E-1)p + (2.42E-3)p^2$
	P(15)	1952.904	$(7.98E-2)p + (1.49E-3)p^2$
	P(14)	1957.049	$(3.75E-1)p - (2.27E-3)p^2$
5-4	P(17)	1970.128	$(1.28E-1)p + (2.12E-3)p^2$
	P(16)	1974.373	$(3.71E-2)p + (1.25E-3)p^2$
	P(15)	1978.585	$(3.38E-2)p + (9.12E-4)p^2$

Group II (1977a)

6-5	P(14)	1957.049	$(3.4E-1)p - (2.15E-3)p^2$
5-4	P(15)	1978.585	$(3.25E-2)p + (4.96E-4)p^2$
4-3	P(13)	2012.734	$(5.05E-2)p + (3.02E-4)p^2$
	P(10)	2025.079	$(3.77E-2)p + (2.06E-4)p^2$

Group III (1977b)

5-4	P(9)	2003.165	$(3.83E-2)p + (3.15E-4)p^2$
4-3	P(15)	2004.337	$(3.96E-2)p + (1.756E-4)p^2$
	P(9)	2029.128	$(1.67E-2)p + (1.704E-4)p^2$
3-2	P(13)	2038.625	$(4.06E-2)p + (2.93E-4)p^2$

Measurements of absorption coefficient  $k(\text{km}^{-1}) = Ap + Bp^2$  with water pressure  $p$  in Torr for CO laser lines. Total pressure using  $\text{N}_2$  buffer gas was 760 Torr and temperature approximately  $23^\circ\text{C}$  for all lines.

Table V

Group I (1973)

Line	Iden.	Computed (SuperLorentz)	Measured	Diff. %
11-10	P(12)	2.06E2	1.79E2	+15
10-9	P(14)	4.73	5.22	-9.4
9-8	P(14)	3.17	3.47	-8.6
	P(16)	15.2	19.6	-22.4
8-7	P(14)	4.57	4.92	-7.1
7-6	P(15)	3.13	2.99	+4.7
	P(14)	1.93	2.12	-9.
6-5	P(16)	2.93	2.63	+11.4
	P(15)	1.26	1.44	-12.5
	P(14)	4.16	4.89	-14.9
5-4	P(17)	2.26	2.26	0
	P(16)	.599	.783	-23.4
	P(15)	.415	.667	-38.

Group II (1977a)

6-5	P(14)	4.16	4.42	-5.9
5-4	P(15)	.415	.566	-27.
4-3	P(13)	.697	.784	-11.
	P(10)	.610	.581	+5.

Group III (1977b)

5-4	P(9)	.492	.612	-19.6
4-3	P(15)	.422	.602	-30.
	P(9)	.251	.274	-8.
3-2	P(13)	.465	.640	-27.

Comparison of measured and computed absorption coefficients for CO laser  
lines at 14.3 Torr H<sub>2</sub>O pressure, 760 Torr total.

Table VI



Figures 82-85 present the experimental White cell data for the latest group of lines (1977b in Table V). Several conclusions can be reached from this study. There are many CO laser lines with absorption coefficients small enough to be useful candidates for applications even in the lower atmosphere. The number of such lines and the best attenuation improve if the laser can operate on the 5-4 and lower vibrational bands. However, there is a serious problem with our ability to model the observed absorption using the AFGL data tape. The use of the enhanced wing line shape is a stop gap measure. Additional fundamental investigations should be pursued in such areas as line shape, foreign and self broadening effects, etc. in order to improve the modeling capability in this wavelength region.



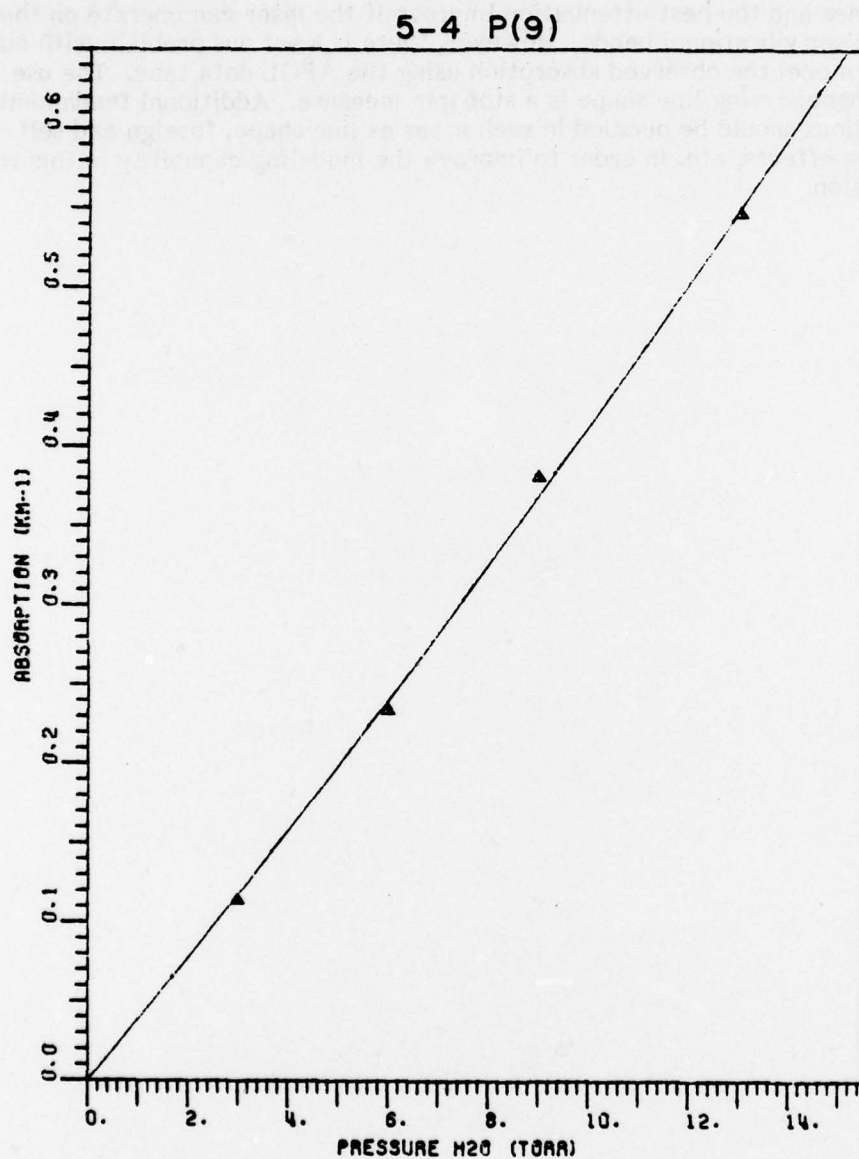


Figure 82. Measurement of water vapor absorption coefficient,  
760 Torr  $N_2$  and  $H_2O$ ,  $T=22C$ , 5-4 P(9) CO laser  
line at  $2003.165\text{ cm}^{-1}$ .

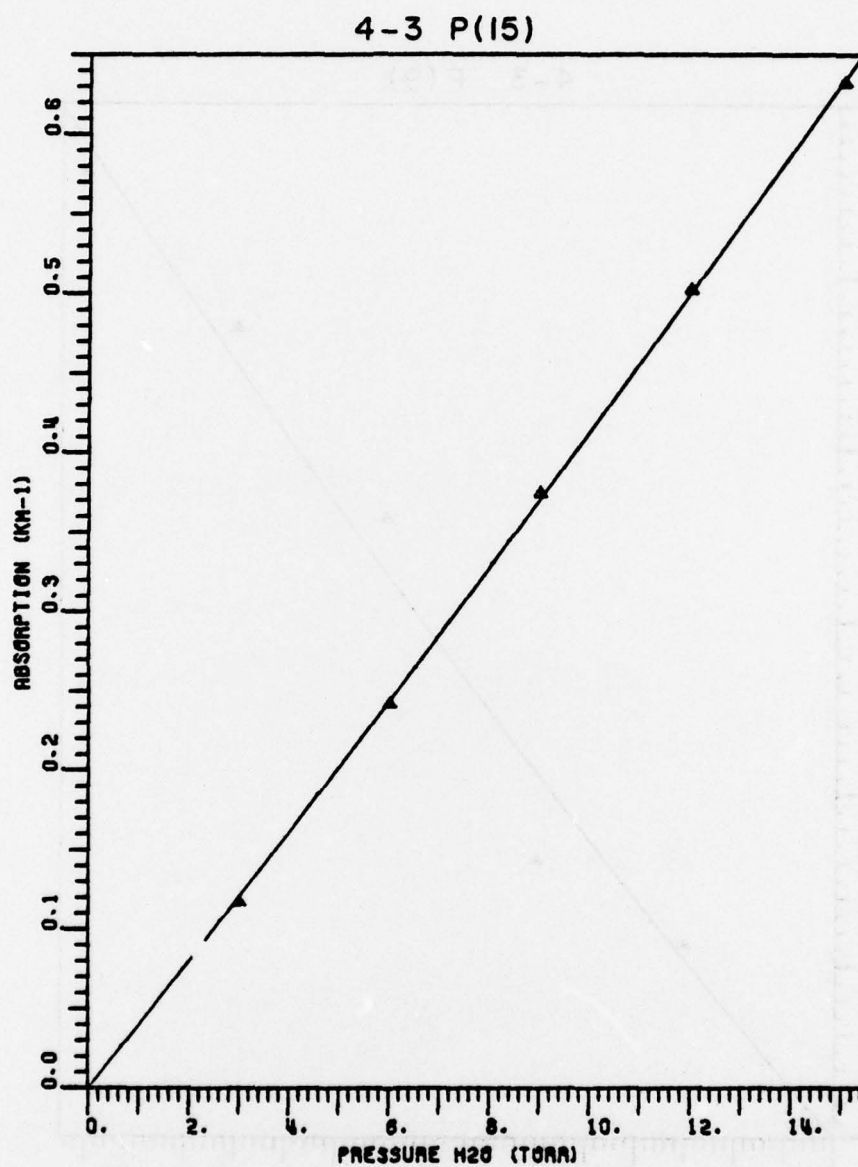


Figure 83. Measurement of water vapor absorption coefficient, 760 Torr  $N_2$  and  $H_2O$ ,  $T=22^\circ C$ , 4-3 P(15) CO laser line at  $2004.337\text{ cm}^{-1}$ .

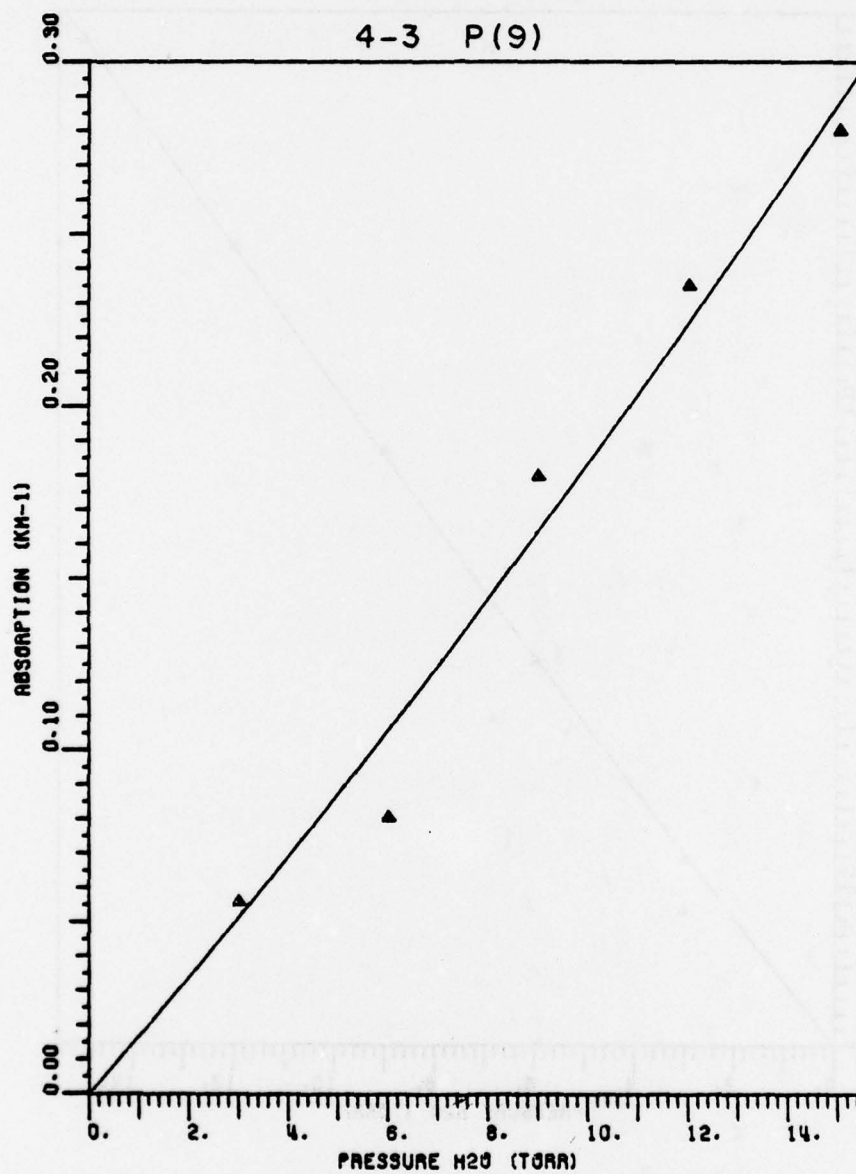


Figure 84. Measurement of water vapor absorption coefficient,  
760 Torr N<sub>2</sub> and H<sub>2</sub>O, T=22.5C, 4-3 P(9) CO laser  
line at 2029.128 cm<sup>-1</sup>.

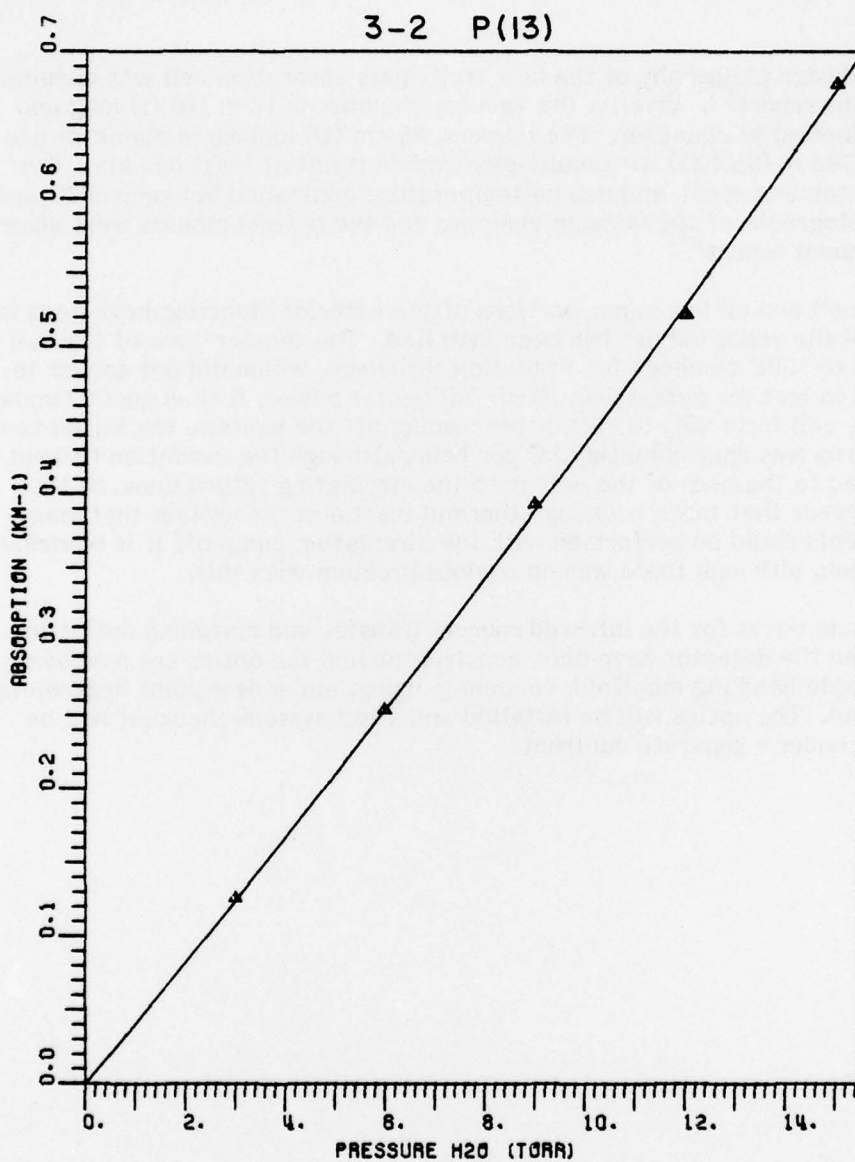


Figure 85. Measurement of water vapor absorption coefficient,  
760 Torr N<sub>2</sub> and H<sub>2</sub>O, T=22C, 3-2 P(13) CO laser  
line at 2038.625 cm<sup>-1</sup>.

### SECTION III CONSTRUCTION OF A NEW LONG PATH ABSORPTION CELL

The design philosophy of the new multi-pass absorption cell was documented in a previous report<sup>13</sup>. Briefly, the vacuum chamber is 12 m (40 ft) long and 0.6 m (24 inches) in diameter. The mirrors, 25 cm (10 inches) in diameter are spaced 10.785 m (35.4 ft) with multi-pass capability of at least one km. The system is stainless steel, and can be temperature controlled between -60C and +60C. Photographs of the vacuum chamber and the optical mounts were shown in a subsequent report<sup>14</sup>.

The cell and all but minor portions of the exterior plumbing have been insulated and the vapor barrier has been installed. The temperature of the cell was raised to +50C to check for insulation shrinkage, which did not appear to occur, and to test for outgassing. With full heater power, it took about two hours to heat the cell from 25C to 50C; after turning off the heaters, the initial temperature drop was approximately 1C per hour, although the insulation had not been applied to the ends of the cell or to the circulating return lines, so that it would appear that there is enough thermal inertia in the system that many measurements could be performed with the circulating pump off if it contributes any vibration, although there was no obvious problem with this.

Vacuum boxes for the infrared source, transfer and matching optics to the cell, and the detector have been constructed and the optics are now being installed. A sample handling manifold, vacuum gauging, and a dew-point hygrometer are installed. The optics will be installed and a full system checkout will be performed under a separate contract.



## SECTION IV DEVELOPMENT OF A SMALL SINGLE-MODE CW HF-DF LASER

### A. Introduction

#### 1. Background

The continuous wave HF-DF chemical laser described in this report was designed and constructed for use as a source of highly directional, monochromatic radiation in experiments measuring the absorption of such radiation by various molecular gases. This type of experimentation demands a laser with the following characteristics - a high degree of stability, single-mode operation over a broad spectral range, and sufficient power to provide a good signal-to-noise ratio in the acquisition of experimental data. The fulfillment of all these requirements has recently been made possible by the development of small HF-DF mixing lasers<sup>15,16,17</sup>.

Chemical lasers have been in existence for twelve years, since the successful achievement of laser emission from a HCl "explosion" system by Kasper and Pimentel in 1965<sup>18</sup>. At this time it was recognized that certain highly exothermic chemical reactions resulted in the creation of "excited" reaction products - molecules boosted to a higher quantum state by energy released in the reaction. Laser radiation resulted when the ratio of population density of excited molecules to those in the unexcited or "ground" state was sufficiently high to provide an amplifying medium for the stimulated emission of radiation.

The reaction of molecular hydrogen with dissociated atomic fluorine was one of the first ones investigated<sup>19</sup>. This reaction releases  $1.31 \times 10^5$  joules of energy per mole, which is sufficient to populate the first three vibrational levels above ground state in the HF molecule, while the corresponding reaction involving deuterium is enough to populate the first four vibrational levels of excitation for that molecule.

The major physical limitation in HF-DF laser systems arises from the fact that ground state molecules in both cases are very effective collisional deactivators of excited molecules in addition to being strong absorbers of the radiation emitted by these molecules<sup>20</sup>. Creation of a high degree of population inversion in a given volume, such as that comprising the optical cavity region in an oscillatory laser system, necessarily implies a high flow rate of reactants through this region in order to keep the concentration of "spent" reaction products as low as possible.

This principle was incorporated in the first continuous wave HF-DF laser system built by Spencer et al. in 1969<sup>21</sup>. This system was studied extensively and refined to the point where a power output of 1700W at a 10% chemical efficiency was achieved. Although these figures are impressive, this large-scale supersonic flow system involved engineering too complex to allow it to be scaled down to more moderate laboratory requirements. Moreover, the turbulent nature of the mixing process and huge vacuum pumps required precluded realization of good stability in power output or high beam quality.

These requirements were met with the development of subsonic flow electrical discharge driven lasers by several researchers<sup>15,16,17</sup>. Although these devices have a markedly lower efficiency than supersonic systems, they are comparatively simple and inexpensive to build. The laser described in this report is based on a design derived by Dr. J. J. Hinchey<sup>16</sup> and represents the current state-of-the-art where stability, economy of operation and simplicity of technology are the desired features.

## 2. Research Objectives

The efforts described below cover the construction of the laser system and subsequent investigations of its performance and the parameters governing it in hopes of determining optimum operating conditions as well as any design modifications that would enhance performance. The following research agenda was drawn up, covering several lines of inquiry:

- a) Construction of laser system.
- b) Attempts to achieve multiline HF lasing through variation of reactant and diluent flow rates, discharge current and voltage, optical alignment and transverse positioning of the optical cavity to determine necessary and correct values. On achievement of lasing, variation of each parameter to determine its effect on multiline power output.
- c) Repeat of b) using deuterium in place of hydrogen. Comparison of output characteristics as a function of parameter variations listed above.
- d) Installation of diffraction grating to allow narrow band frequency tuning of the optical cavity, i.e., selective single line output on a range of specific vibrational-rotational laser transitions.
- e) Spectrometer identification of observed transitions.
- f) Variation of operating parameters to determine means of maximum enhancement of individual laser lines.
- g) Output coupling studies to determine optimal output mirror reflectivity.
- h) Short-term stability measurements using a fast detector.

It should be emphasized here that the approach taken in these studies was highly empirical. The theoretical modeling of chemical mixing lasers is an extremely involved problem in chemical kinetics and fluid mechanics, and so has entered into our treatment only in a general and qualitative manner. Although experimental lines of inquiry were drawn largely from the work of previous researchers rather than by application of theoretical hypothesis, our approach was ultimately productive, with laser performance that in several respects surpasses that reported in Reference 16.

Although some conclusions as to how this system might be further refined were arrived at, it should be recognized that this process is open-ended. Limitations on time and resources precluded the implementation of some of these conclusions as well as the investigation of some other facets of the lasers operation. It is believed, however, that the work described below has resulted in a system of sufficient power, stability and range of operating frequency to make it a valuable tool in spectroscopic analysis.

#### B. System Configuration

A diagram of the HF-DF laser system is shown in Figure 86. A mixture of sulfur hexafluoride gas ( $\text{SF}_6$ ) and helium and oxygen diluent is injected through a circular array of hollow nickel electrodes comprising the cathode of the electric discharge tube. These electrodes are individually connected through  $350\text{K}\Omega$  ballast resistor chains to the high voltage terminal of the power supply. This arrangement decouples the arcs produced at each electrode, while allowing maximum use of the discharge tube volume. The tube is made of Pyrex, and is 69 cm long with an I.D. of 27 mm. A water jacket flow system surrounds the tube to carry away the heat generated by the discharge. The discharge causes fluorine atoms to break off from the  $\text{SF}_6$  molecules. The addition of oxygen enhances this process, while the effect of the helium is to cool and stabilize the discharge.

The plasma containing the dissociated fluorine atoms flow into the mixing cell, where it is broadened and flattened into a stream 10 cm wide by 3 mm high in cross-section. The mixing cell is made of electro deposited nickel to make it impervious to corrosion by the reactants and reaction products. The  $\text{H}_2\text{-D}_2$  injection manifold is located about 3.5 cm downstream from the entrance to the mixing chamber. Here hydrogen or deuterium is injected through two linear arrays of 30 holes 0.25 mm in diameter running transverse to the direction of plasma flow along the upper and lower faces of the chamber. The small size of the holes ensures the rapid and localized combination of reactants necessary for good population inversion. The cell is also cooled by water flowing through copper piping soldered to the outer surface to carry away heat generated by the chemical reaction. The reaction products are evacuated through a soda ash ( $\text{Na}_2\text{CO}_3$ ) scrubbing filter into a model 1398 Welch Duo-seal vacuum pump with a capacity of 55 cfm (20 l/sec), which results in a linear flow velocity in the mixing chamber of about 50m/sec.

Laser windows for the optical cavity are located in the mixing region, and provide for location of the optical cavity axis anywhere from 3 mm upstream to 5 mm downstream of the injection point. The windows are  $\text{CaF}_2$ , mounted at the Brewster angle on mounts equipped with a He purge line to sweep out ground state HF-DF and to keep deposits from forming on the windows. The windows are sealed in place with silicone rubber compound to allow for easy removal and replacement during periodic cleaning.

The optical cavity is 30 cm long. The end reflector mount, which holds a plane first-surface mirror for multiline operation and a diffraction grating for single-line operation, was designed by Professor E. K. Damon of Ohio State University for use in tunable laser systems. The angle of the reflector is adjusted



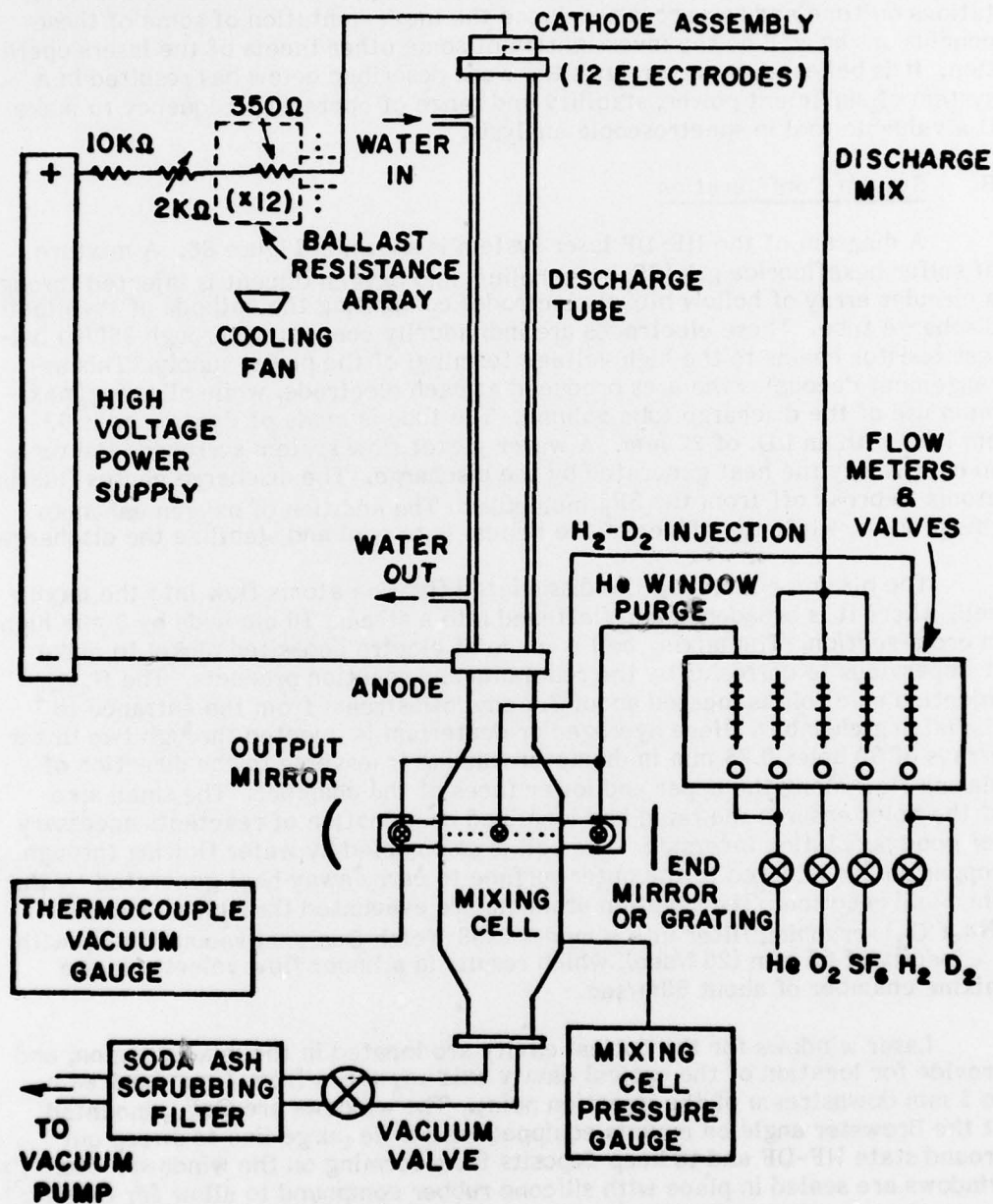


Figure 86. HF-DF laser system configuration.

by a micrometer drive in a manner so as to maintain a linear ratio between the change in position registered by the micrometer and change in wave number for which the cavity is aligned. This feature is helpful in the identification of laser transitions.

The output mirror mount is a Burleigh Gimbal Star mount equipped with two micrometer drives for the elevational and azimuthal orientation of the mirror. The mount is also equipped with a 3-element piezo-electric aligner/translator, driven by a Burleigh PZ-61 dc power supply to allow fine adjustment of mirror tilt and cavity length over distances on the order of a wavelength ( $3\text{ }\mu\text{m}$ ). This arrangement guarantees optimum mirror orientation.

Since the gain of the laser is a function of the relative location of the optical cavity axis with respect to the injection point, the output mirror mount is mounted in turn on a micrometer-driven translational base, which allows for easy shifting of the cavity axis up and down stream from the mix point, and hence provides for expeditious determination of the region of maximum gain. A close-up photograph of the mixing cell and optical cavity is shown in Figure 87.

### C. Operation and Output Characteristics

#### 1. Multiline Operation

The fact that this laser resembles the one described in Reference 16 in geometry and configuration allowed us to assume that duplication of the operating specifications reported in this reference would be the most likely means of achieving laser operation. Accordingly, initial attempts to achieve lasing involved the individual variation by increments of those parameters deemed to have an effect on laser operation, i.e., reactant-diluent ratios, total internal cell pressure, discharge voltage and current, optical alignment and translational position of the cavity axis. Reference 16 specifications were used as a mean value in each case. Trials were run using a first-surface plane mirror as the end reflector, with an 80%<sup>±</sup>3 broadband reflective germanium mirror of 20 m radius of curvature used as the output mirror for HF, and a ZnSe 2 m radius of curvature mirror 95%-98% reflective from 3.5-4.1  $\mu\text{m}$  for DF. This painstaking and time consuming process was not productive.

Lasing was finally achieved upon substitution of oxygen for helium as a diluent, a possibility that had not been investigated initially because the optimum diluent reactant mix reported in Reference 16 had contained no oxygen. This had the effect of increasing discharge impedance and heat generated by chemical reaction. The germanium mirror and first-surface flat were used, and a maximum multiline power out of 0.5W was eventually achieved. Voltage and current delivered to the ballast resistors and discharge tube for this value was 14.2K at 98 mA. Total internal cell pressure was 17 mbar, with the following component breakdown: 2.5 mbar  $\text{H}_e$  (window purge), 6.5 mbar  $\text{O}_2$ , 5 mbar  $\text{SF}_6$  and 3 mbar  $\text{H}_2$ .

Gas flows, discharge power and optical cavity orientation were varied as described above in hopes of determining the effect of each multiline power output. The following observations were made:



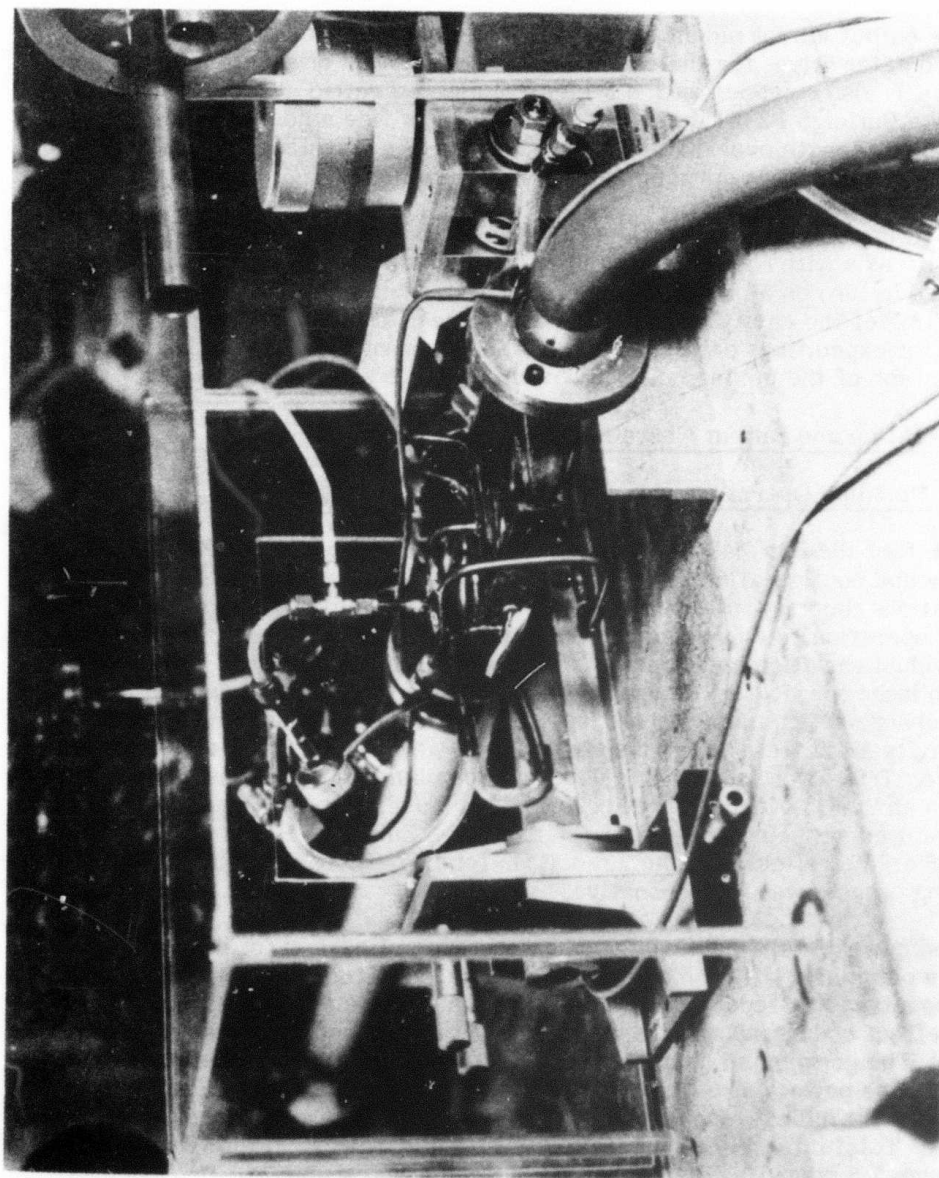


Figure 87. Mixing cell and optical cavity.

a) The most critical factor in maintaining good multiline power output is cavity alignment and stability. The slightest adjustment of the elevational or azimuthal drives or even simple pressure on the output mirror mount was found to be enough to drastically reduce or eliminate output. However, the relative positioning of the cavity axis with respect to the injection point was not found to be a very critical factor, with roughly comparable (less than a factor of 2) power outputs observed anywhere from 1 mm upstream to 3mm downstream of the point of injection for a given gas mixture.

b) Although variations in reactant and diluent flow rates had a pronounced effect on discharge impedance, the corresponding effect on laser power output was markedly less.

c) For multiline HF lasing, power output was surprisingly observed to decrease with increasing voltage and current. With the ballast resistance used at this point, the discharge was unable to sustain itself below 90mA. It was decided therefore to add a total of 10-20 kilohms adjustable resistance between the power supply and the ballast resistor array to investigate the possibility of achieving still greater power out at currents below 90mA. However, it was found that, for multiline operation, maximum power out was achieved over the range of 90-100mA. The addition of the extra resistance raised the operating power supply output voltage to 15-16KV.

d) A tendency was noticed for the laser to "self-maximize" its output, where if adjustment of output mirror orientation resulted in a power output of greater than about 25mW, laser power would continue to increase in the absence of any adjustment whatsoever for about 15 seconds. No determination of the cause for this behavior was made, although deformation of the windows or output mirror due to absorption of laser radiation, resulting in a favorable slight re-alignment of the cavity, may account for it.

With the information gained from successful HF laser operation, DF operation was rapidly achieved using the 98% reflective output mirror mentioned above. Reactant-diluent flows and discharge voltage-current values were the same as for HF and a maximum power out of 0.5W was also achieved in this case. Since DF gain has invariably been reported to be less than HF gain, this raised the question whether the 20% output coupling of the germanium mirror was excessive. This possibility was further investigated in the single line studies below.

## 2. Single Line Operation

Attempts were made to achieve single line HF lasing using a Bausch and Lomb 300 line/mm plane diffraction grating, blazed at 3.5 microns, and the germanium mirror mentioned above. No laser oscillation was observed. Since the germanium mirror had the highest reflectivity in the HF laser spectral region ( $2.8\mu\text{m}$ ) available in the laboratory at this time, our only choice was to use a grating of sufficiently high efficiency to keep cavity losses low enough to sustain oscillation. Investigation of the grating specifications revealed that its efficiency at HF laser frequencies was only 60%. A grating blazed at  $3\mu\text{m}$ , 80%-85% efficient over this region, was substituted, but no lasing was observed. This confirmed the need for a high reflectivity output mirror. A theoretical case for overcoupling in this system is presented in Appendix A.

Single-line operation with DF using the first grating mentioned above was, by contrast, very successful. Lasing was observed on a total of 21 separate vibrational-rotational transitions covering the 3-2, 2-1 and 1-0 groups. A complete listing of these transitions and their spectral locations is given in Table VII.

The strongest observed laser lines were P(5)-P(10) on the 2-1 band, with power outputs ranging from about 50-120 mW. Positive identification of these lines was made using an Optical Engineering DF Laser spectrum analyzer. As shown in Figure 88, the output beam was reflected by a diagonal mirror into the entrance slit of the analyzer.

Because of the small ( $1 \frac{1^0}{2} \times 2 \frac{1^0}{2}$ ) input beam acceptance angle of this device, a no. 8 infrared fluorescent detection screen was used to determine the correct reflected beam orientation. Observed spectrometer readings corresponded to tabulated values to within the limits of resolution of the device ( $.002 \mu\text{m}$ ). Identification of weaker transitions too low in intensity to be observed on the spectrometer detection screen ( $< 40 \text{ mW}$ ) was made by measuring the intervals between micrometer settings of the grating mount for spectrometer-identified transitions to derive the ratio between shift in setting and shift in observed wavenumber, taking advantage of the linearity feature of the mount mentioned above, and correlation extrapolated wavenumbers with their tabulated values. As can be seen in the table, this procedure proved to be reliable.

Once the identity of the various transitions had been established, experiments were run, as in the multiline case, to determine how these individual lasing transitions might be enhanced. Both helium and oxygen diluents were used in varying ratios of partial pressure. Parameters known to affect output power were varied singly and in combination to determine to what extent, if any, these effects would reinforce or cancel one another.

It was discovered early in this investigation that variation of these parameters had differing effects on the three vibrational "families", although the effect on the P-branch constituents of each was fairly uniform. 1-0 transitions were enhanced by running a comparatively high current discharge with a comparatively rich admixture of oxygen diluent. The addition of oxygen resulted in a steady increase in power output up to an  $\text{O}_2$  partial pressure of 8 mbar while, for a given gas mixture, an increase in discharge current up to about 135 mA resulted in a linearly proportional output power increase. Conversely, a decrease in oxygen component resulted in a sharp loss of power, with 1-0 transitions ceasing entirely at  $\text{O}_2$  partial pressures below 3 mbar, regardless of variations in discharge current.

3-2 transitions, on the other hand, were enhanced as current was decreased from the base settings determined in the multiline studies - in fact, no transitions were observed at all at settings above 110 mA. While addition of oxygen did have some positive effect on power output, the addition of helium to the discharge was much more effective. Optimum settings for 3-2 transitions were a discharge current of 75 mA and partial pressures for He and  $\text{O}_2$  of 7 mbar and 2 mbar respectively.



	Wave No. (cm <sup>-1</sup> )	Micrometer Setting	Power
1-0 P(5)	2792.434	4.54	weak
1-0 P(6)	2767.968	4.68	weak
1-0 P(7)	2742.998	4.83	moderate
2-1 P(4)	2727.309	4.92	weak
1-0 P(8)	2717.539	4.98	moderate
2-1 P(5)	2703.999	5.06	moderate
1-0 P(9)	2691.607	5.13	weak
2-1 P(6)	2680.179	5.21	strong
1-0 P(10)	2665.219	5.29	weak
2-1 P(7)	2655.863	5.36	strong
1-0 P(11)	2638.392	5.46	weak
2-1 P(8)	2631.068	5.51	strong
1-0 P(12)	2611.142	5.64	weak
2-1 P(9)	2605.807	5.69	strong
3-2 P(6)	2594.198	5.75	weak
2-1 P(10)	2580.097	5.85	strong
3-2 P(7)	2570.522	5.92	weak
2-1 P(11)	2553.953	6.03	moderate
3-2 P(8)	2546.375	6.08	moderate
3-2 P(9)	2521.769	6.24	weak
3-2 P(10)	2496.721	6.42	weak

weak - 10 - 30 mW  
moderate - 30 - 60 mW  
strong - 60 - 120 mW

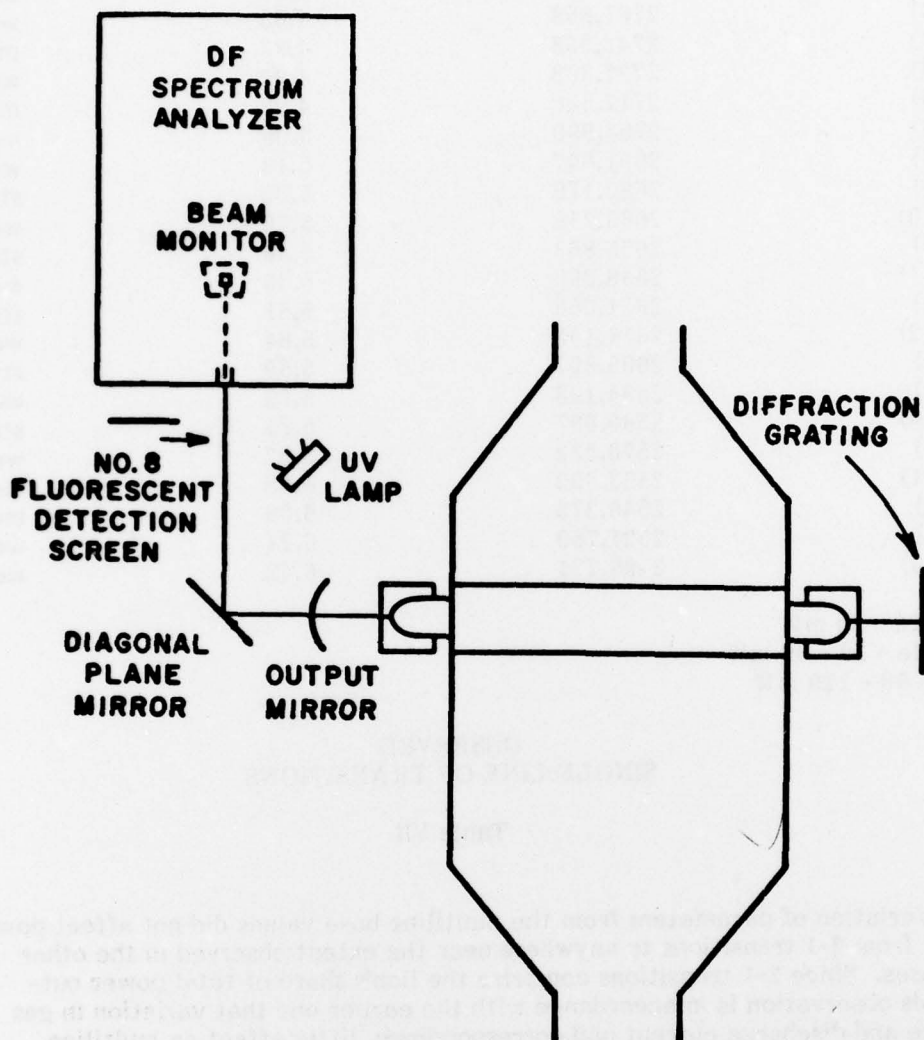
#### OBSERVED SINGLE-LINE OF TRANSITIONS

Table VII

Variation of parameters from the multiline base values did not affect power output from 2-1 transitions to anywhere near the extent observed in the other two cases. Since 2-1 transitions comprise the lion's share of total power output, this observation is in accordance with the earlier one that variation in gas mixture and discharge current had correspondingly little effect on multiline power output.

### 3. Conclusions

The observations collected from both the multiline and single line studies conform, in large part, to theoretical and experimental knowledge derived to date. Although the reasons for our lack of success in achieving lasing using helium as the only diluent remain unclear, a possible explanation may lie in the fact that, because our discharge tube is 15 cm longer than that used in Reference 16, the wall recombination rate of dissociated fluorine may be great enough to prevent the development of a sufficient population of excited HF-DF molecules. This conjecture is supported by the fact that oxygen is known to enhance



**Figure 88.** Experimental set-up for identification of specific vibrational-rotational transitions.



the dissociation of  $\text{SF}_6^{22}$ , which also would account for the increase in chemical reaction heat generated upon introduction of oxygen as a diluent.

The effect of helium in a discharge laser of this type is to lower the temperature of the discharge and mixing region, where the lower collision rate results in a higher partial inversion of the medium<sup>23</sup>. This phenomenon would account for the strong enhancement of 3-2 DF lasing in helium diluent and comparatively low currents. The strong 1-0 DF lasing observed with high currents is probably due to the higher temperature and collision rate, shifting the mean population in each vibrational level in favor of the lower levels. The fact that the 2-1 transition occupies the middle position in this dynamic, coupled with the fact that this excited DF level is the most heavily populated to start with, would account for the comparative lack of effect of parameter variations on 2-1 transitions in this case.

#### D. Output Coupling Studies

In the course of the construction of this laser, it was realized that, in the interest of achieving laser action on a large number of transitions, output coupling should be relatively low. The choice of the 98% reflecting DF output mirror mentioned above was made with this in mind. Undercoupling the system in this manner allowed us to run experiments to determine the optimum amount of output coupling for a given DF transition, using the grating blazed at  $3.5\mu\text{m}$ . It was hoped that this data would help us to determine the desired degree of general output coupling to assure the best trade-off between power output and number of lasing transitions.

The experimental procedure used was a simple but effective technique developed by T. F. Johnston, Jr. of Hughes Electron Dynamics Division, Torrance, California<sup>24</sup>. A "knife-edge" cubical aluminum mirror, 1 inch on a side, was mounted on a micrometer driven translational stage with the cube faces oriented at a  $45^\circ$  angle with respect to the optical cavity axis, as shown in Figure 89. As the knife-edge is moved inward to the point where it begins to occlude the laser beam, power is coupled out at right angles to the cavity. Since the laser power in the cavity  $P_c = P_{\text{OUT}}/t$ , the expression for the ratio of power coupled out to the available cavity power - that is, the amount of inserted loss - is  $L = P_{\text{IN}}/P_c = P_{\text{IN}}/P_{\text{OUT}}t$ , where  $P_{\text{IN}}$  is the power coupled out by the knife-edge,  $P_{\text{OUT}}$  the power coupled out by the output mirror, and  $t$  the known transmissivity of the mirror. As more and more intracavity power is coupled out by the knife-edge in an undercoupled system, the sum of  $P_{\text{IN}}$  and  $P_{\text{OUT}}$  reaches a maximum value. This is the point at which total output coupling is at its optimum value for the transition in question and an expression for the desired output mirror transmissivity can be readily derived:

$$T_{\text{OPT}} = \left(1 + \frac{P_{\text{IN}}}{P_{\text{OUT}}}\right)t \text{ where } P_{\text{IN}} + P_{\text{OUT}} \text{ is maximum.}$$

A strong transition (2-1 P(7)) and a weak one (3-2 P(7)) were each investigated for respective degrees of undercoupling. In each case, the knife-edge was introduced into the cavity to the point where lateral output coupling was

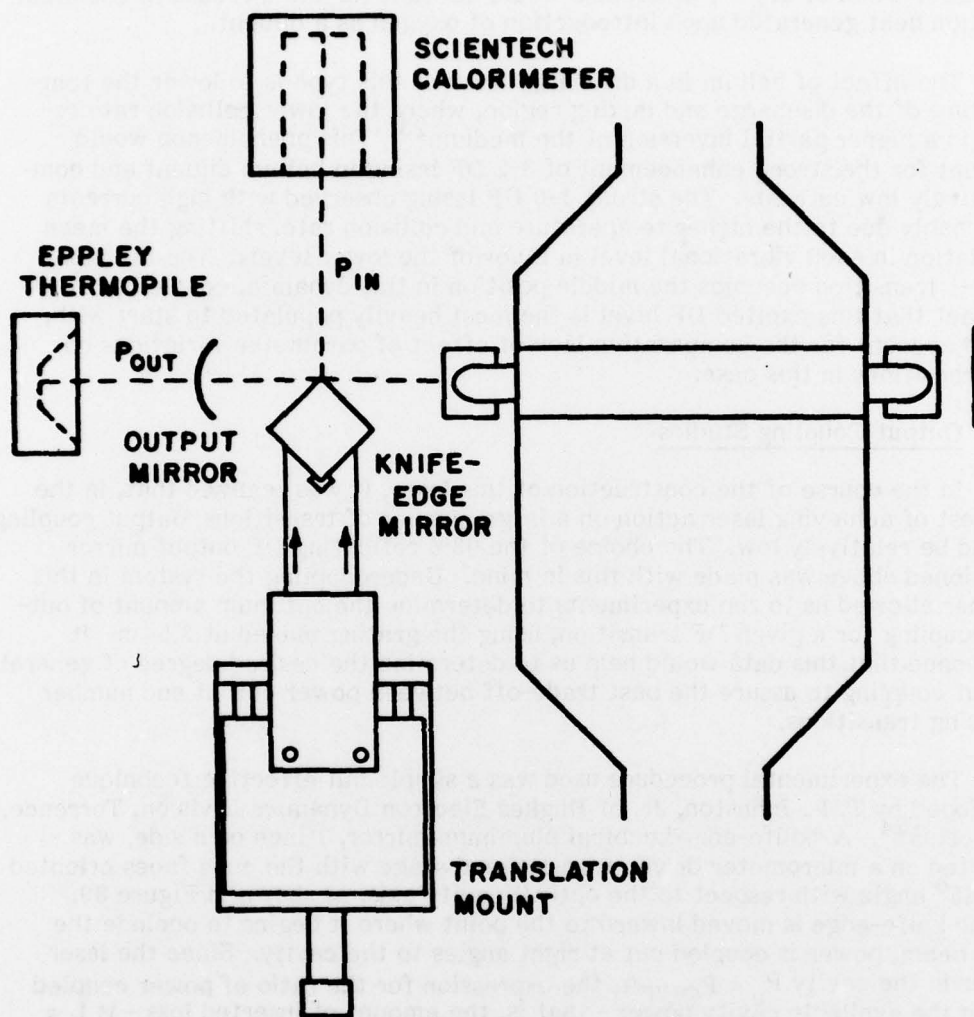


Figure 89. Experimental set-up for output coupling studies.

first observed. An Eppley thermopile was used to measure this beam intensity, while a Scientech calorimeter was used to measure the power output of the main beam. Power readings were taken at .005" (.125 mm) increments from this point until measurements for both  $P_{IN}$  and  $P_{OUT}$  began to decline, indicating obvious overcoupling. The measurements were then repeated to establish the consistency of laser performance and reliability of the data. Graphs of these results are shown in Figures 90,91. The figures for  $P_{IN}$  take into account the reflectivity of the cube faces at  $45^\circ$  incidence, measured in the laboratory at  $85\% \pm 1$ .

For the strongest lines, like 2-1 P(7), the optimum output coupling can be seen to occur where the power coupled into each detector is nearly the same amount. This indicates that optimum transmissivity for these lines is about:

$$t_{OPT} = (1+1)(2\%) \text{ or } 4\%.$$

For weaker lines like 3-2 P(7), however, optimum coupling is seen to occur where  $P_{OUT}$  is almost three times  $P_{IN}$ , indicating that optimum transmissivity for this line is  $(1 + 1/3)(2\%)$  or  $\sim 2.7\%$ . We can conclude, therefore, that our original choice of the 98% reflecting mirror was close to the optimum desired value, especially since undercoupled output from strong lines is only about 30% less than theoretical maximum.

#### E. Short-Term Stability Measurements

The purpose of the investigation described in this section was to determine the extent and, if possible, the causes of single-line amplitude instability not registered by calorimeter or thermopile measurements because of the slow time constants associated with these devices. Measurements with the thermopile did reveal a necessity for periodic tweaking of grating position or the PZT aligner to counteract the tendency for the cavity resonance frequency to drift away from the center of the frequency vs. gain profile of a given transition. Short term measurements using a fast detector were made to shed more light on this phenomenon.

The detector used was a 4mm x 4mm chip of lead selenide (Pb Se) furnished by the Santa Barbara Research Center, and was used in previous research at this laboratory by Dr. F. S. Mills<sup>25</sup>. The original electronics (reprinted in Figure 92a), were used to bias the detector and provide a suitable output signal to be monitored by oscilloscope. The detector time constant is on the order of a few microseconds.

In view of the fragility and sensitivity of these devices it was deemed prudent to expose the detector only to average power levels not in excess of those encountered in previous use (about 5 mW). Accordingly, a beam chopper was constructed to cut the exposure cycle to about 5%. Four  $4-1/2^\circ$  wedges were cut to  $90^\circ$  intervals from an aluminum disc 6 inches in diameter. The disc was mounted on a bearing and belt-driven by an electric motor running at 780 rpm, giving us a beam sampling frequency of approximately 52 Hz. The beam was sampled directly as shown in Figure 92b. Beam power was monitored for both strong and weak transitions.



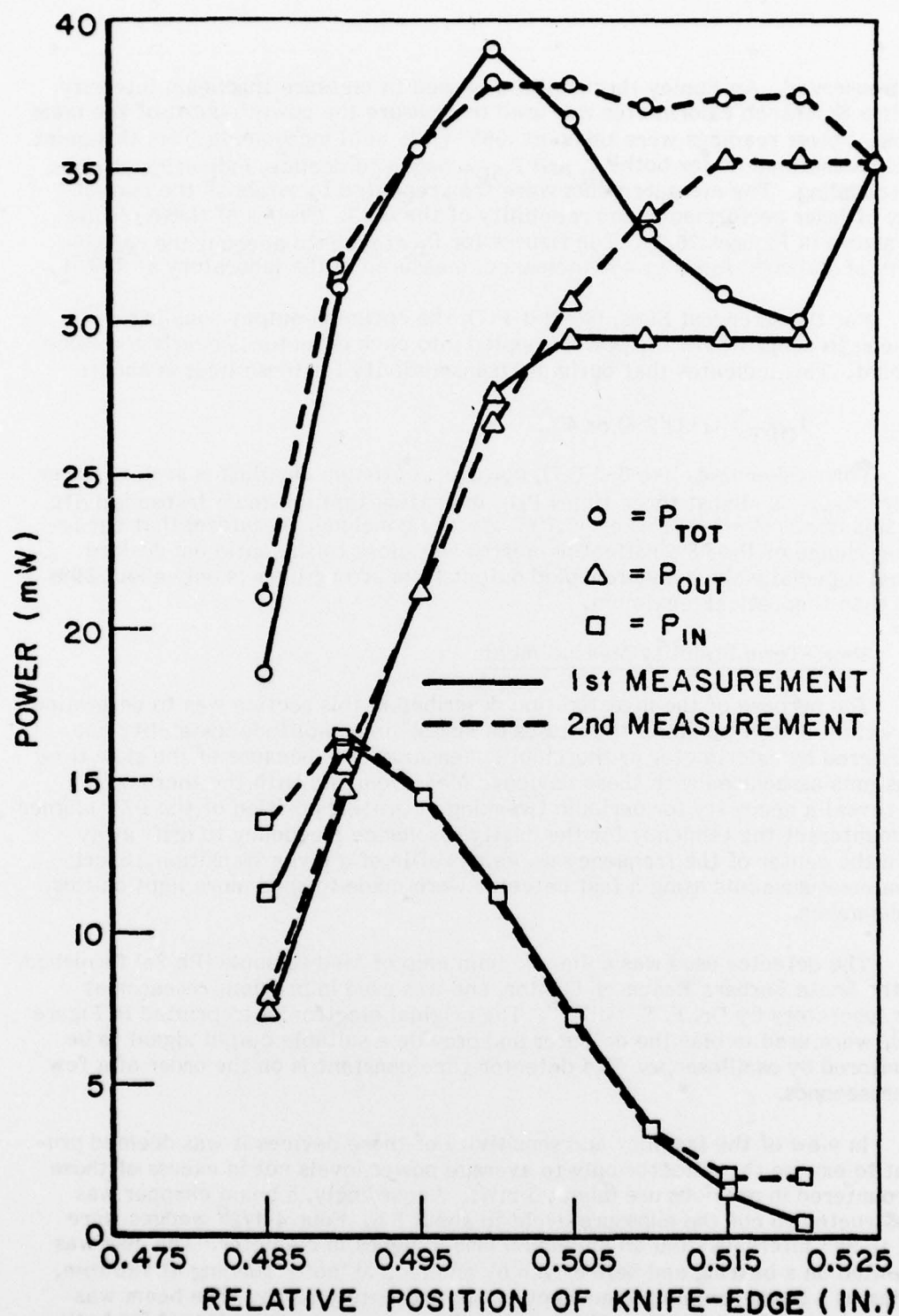


Figure 90. Output coupling measurements with the 2-1 P(7) DF laser line.

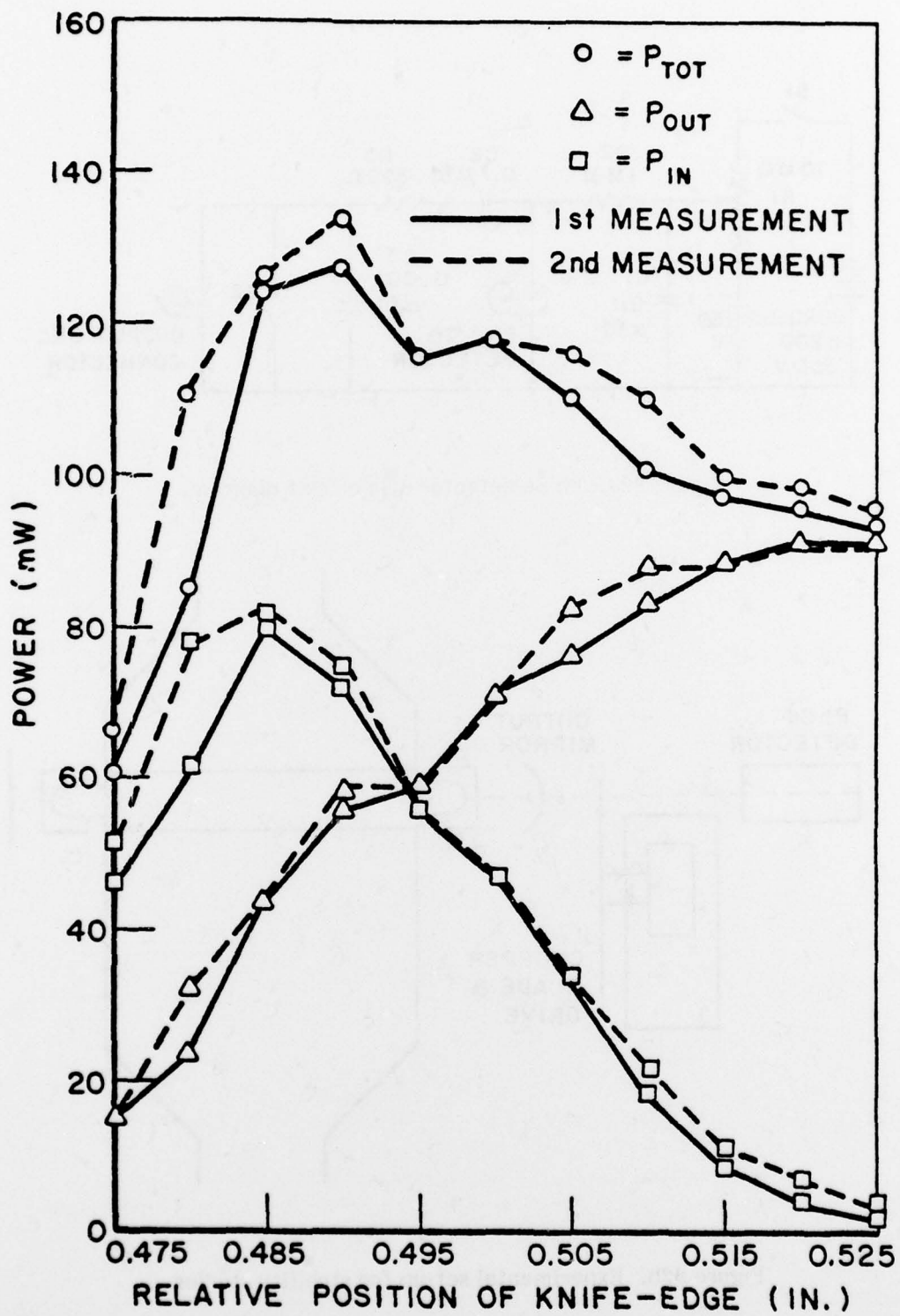


Figure 91. Output coupling measurements with the 3-2 P(7) DF laser line.



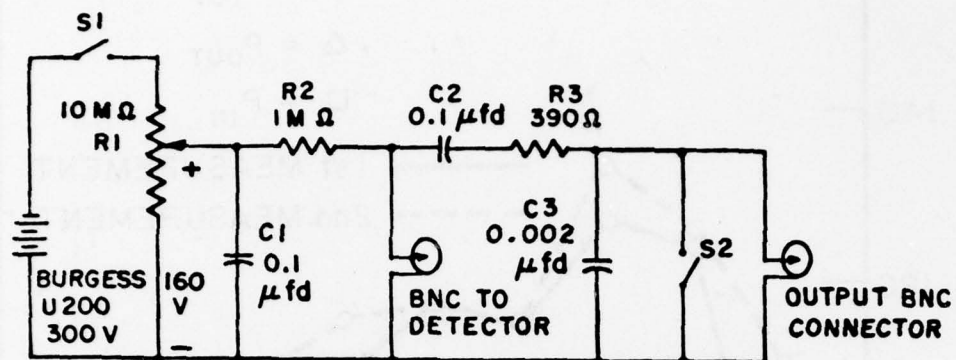


Figure 92a. Pb Se detector bias circuit diagram.

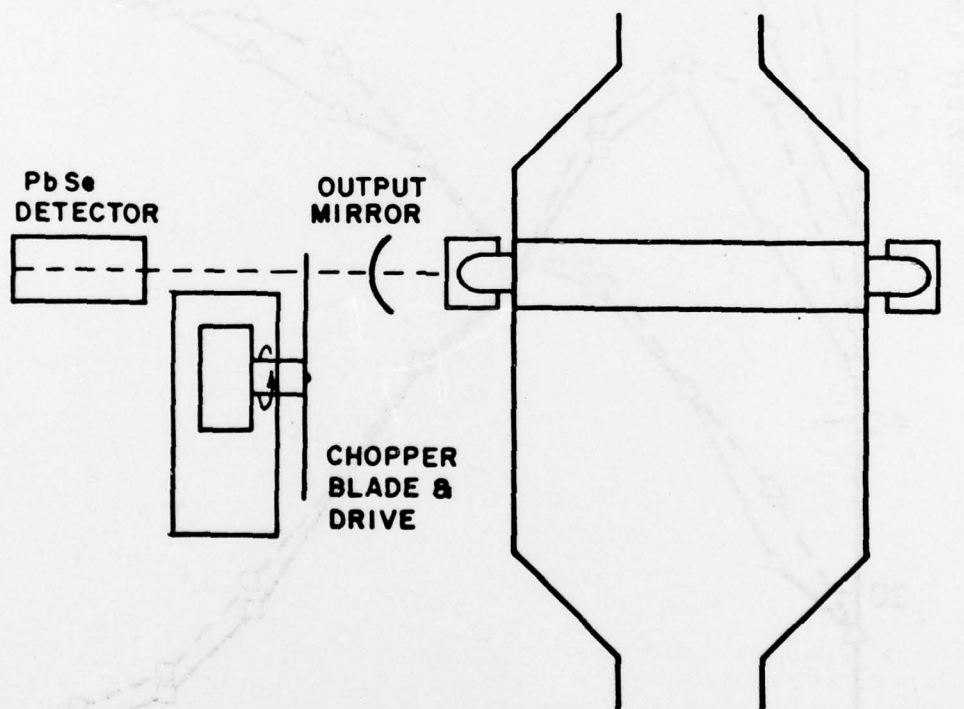


Figure 92b. Experimental set-up for stability studies.

As can be seen in Figure 93a, stability of output at maximum gain is good. Although exact figures could not be determined due to lack of data concerning detector non linearities, the amplitude variation shown on the oscilloscope was  $\pm 10\%$ . It is reasonable to assume that the actual figure is not far from this.

If the cavity is tuned away from maximum gain, however, output becomes extremely erratic, as shown in Figure 93b. Weak transitions predictably were found to be affected to a greater extent in this regard than strong ones.

It can reasonably be concluded that instability in this laser is largely due to variations in the cavity resonance frequency, which are characterized by rapid fluctuations around a slowly drifting mean value. The observations detailed above can be explained with the aid of Figure 93c. Around the central maximum of our gain vs. frequency profile (assumed to be Lorentzian), the change in gain with frequency is low, leading to maximum stability of maximum power. If the mean resonance frequency of the cavity is on the slope of the gain profile "hill", however, the change in gain with frequency is great, leading to erratic output.

The sources of the rapid variations are fairly obvious. The two optical mounts are anchored to a limestone base but are not directly structurally linked in any way. Cavity length therefore is influenced by the vibrations generated by sources like the vacuum pump (located directly beneath the lab table on which the laser rests) and the breeze from the fan used to cool the ballast resistors. A quick check revealed that blocking the breeze from the optical cavity region did have a perceivable effect in reducing the instability seen in the off-maximum case.

The reasons for the slow drift in resonance frequency are more difficult to uncover. A possible explanation is that the fan breeze cools the surfaces of the mounts, causing them to contract slightly. In any event, some form of low-thermal expansion structural framework for the cavity is desirable.

Much of the instability in this laser could be eliminated by incorporating the longitudinal translator of the PZT pusher in a servo-loop controlled by a signal which is a function of power output variation. Direct power measurement could serve in cases where the gain profile of a transition exhibits an inflection point at line center (Lamb dip), while a slope-sensitive signal could be used if this were not so. Laser power could be monitored by placing an angled window in the optical cavity to reflect out a small, but constant, portion of the power.

#### F. Summary and Conclusions

The object of the efforts described above was to develop an economical, single mode continuous wave HF-DF laser system of sufficient stability and spectral range to be useful in spectroscopic analysis. To this end we were largely successful, with the achievement of substantial single-mode power output on a large number of vibrational-rotational transitions covering a broad portion of the infrared spectrum.

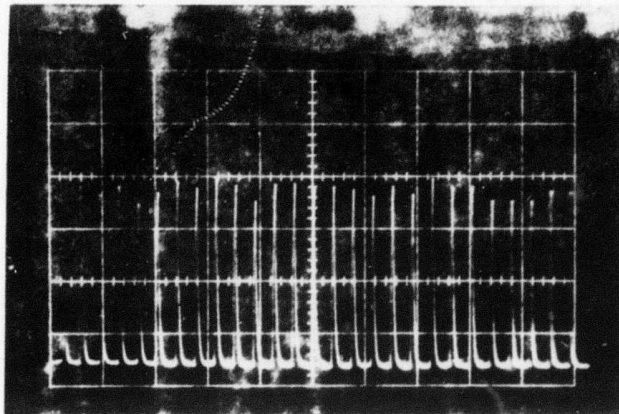


Figure 93a. Stability at line-center (vert. 200mV/cm, horiz. 50m/cm).

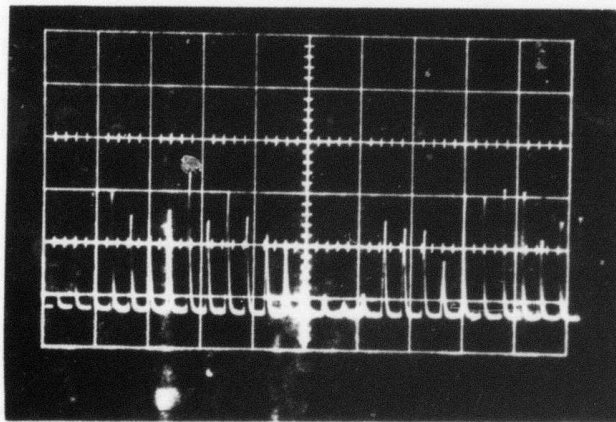


Figure 93b. Stability off line-center (vert. 200mV, horiz. 50ms/cm).

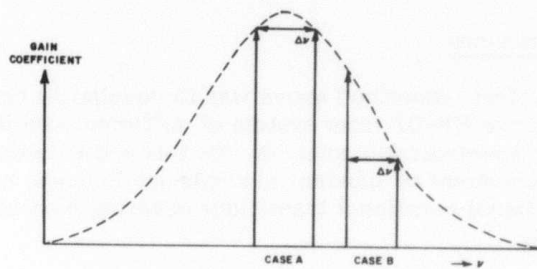


Figure 93c. Variation in gain with frequency.

The two major areas in which work should be continued are readily apparent - in order to achieve single line HF lasing, an output mirror of 93-95% reflectivity around  $2.8\mu$  should be procured, and studies similar to those described above repeated for the HF transitions observed. Secondly, a structural frame for the optics should be designed and tested, and a servo-loop stabilization system should be devised, with detailed followup observations to determine the degree of stability achieved and, if possible, the limiting factors responsible.



## APPENDIX A OVERCOUPLING OF HF OUTPUT MIRROR

Lack of success in achieving single-line HF lasing prompted the following theoretical analysis, using gain data reported by Hinchey in Reference 16. For the laser described therein, similar to our own in size, configuration and output power, a maximum gain coefficient of about  $.03 \text{ cm}^{-1}$  was reported. Losses within our own optical cavity were conservatively estimated at 20% to output coupling and 15% to grating losses. No attempt was made to account for other sources, such as optics size or window loss. Using the following formula for theoretical optimum output coupling:

$$\frac{1}{2} \ln \left( \frac{1}{R_{\text{OPT}}} \right) = T_{\text{OPT}} = \sqrt{go\mathcal{L} - \mathcal{L}} \quad (1)$$

where  $go = .3 = (.03 \text{ cm}^{-1}) \times 10 \text{ cm} = \text{fractional power gain per pass}$ ,

and  $\mathcal{L} = \frac{1}{2} \ln \left( \frac{1}{R_{\text{GRAT}}} \right) = .0813 = \text{fractional power loss per pass}$ ,

so  $T_{\text{OPT}} = \sqrt{.3(.0813)} - .0813 = .156 - .0813 = .0749$

$R_{\text{OPT}} = e^{-2(.0749)} = .861$  so optimum output coupling is 13.9% for the strongest HF transition.

Even under the conservative, simplistic conditions stipulated, the degree of overcoupling is substantial. We can therefore conclude that a reflectivity of over 90% is needed if we take into account unaccounted for loss and the lower gains of weaker lasing lines. In view of our experience with DF lasing, a choice of 5% output coupling would be good. Exact optimums could then be determined experimentally.



## REFERENCES

1. J. H. McCoy, D. B. Rensch, and R. K. Long, Appl. Opt. 8, 1471 (1969).
2. J. C. Peterson, "A Differential Spectrophone of Unique Design," MS Thesis, The Ohio State University, 1976.
3. R. K. Long, E. K. Damon, R. J. Nordstrom, J. C. Peterson, M. E. Thomas, J. Sherman, "Laser Atmospheric Absorption Studies," Report 4232-4, May 1977, The Ohio State University ElectroScience Laboratory, Department of Electrical Engineering; prepared under Contract F30602-76-C-0058 for Rome Air Development Center. (RADC-TR-77-248) (AD A045821)
4. V. N. Arefev and V. I. Dianov-Klokov, Opt. Spectrosc. 42, 488 (1977).
5. W. H. Thomason and D. C. Elbers, "An Inexpensive Method to Stabilize the Frequency of a CO<sub>2</sub> Laser," 1974, Louisiana State University, Department of Chemistry, private communication.
6. F. S. Mills, "A Computer Controlled Data Acquisition System for Atmospheric Propagation Studies," MS Thesis, August 1971, The Ohio State University; also Report 2834-1, August 1971, The Ohio State University ElectroScience Laboratory, Department of Electrical Engineering. prepared under Contract DAAG05-69-C-0782 for White Sands Missile Range, New Mexico.
7. G. L. Trusty, "Absorption Measurements of the 10.4 Micron Region Using a CO<sub>2</sub> Laser and a Spectrophone," Report 2819-4, January 1973, The Ohio State University ElectroScience Laboratory, Department of Electrical Engineering; prepared under Contract F33615-69-C-1809 for Air Force Avionics Laboratory. (AFAL-TR-72-413) (AD 909549)
8. "Measured Water Vapor Absorption Coefficients for Two Highly Absorbed CO Laser Lines," RADC-TR-73-225 (AD 764-376) June 1973.
9. R. K. Long, E. K. Damon, R. J. Nordstrom, J. C. Peterson, M. E. Thomas, J. Sherman, op. cit.
10. R. K. Long, F. S. Mills and G. L. Trusty, "Experimental Absorption Coefficients for Eleven CO Laser Lines," Report 3271-5, March 1973, The Ohio State University ElectroScience Laboratory, Department of Electrical Engineering; prepared under Contract F30602-72-C-0016 for Rome Air Development Center. (RADC-TR-73-126) (AD 760140)
11. R. K. Long, F. S. Mills and G. L. Trusty, "Calculated Absorption Coefficients for DF Laser Frequencies," Report 3271-7, November 1973, The Ohio State University ElectroScience Laboratory, Department of Electrical Engineering; prepared under Contract F30602-72-C-0016 for Rome Air Development Center. (RADC-TR-73-389) (AD 775373)

12. A. Metromopoulos, "Line Shape Parameters for H<sub>2</sub>O in Air," MS Thesis, University of Maryland, 1973.
13. R. K. Long, E. K. Damon, J. C. Peterson, M. E. Thomas, "Laser Atmospheric Absorption Studies," Report 4232-1, July 1976, The Ohio State University ElectroScience Laboratory, Department of Electrical Engineering; prepared under Contract F30602-76-C-0058 for Rome Air Development Center. (RADC-TR-76-330) (AD A036653)
14. R. K. Long, E. K. Damon, R. J. Nordstrom, J. C. Peterson, "Laser Atmospheric Absorption Studies," Report 4232-2, September 1976, The Ohio State University ElectroScience Laboratory, Department of Electrical Engineering; prepared under Contract F30602-76-C-0058 for Rome Air Development Center. (RADC-TR-76-389) (AD A036872)
15. J. J. Hinchey and C. M. Banas, Appl. Phys. Lett., 17 (1970) p. 386.
16. J. H. Hinchey, J. Appl. Phys., 45 (1974) p. 1818.
17. J. A. Glaze and G. J. Linford, Rev. Sci. Instrum. 44 (1973), p. 600.
18. J. V. V. Kasper and G. C. Pimentel, Phys. Rev. Lett. 14 (1965) p. 352.
19. K. L. Kompa and G. C. Pimentel, J. Chem. Phys. 47 (1967) p. 857.
20. R. W. F. Cross and J. F. Bott, ed., Handbook of Chemical Lasers, (John Wiley and Sons, New York, 1976) p. 21.
21. D. J. Spencer, T. A. Jacobs, H. Mirels and R. W. F. Gross, Int. J. of Chem Kinet. 1 (1969) p. 493; also Appl. Phys. Lett 16 (1970) p. 235.
22. Handbook of Chemical Lasers, p. 226.
23. Handbook of Chemical Lasers, p. 236.
24. T. F. Johnston, Jr., J. Quant. Elect QE-12 (1976), p. 310.
25. F. S. Mills, "Absorption of Deuterium Fluoride Laser Radiation by the Atmosphere," Report 4054-3, September 1975, The Ohio State University ElectroScience Laboratory, Department of Electrical Engineering; prepared under Contract F30602-75-C-0029 for Rome Air Development Center. (RADC-TR-76-105) (AD/A 025402)

## *MISSION of Rome Air Development Center*

RADC plans and conducts research, exploratory and advanced development programs in command, control, and communications (C<sup>3</sup>) activities, and in the C<sup>3</sup> areas of information sciences and intelligence. The principal technical mission areas are communications, electromagnetic guidance and control, surveillance of ground and aerospace objects, intelligence data collection and handling, information system technology, ionospheric propagation, solid state sciences, microwave physics and electronic reliability, maintainability and compatibility.

